CATCHING OUR FUTURE

Collection 07:

Process modelling, Scale-up and Cost reduction

TECHNOLOGY CENTRE MONGSTAD

RESEARCH PAPERS BY
TECHNOLOGY CENTRE MONGSTAD (TCM)

07 / 11

At TCM we are committed to promote the competitive deployment of carbon capture technologies to help combat climate change. We do that by supporting technology vendors to derisk at the largest scale before commercialization and by providing invaluable knowledge to project owners throughout their project cycle.

The owners' intentions

«We see an increasing interest for testing at TCM, and we are very pleased that we can continue our important work with testing and research necessary for the deployment of large-scale carbon capture.»

GASSNOVA

«TCM has contributed to maturing the carbon capture supplier market and will remain relevant with the increasing number of technology suppliers lining up for testing.»

equinor

«TCM plays a key role in further developing and reducing the cost of CCS – a crucial technology to help society and economies thrive through the energy transition.»

Shell

«In our climate ambition, carbon capture is key. TCM is the best platform to learn, test technologies and accelerate the technology scale up for implementation on our assets.»

TotalEnergies

07

Contents

CATCHING OUR FUTURE

Application of Sequential Design of Experiments (SDoE) to Large Pilot-Scale Solvent-Based CO_2 Capture Process at Technology Centre Mongstad (TCM)

(2021)

15th International Conference on Greenhouse Gas Control Technologies, GHGT-15

15th 18th March 2021 Abu Dhabi, UAE

Application of Sequential Design of Experiments (SDoE) to Large Pilot-Scale Solvent-Based CO_2 Capture Process at Technology Centre Mongstad (TCM)

Joshua C. Morgan[a,b,*], Benjamin Omell[a], Michael Matuszewski[a], David C. Miller[a], Muhammad Ismail Shah[c], Christophe Benquet[c], Anette Beate Nesse Knarvik[c], Thomas de Cazenove[c], Christine M. Anderson-Cook[d], Towfiq Ahmed[d], Charles Tong[e], Brenda Ng[e], Debangsu Bhattacharyya[f]

[a]*National Energy Technology Laboratory, 626 Cochrans Mill Road, P.O. Box 10940, Pittsburgh PA 15236-0940, USA*
[b] *NETL Support Contractor, 626 Cochrans Mill Road, P.O. Box 10940, Pittsburgh PA 15236-0940, USA*
[c]*CO_2 Technology Centre Mongstad, Mongstad 71, 5954 Mongstad, Norway*
[d]*Los Alamos National Laboratory, P.O. Box 1663, Los Alamos NM 87545, USA*
[e]*Lawrence Livermore National Laboratory, 7000 East Ave, Livermore CA 94550, USA*
[f]*West Virginia University, Department of Chemical and Biomedical Engineering, 1306 Evansdale Drive, P.O. Box 6102, Morgantown WV 26506-6102, USA*

Abstract

The United States Department of Energy's Carbon Capture Simulation for Industry Impact (CCSI^2) program has developed a framework for sequential design of experiments (SDoE) that aims to maximize knowledge gained from budget- and schedule-limited pilot scale testing. SDoE was applied to the planning and execution of campaigns for testing CO_2 capture systems at pilot-scale in order to optimally allocate resources available for the testing. In this methodology, a stochastic process model is developed by quantifying the parametric uncertainty in submodels of interest; for a solvent-based CO_2 capture system, these may include physical properties and equipment performance submodels (e.g., mass transfer, interfacial area). This uncertainty is propagated through the full process model, over variable operating conditions, for estimating the resulting uncertainty in key model outputs (e.g., percentage of CO_2 capture, solvent regeneration energy requirement). In developing a data collection plan, the predicted output uncertainty is incorporated into an algorithm that seeks simultaneously to select process operating conditions for which the predicted uncertainty is relatively high and to ensure that the entire space of operation is well represented. This test plan is then used to guide operation of the pilot plant at varying steady-state conditions, with resulting process data incorporated into the existing model using Bayesian inference to refine parameter distributions. The updated stochastic model, with reduced parametric uncertainty from data collected, is then used to guide additional data collection, thus the sequential nature of the experimental design.

The SDoE process was implemented at the pilot test unit (12 MWe in scale) at Norway's Technology Centre Mongstad (TCM) in a summer 2018 test campaign with aqueous monoethanolamine (MEA). During the test campaign, the varied operating conditions included the flowrates of circulated solvent, flue gas, and reboiler steam and the CO_2 concentration in the flue gas. The process data were used to update probability distributions of mass transfer and interfacial area parameters of a stochastic process model developed by the CCSI^2 team. Two iterations of the SDoE process were executed, resulting in the uncertainty in model predicted CO_2 capture percentage decreasing by an average of 58.0 ± 4.7% over the full input space of interest. This work demonstrates the

* Corresponding author. *E-mail address:* joshua.morgan@netl.doe.gov

potential of the SDoE process for model refinement through reduction in process model parametric uncertainty, and ultimately risk in scale-up, in CO_2 capture technology performance.

Keywords: post-combustion carbon capture; pilot-scale testing; uncertainty quantification; design of experiments

1. Introduction

The United States Department of Energy's Carbon Capture Simulation for Industry Impact (CCSI^2) program is a collaboration of national laboratories, universities, and industrial organizations that provides research and development support for novel CO_2 capture technologies with the objective of reducing risk and accelerating their commercialization. These efforts involve continuing advancements in and applications of the open-source toolset[1] developed as part of its predecessor project, the Carbon Capture Simulation Initiative (CCSI). The CCSI Toolset includes a suite of computational tools and models with the overarching goal of accelerating the development, deployment, and scale-up of CO_2 capture technologies. The toolset includes a rigorous process model, implemented in Aspen Plus®, of the aqueous monoethanolamine (MEA) solvent system, which is the industrial standard for solvent-based CO_2 capture. This model includes quantification of parametric uncertainty for solvent physical property models such as viscosity, density, and surface tension [1], the thermodynamic framework [2], and packing-specific models such as mass transfer, interfacial area, and hydraulics [3]. These submodels combine with a full process model that was validated with process data from the 0.5 MWe pilot test unit at the National Carbon Capture Center (NCCC) in 2014 [4]. In 2017, an additional test campaign for the aqueous MEA system was held at NCCC, incorporating the CCSI^2 framework for SDoE. In this methodology, the existing process model is leveraged to inform collection of data that are subsequently used to refine the model and modify the test plan accordingly [5,6]. Over two iterations of the SDoE process, parametric distributions for process submodels were refined through experimental observations of absorber CO_2 capture percentage, resulting in an average uncertainty reduction of approximately 50% for the model prediction of CO_2 capture percentage throughout the input space of interest.

The CCSI aqueous MEA process model was scaled up to 12 MWe for consistency with the pilot test unit at Norway's Technology Centre Mongstad (TCM) and was used in the planning and execution of a test campaign at TCM in summer 2018. TCM is one of the world's largest facilities for testing carbon capture technologies, and previous test results with the MEA solvent system have been reported in the open literature [7-12], including variation in many process variables and both steady-state and dynamic operation. The pilot plant at TCM notably has two sources of flue gas: combined cycle gas turbine (CCGT) based heat and power plant (CHP), with ~3.5 vol% CO_2, and residual fluidized catalytic cracker (RFCC) unit, with ~13-14 vol% CO_2. The TCM plant also contains two stripper columns, each designed for process operation with one of the flue gas sources. This work focused on collecting additional data for the MEA process at TCM with variation in the flowrates of solvent, flue gas, and reboiler steam, the concentration of CO_2 in the flue gas, the packing height of the absorber, and the stripper configuration. During the first three weeks of the test campaign, which are the primary focus of this paper, the SDoE framework was used to guide the collection of process data using the existing MEA process model and multiple test objectives. The data were used to update the model by refining the distributions of parameters in the mass transfer and interfacial area submodels, ultimately resulting in a reduction of predicted uncertainty in the CO_2 capture percentage from 10.5 ± 1.5% to 4.4 ± 0.4%, or an average reduction of 58.0 ± 4.7%, over the full input space of interest. In the final two weeks of the campaign, data were collected for a modified process configuration in which the packing height of the absorber was reduced to 18 meters, and eventually 12 meters, and the stripper configuration was modified so that a fraction (~20%) of the rich solvent exiting the absorber bypasses the lean-rich heat exchanger and is heated in the water wash of the stripper. This work, along with the previous test campaign at NCCC, demonstrates the potential of the SDoE methodology for refining predictions of stochastic process models through strategic data collection. The reduction of model uncertainty effectively reduces expected risk in process design and operation, thus improving confidence when predicting process performance and conducting economic analyses.

[1] Available at https://github.com/CCSI-Toolset/

2. Methodology

2.1. SDoE Methodology

The SDoE process developed by CCSI[2] uses a stochastic model, with parametric uncertainty quantified in the submodels, to inform collection of process data in order to maximize the value of data obtained during a test campaign. Moreover, it provides a framework for directly reducing uncertainty in model prediction of capture rates based on new process knowledge gained from data collection. The SDoE process is represented schematically in Fig. 1.

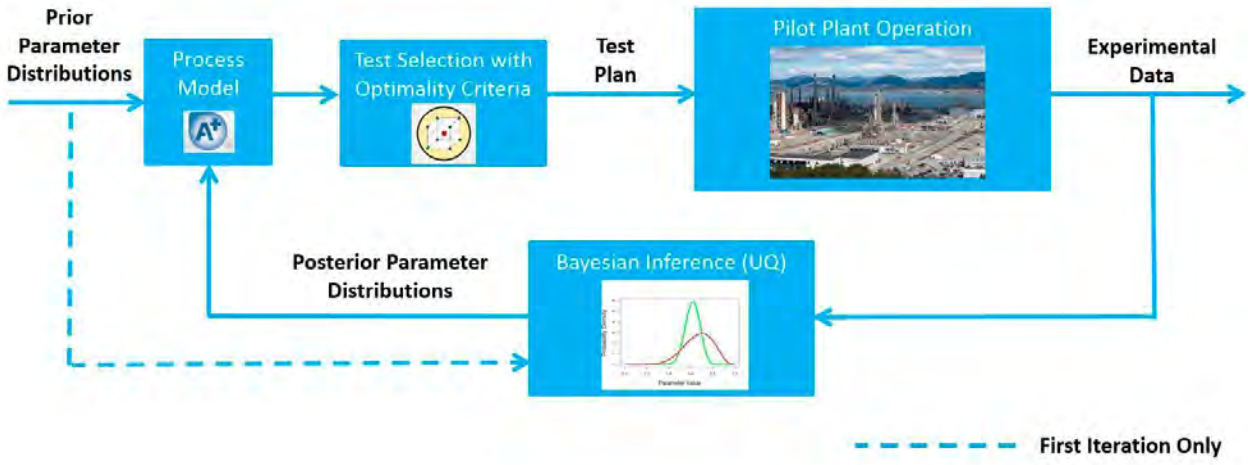

Fig. 1. Schematic representation of SDoE methodology

As shown in Figure 1, *a priori* probability distributions of submodel parameters are propagated through a process model, denoted as $y(\boldsymbol{x}, \boldsymbol{\theta}, \boldsymbol{\theta}^*)$, where $\boldsymbol{x}$ is a set of input variables that can be manipulated in plant operation and $\boldsymbol{\theta}$ and $\boldsymbol{\theta}^*$ are sets of model parameters. These sets differ in that $\boldsymbol{\theta}$ contains parameters for which uncertainty is reduced over the course of executing the SDoE methodology whereas $\boldsymbol{\theta}^*$ has parameters with irreducible uncertainty based on the type of data collected. For the example of a solvent-based CO_2 capture system, $\boldsymbol{\theta}$ includes process specific parameters from submodels such as mass transfer or interfacial area that may be informed through collection of plant data (e.g. CO_2 capture percentage in the absorber column). Conversely, $\boldsymbol{\theta}^*$ includes parameters from physical property submodels, for which uncertainty is readily estimated through direct measurements of the corresponding properties and cannot reasonably be informed from plant level data. If the process model y is sufficiently complex, it may be necessary to replace it with a surrogate model, denoted as $\hat{y}(\boldsymbol{x}, \boldsymbol{\theta}, \boldsymbol{\theta}^*)$, developed and validated over the full input space. For a given point in the input space, a confidence interval for the model prediction are computed by propagating the uncertainty in the full set of parameters ($\boldsymbol{\theta}^{\boldsymbol{T}} = [\boldsymbol{\theta} \quad \boldsymbol{\theta}^*]$) through the surrogate model. The 95% confidence interval, estimated by taking a sample of size M over the full parameter space ($\boldsymbol{\theta}^{\boldsymbol{T},(j)}, \forall\, j = 1, \ldots M$), is given as:

$$CI|_{\boldsymbol{x}^{(i)}} = F_{0.975}\left(\left\{\hat{y}\left(\boldsymbol{x}^{(i)}, \boldsymbol{\theta}^{\boldsymbol{T},(\mathbf{1})}\right), \ldots, \hat{y}\left(\boldsymbol{x}^{(i)}, \boldsymbol{\theta}^{\boldsymbol{T},(\boldsymbol{M})}\right)\right\}\right) - F_{0.025}\left(\left\{\hat{y}\left(\boldsymbol{x}^{(i)}, \boldsymbol{\theta}^{\mathbf{T},(1)}\right), \ldots, \hat{y}\left(\boldsymbol{x}^{(i)}, \boldsymbol{\theta}^{\boldsymbol{T},(\boldsymbol{M})}\right)\right\}\right) \quad (1)$$

where $\left\{\hat{y}\left(\boldsymbol{x}^{(i)}, \boldsymbol{\theta}^{\boldsymbol{T},(\mathbf{1})}\right), \ldots, \hat{y}\left(\boldsymbol{x}^{(i)}, \boldsymbol{\theta}^{\boldsymbol{T},(\boldsymbol{M})}\right)\right\}$ is the set of values of an output variable calculated from propagating all of the individual $\boldsymbol{\theta}^{\boldsymbol{T},(j)}$ through the surrogate model and F_k represents the k^{th} percentile of this set. The values of $CI|_{\boldsymbol{x}^{(i)}}$ for individual $\boldsymbol{x}^{(i)}$ are considered in the test selection method; the specific optimality criterion used in this work is G-optimality [13], which minimizes the maximum prediction variance. This aim targets experimental settings $\boldsymbol{x}^{(i)}$ for which the predicted uncertainty (i.e., $CI|_{\boldsymbol{x}^{(i)}}$) is relatively large, so that the collection of data at these settings represents high potential for uncertainty reduction. Moreover, the algorithm used in this work for test selection simultaneously seeks to ensure that the full input space is well-represented in the test plan, balancing good representation of design points throughout the region while making locations with large confidence interval widths more likely to be selected.

The test plan is then implemented by running the plant accordingly, resulting in collection of experimental data (denoted Z). The data are incorporated into a Bayesian inference framework, using the PSUADE[2] software package. For model parameters of fixed uncertainty, a sample ($\boldsymbol{\theta}^{*,(j)}; \forall\, j = 1, \ldots, N$) is drawn from their probability distribution $P(\boldsymbol{\theta}^{*})$. For each sample point $\boldsymbol{\theta}^{*,(j)}$, a posterior distribution for the remaining parameters ($\boldsymbol{\theta}$) is calculated:

$$\pi_j\left(\boldsymbol{\theta}|Z, \boldsymbol{\theta}^{*,(j)}\right) \propto P(\boldsymbol{\theta}) L\left(Z|\boldsymbol{\theta}, \boldsymbol{\theta}^{*,(j)}\right) \tag{2}$$

and given in the form of a set of sample points. Here, $L\left(Z|\boldsymbol{\theta}, \boldsymbol{\theta}^{*,(j)}\right)$ represents the likelihood (some metric used to express the distance between simulation predictions and experimental data) of observing a set of experimental data (Z) conditioned on the values of the parameters, $P(\boldsymbol{\theta})$ the prior distribution of the parameters for which uncertainty is updated, and $\pi_j\left(\boldsymbol{\theta}|Z, \boldsymbol{\theta}^{*,(j)}\right)$ the posterior distribution of $\boldsymbol{\theta}$ conditioned on the observed experimental data and the value of $\boldsymbol{\theta}^{*}$ for sample j. The overall posterior distribution $\pi\left(\boldsymbol{\theta}|Z, \boldsymbol{\theta}^{*,(j)}\right)$ is obtained through the process of marginalization, combining all individual $\pi_j\left(\boldsymbol{\theta}|Z, \boldsymbol{\theta}^{*,(j)}\right)$. The updated stochastic model, with refined estimates of parameter uncertainties, is then used to re-calculate $CI|_{\boldsymbol{x}^{(i)}}$ throughout the input space. For all subsequent iterations of SDoE, the prior distribution $P(\boldsymbol{\theta})$ is replaced by the posterior distribution $\pi_j\left(\boldsymbol{\theta}|Z, \boldsymbol{\theta}^{*,(j)}\right)$ from the previous iteration.

2.2. Overview of TCM Test Campaign

The TCM test campaign ran for five weeks in summer 2018, in five distinct test phases as outlined in Table 1.

Table 1. Phases of MEA test campaign at TCM

Phase No.	Absorber Packing Height (m)	CO_2 in Flue Gas (vol%)	No. of Data Sets	Stripper Configuration	Description of SDoE Criterion
1	24	8	14	Simple	Space-Filling Design
2	24	8 & 10	10	Simple	Selection of points with optimal economic performance
3	24	8 & 10	41	Simple	Sequential SDoE targeting uncertainty reduction
4	18	10	14	With Bypass	Minimization of specific reboiler duty (SRD)
5	12	10	19	With Bypass	Minimization of SRD

In the first three phases of the campaign, the absorber column was operated with all three packing beds (total height of 24 meters). A conventional stripper configuration was used in which the full amount of rich solvent exiting the absorber is heated in the lean-rich heat exchanger and sent to the top of the stripper column. Throughout the test campaign, flue gas from the CCGT plant (3.5 vol% CO_2) was combined with recycle of the captured CO_2, increasing the flue gas concentration to 8 or 10 vol% CO_2 as required by the test plan. Due to the increased CO_2 concentration in the flue gas, and the corresponding increase in the required solvent circulation rate for capturing CO_2, the larger stripper intended for use with RFCC flue gas was used during this campaign in lieu of the smaller stripper intended for CCGT flue gas. In Phases 4-5, the packing height of the absorber was reduced by changing the number of beds and the stripper configuration was modified so that approximately 20% of the rich solvent exiting the absorber column bypassed the lean-rich heat exchanger and was instead heated with hot vapor leaving the top of the stripper. This portion of the test campaign, also guided with use of the process model, was focused on identifying the optimal solvent circulation for minimizing the specific reboiler duty for the process. Other process variables were fixed for this portion of the test campaign, including a flue gas flowrate of 50,000 sm^3/hr with 10 vol% CO_2 and 85% CO_2 capture. For the purpose of brevity, the details of Phases 4-5 are not included in this paper.

[2] Problem Solving Environment for Uncertainty Analysis and Design Exploration (https://computing.llnl.gov/projects/psuade-uncertainty-quantification)

The first three phases differed in the choice of criteria used for developing the test plan. Phase 1 used a space-filling design to ensure that the process model predicts key outputs such as CO_2 capture and specific reboiler duty with reasonable accuracy. Phase 2 focused on collecting data in regions where the model predicts optimal economic performance. Phase 3 focused on collecting data to target regions where the model predicts high uncertainty based on the SDoE procedure in Section 2.1. For all three phases, a desired region of process operation was established based on ranges of operation for flue gas flowrate (G), CO_2 capture percentage (CAP), CO_2 loading in the lean solvent entering the absorber column (α_{lean}), and the volume fraction of CO_2 in the flue gas (y_{CO_2}), with ranges:

$$G \in [36{,}000 - 75{,}000]\ kg/hr \tag{3a}$$

$$CAP \in [80 - 95]\ \% \tag{3b}$$

$$\alpha_{lean} \in [0.10 - 0.25]\ mol\ CO_2/mol\ MEA \tag{3c}$$

$$y_{CO_2} \in \{0.08, 0.10\} \tag{3d}$$

The first three variables are treated as continuous whereas the CO_2 fraction in the flue gas is treated as a categorical variable with two process operation levels. For each value of CO_2 fraction, a test set consisting of candidate experiments with a unique combination of variables $\{G, CAP, \alpha_{lean}\}$ is generated by sampling independently from uniform distributions for each variable with upper and lower limits based on the ranges given in Eq. 3. An Aspen Plus simulation is run for each point in the candidate set to estimate the corresponding values of lean (L_{lean}) and rich (L_{rich}) solvent flowrate, steam flowrate (S) and mass of CO_2 captured ($\dot{m}_{CAP}$). To be included in the final candidate set, a point must satisfy the following conditions based on operational limits for the TCM plant:

$$\dot{m}_{CAP} < 8{,}000\ kg/hr \tag{4a}$$

$$S < 14{,}000\ kg/hr \tag{4b}$$

Separate candidate sets (for $y_{CO_2} = 0.08$ and $y_{CO_2} = 0.10$) were developed using a space-filling approach based on the input vector $\boldsymbol{x} = [G\ S\ \alpha_{lean}]$. These candidate sets were used in Phases 1 and 3, although Phase 1 used a space-filling design on the model input space while Phase 3 incorporated the predicted uncertainty in the model output, using the methodology described in Section 2.1. Moreover, only the candidate set for 8 vol% CO_2 in flue gas was implemented during Phase 1 of the test campaign due to time considerations.

Phase 2, however, was designed based on an optimization problem of the form:

$$\min_{\boldsymbol{x}} f(\boldsymbol{x}) = \frac{CAPEX\left(\frac{A}{P}, i, n\right) + OPEX}{\dot{m}_{CAP}} \tag{5a}$$

$$\left(\frac{A}{P}, i, n\right) = \frac{i(1+i)^n}{(1+i)^n - 1} \tag{5b}$$

$$\boldsymbol{x} = \begin{bmatrix} L_{lean} \\ G \\ \alpha_{lean} \end{bmatrix} \tag{5c}$$

subject to:

$$\boldsymbol{x^L} \leq \boldsymbol{x} \leq \boldsymbol{x^U} \tag{5d}$$

$$h(\boldsymbol{x}) = 0 \tag{5e}$$

$$g(\boldsymbol{x}) \leq 0 \tag{5f}$$

The objective function is the ratio of the equivalent annual operating cost (EAOC) associated with the CO_2 capture to the mass of CO_2 captured. The EAOC is the sum of the capital cost (CAPEX) multiplied by an annuity factor ($\frac{A}{P}, i, n$) and the operating cost (OPEX). Within the annuity factor, $\frac{A}{P}$ is the ratio of annuity to present value, i is the interest rate, and n is the number of years. The vector of decision variables is denoted as $\boldsymbol{x}$ with lower and upper bounds $\boldsymbol{x^L}$ and $\boldsymbol{x^U}$. The equality constraints denoted by $h(\boldsymbol{x})$ includes heat and material balances, and the inequality constraints

denoted by $g(\boldsymbol{x})$ includes the constraints for process operation listed in Eq. 4. The optimization was performed separately for the cases with 8 and 10 vol% CO_2 in flue gas. In addition the optimal points in the test plan, additional test points near the optimal points were included. The space surrounding the optimal point can be represented by a cube created by perturbing the input variable values by a chosen amount (10% for this study) from their estimated optimal values. A design that permutes each factor away from this estimated optimum one at a time would require seven test points, or six for the center of each face of the cube (if each factor is manipulated one at a time) and one for the center (optimal) point. As shown in Fig. 2., the design size was reduced to five by considering a fractional factorial structure, which also allows exploration of potential interactions between input factors around the optimum [14].

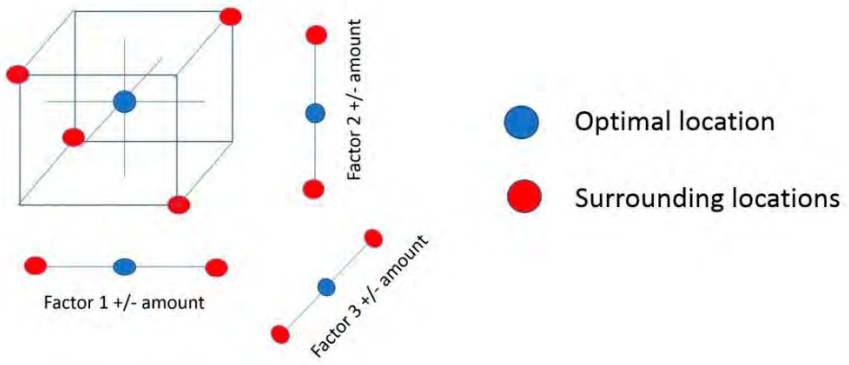

Fig. 2. Space-filling in region around optimal point for Phase 2 test plan

Since two levels of y_{CO_2} were included in the analysis, the reduction of the overall number of points required for the Phase 2 test plan from 14 to 10 was highly beneficial due to the limited amount of time available for the test campaign.

3. Results

3.1 Phase 1

In Phase 1, the test plan was developed using a minimax space-filling methodology [15] to provide an initial data set that was well-representative of the process. For all testing in this phase, the CO_2 concentration in the flue gas was fixed at 8 vol%. The set of input variables included in the test matrix differs from that used for space-filling design in that the input variables for the space-filling design were chosen for modeling convenience whereas the input variables in the test matrix were those directly manipulated in the plant operation. In developing the test matrix, the Aspen simulation was used to estimate the rich solvent flowrate and the flue gas flowrate was converted from mass to volumetric units. The test matrix, which was organized in terms of increasing flue gas flowrate for ease of process operation, for Phase 1 is given in Table 2.

Table 2. Test matrix for Phase 1 design of MEA test campaign at TCM

Test	Rich Solvent Flowrate (kg/hr)	Flue Gas Flowrate (Sm^3/hr)	Steam Flowrate (kg/hr)	CO_2 Capture Percent Estimate
1A	55,300	31,800	5,500	86.1
1B	54,200	36,000	7,200	88.0
1C	92,100	37,300	7,400	92.5
1D	81,400	43,800	7,700	84.9
1E	81,300	45,900	8,900	93.4
1F	120,800	53,700	10,700	92.2
1G	88,900	56,500	12,100	90.4
1H	90,300	57,100	9,800	82.7

When obtaining data for test cases 1A-1B, it was noted that the CO_2 capture percentage was substantially lower than the model predictions. This discrepancy was attributed to solvent maldistribution, or uneven flow through the packing, in the RFCC stripper column, resulting in inefficient performance of the column. This stripper was designed to operate at a solvent flowrate of approximately 200,000 kg/hr, or almost four times higher than the solvent flowrate in cases 1A-1B. Therefore, the lean solvent loading for these test runs was substantially higher than

that predicted by the model, and the CO_2 capture percentage lower. This issue was addressed by dividing each subsequent test run into two intervals with distinct operating goals, so that two data sets were collected for test runs 1C-1H. First, the test was executed with the value of steam flowrate specified in the original test matrix. Upon achieving the steady-state, the steam flowrate was manipulated to match the estimated value of CO_2 capture. Parity plots for the model prediction of CO_2 capture percentage in the absorber and steam requirement in the stripper are given in Figure 3.

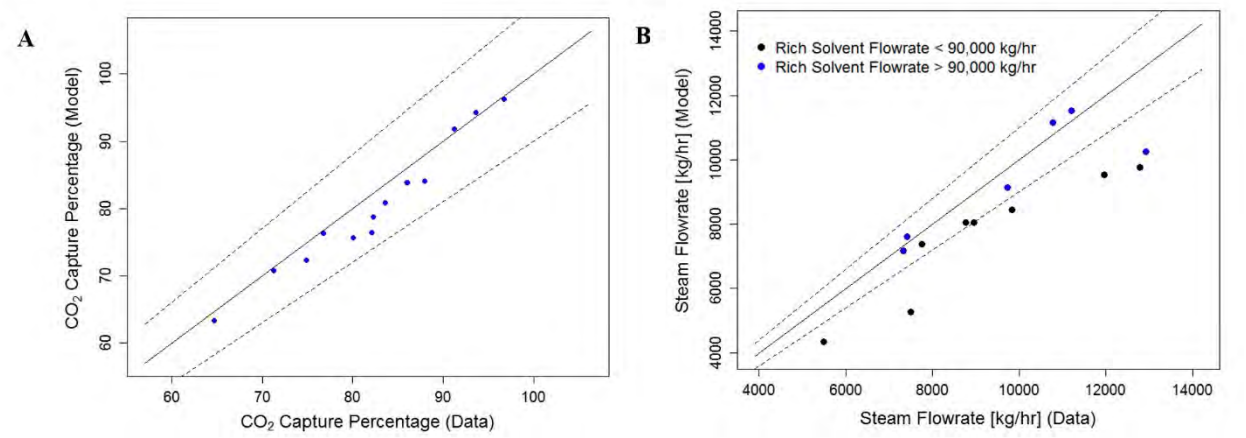

Figure 3. Parity plots for (A) CO_2 capture percentage and (B) steam flowrate required for test runs performed in Phase 1. Dashed lines represent ±10% error.

The original deterministic model, or the model in which all parameters are fixed as point values, predicts the CO_2 capture with a range of ±10% error for all test runs. The average error for CO_2 capture percentage is -2.51 ± 2.29%, with the negative error indicating that the model generally underpredicts the data. The model predicts stripper steam requirement with an average error of -10.83 ± 10.82%, although the error is notably higher for cases in which the solvent flowrate is below 90,000 kg/hr (average error of -16.43 ± 8.49%) than when it is higher than 90,000 kg/hr (average error of -3.67 ± 9.29%). This discrepancy is likely due to liquid maldistribution in the stripper column, as discussed previously. The results obtained in the first phase of the test campaign demonstrated that the initial process model was sufficiently accurate to proceed with the sequential experimental design in subsequent stages.

3.3 Phases 2-3

During the test campaign, data for Phases 2-3 were collected simultaneously and used to update the model parameter distributions through Bayesian inference. The majority of the data for Phase 2 were actually collected after those for Phase 3 due to scheduling convenience. The optimization problem described in Eq. 5 was implemented separately for the 8 and 10 vol% CO_2 cases, and used to develop the test matrix given in Table 3.

Table 3. Test matrix for Phase 2 design of MEA test campaign at TCM

Test	Rich Solvent Flowrate (kg/hr)	Flue Gas Flowrate (Sm^3/hr)	Steam Flowrate (kg/hr)	CO_2 in Flue Gas (vol%)
2A	***107,800***	***40,800***	***10,700***	***10***
2B	107,100	44,100	10,300	8
2C	107,100	44,100	12,500	8
2D	***97,400***	***49,000***	***11,400***	***8***
2E	87,700	53,900	10,300	8
2F	87,700	53,900	12,500	8
2G	97,000	44,900	11,800	10
2H	97,000	44,900	9,600	10
2I	118,600	36,700	9,600	10

In Table 3, the optimal points determined from solving separate optimization problems (Eq. 5) for the $y_{CO_2} = 0.08$ (2A) and $y_{CO_2} = 0.10$ (2D) cases are highlighted, and additional test points were selected by perturbing the variables

by ± 10% from the optimal values. Parity plots for the model prediction of CO_2 capture percentage in the absorber and steam requirement in the stripper are given in Fig. 4.

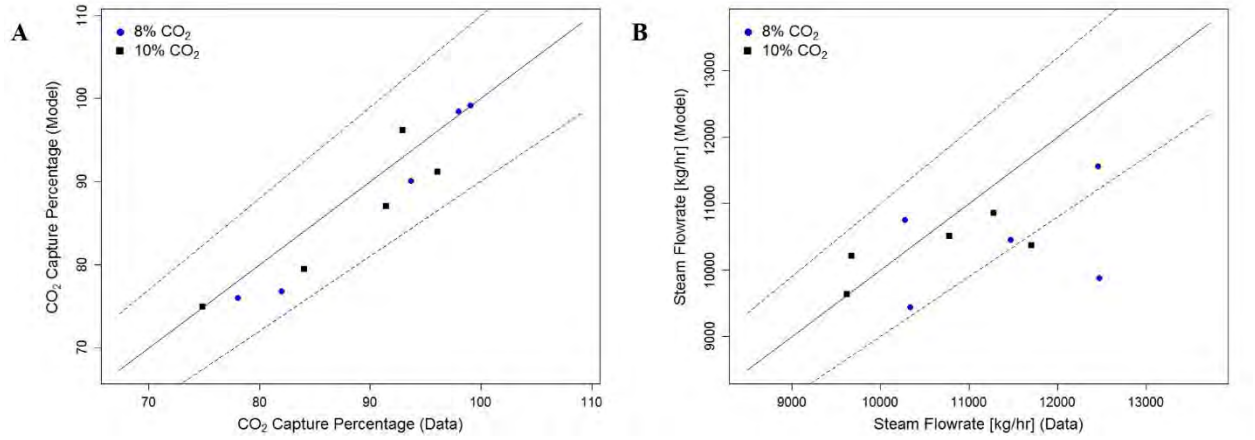

Fig. 4. Parity plots for (A) CO_2 capture percentage and (B) steam flowrate required for test runs performed in Phase 2. Dashed lines represent ±10% error.

As shown in Figure 4, the accuracy of the model for the data collected in Phase 2 is comparable to that in Phase 1. The average percent error for the CO_2 capture prediction and steam requirement prediction is -2.40 ± 3.27% and -5.28 ± 8.00%, respectively. The percentage error for the steam requirement prediction is substantially lower for the data collected in Phase 2 than in Phase 1 due to the absence of test runs with very low (< 85,000 kg/hr) solvent flowrate. Therefore, the model was shown to be sufficiently accurate for the region of the input space likely to be economically optimal.

Phase 3 of the test campaign was focused on data collection in regions where the stochastic model predicts relatively high uncertainty for the absorber CO_2 capture percentage. These data, along with those collected in Phase 2, were used to update the mass transfer and interfacial area model parameter distributions. The test matrix for Phase 3 is shown in Table 4.

Table 4. Test matrix for Phase 3 design of MEA test campaign at TCM (First Iteration)

Test	Rich Solvent Flowrate (kg/hr)	Flue Gas Flowrate (Sm^3/hr)	Steam Flowrate (kg/hr)	CO_2 in Flue Gas (vol%)	CO_2 Capture Percent Estimate
3A	133,900	62,600	11,600	8	85.9
3B	115,400	62,300	10,700	8	81.3
3C	111,900	59,100	11,100	8	89.3
3D	120,200	56,100	10,100	8	84.1
3E	119,500	55,000	9,900	8	83.6
3F	81,500	51,100	10,300	8	90.1
3G	57,500	42,500	8,700	8	81.8
3H	39,300	30,800	6,600	8	80.0
3I	48,300	30,400	8,200	10	80.0
3J	85,600	33,800	7,500	10	85.5
3K	103,100	43,000	9,200	10	82.2

The data collected in Table 4, along with case 2A from Table 3 were used in the Bayesian inference procedure based on Eq. 2. In this work, the parameters contained in $\boldsymbol{\theta}$ included the leading coefficients for the interfacial area and mass transfer submodels developed in previous work [3], and the parameters contained in $\boldsymbol{\theta}^*$ included the thermodynamic model parameters for which distributions were estimated in previous work [2]. Upon obtaining the updated parameter distributions, the refined stochastic model was used to develop a new test matrix, shown in Table 5.

Table 5. Test matrix for Phase 3 design of MEA test campaign at TCM (Second Iteration)

Test	Rich Solvent Flowrate (kg/hr)	Flue Gas Flowrate (Sm^3/hr)	Steam Flowrate (kg/hr)	CO_2 in Flue Gas (vol%)	CO_2 Capture Percent Estimate
3L	96,100	41,300	9,900	10	89.4
3M	94,000	43,500	11,000	10	88.8
3N	119,500	46,500	10,900	10	86.4
3O	150,300	48,200	11,500	10	85.2
3P	130,200	58,400	10,500	8	81.9
3Q	99,900	53,400	10,500	8	90.8
3R	80,800	51,600	12,900	8	88.3
3S	127,500	50,800	10,000	8	88.7
3T	121,200	49,300	9,200	8	85.2
3U	98,200	47,800	8,400	8	81.6
3V	125,500	47,000	9,900	8	94.2

The data collected from the test plan given in Table 5, along with cases 2B-2I in Table 3, were used in a second iteration of the SDoE procedure to update the parameter distributions again. Parity plots for the model prediction of CO_2 capture percentage in the absorber and steam requirement in the stripper for all data collected in both iterations of Phase 3 are given in Figure 5.

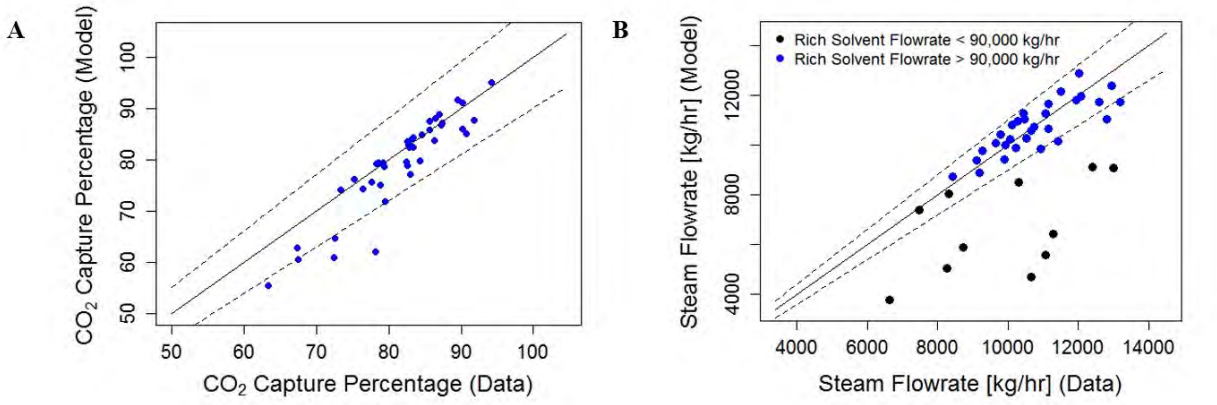

Figure 5. Parity plots for (A) CO_2 capture percentage and (B) steam flowrate required for test runs performed in Phase 3. Dashed lines represent ±10% error.

The average percentage error values for the model predictions of the data collected in Phase 3 are -2.91 ± 5.27% for CO_2 capture percentage and -8.53 ± 17.20% for the steam flowrate. As with the data collected in Phase 1, there is greater discrepancy in the stripper model for cases in which solvent flowrate is low; the average percentage error in the steam requirement is -31.05 ± 17.81% for cases in which the solvent flowrate is below 90,000 kg/hr and -0.27 ± 6.04% when it exceeds 90,000 kg/hr. As previously suggested, the underprediction in steam flowrate is likely due to operation inefficiency of the RFCC stripper caused by solvent maldistribution, as the process is operated at much lower solvent flowrate than the stripper design condition.

The probability density functions of the mass transfer and interfacial area parameters, including the prior and posterior distributions obtained after each SDoE iteration, are given in Fig. 6.

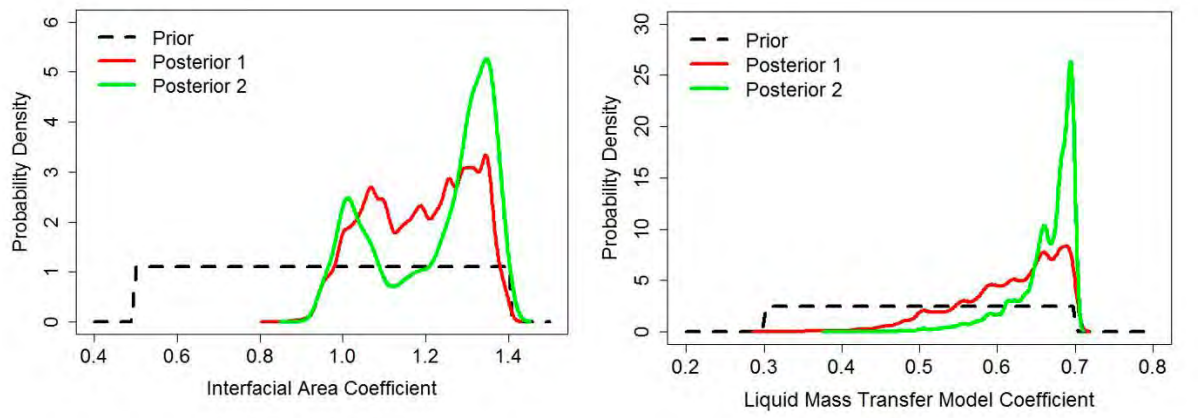

Figure 6. Comparison of prior and posterior distributions of interfacial area and mass transfer model parameters

Uniform prior distributions were initially chosen for the two parameters. The parameter space of plausible values was significantly reduced after incorporating the experimental data from the first iteration of SDoE into the stochastic model through Bayesian inference, with less reduction in the second round of SDoE. The effect of SDoE on model uncertainty reduction is more apparent when considering the model output, namely the CO_2 capture percent in the absorber. The effect of the first iteration of SDoE on reducing model prediction of uncertainty in CO_2 capture percentage is shown in Fig. 7.

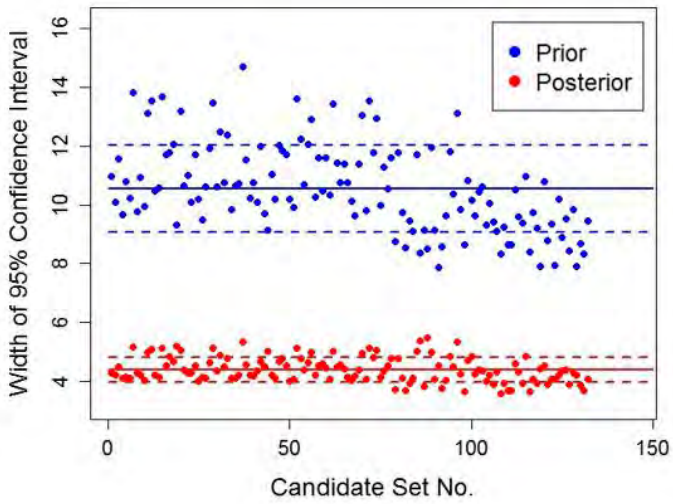

Figure 7. Effect of first round of Bayesian inference on CO_2 capture prediction confidence interval for individual points in candidate set

For the stochastic model prediction using the uniform prior distributions, the average confidence interval width for the CO_2 capture percentage was approximately 10.5% (denoted in Figure 7 by solid line) with standard deviation 1.5% (denoted by dashed lines). For the stochastic model prediction with the posterior distribution obtained after the first iteration of SDoE, the average confidence interval width was approximately 4.4% with standard deviation 0.4%. No further significant reduction in the predicted uncertainty in CO_2 capture percentage was demonstrated in the second round of SDoE. In Figure 7, the candidate set number refers to an index representing a unique combination of input variables (liquid and gas flowrates, CO_2 loading, and CO_2 fraction in flue gas). The percentage of reduction in uncertainty for a given point ($\boldsymbol{x^{(i)}}$) in the candidate set is calculated as:

$$Percent\ Reduction = 100\% \times \frac{[CI|_{x^{(i)}}]_{initial} - [CI|_{x^{(i)}}]_{final}}{[CI|_{x^{(i)}}]_{initial}} \quad (6)$$

where $[CI|_{x^{(i)}}]_{initial}$ and $[CI|_{x^{(i)}}]_{final}$ represent the 95% confidence intervals in the model prediction of CO_2 capture percentage before and after updating the parameter distributions through Bayesian inference, respectively. For the entire candidate set, the average percent reduction in the uncertainty is 58.0 ± 4.7%, which is comparable to the reduction in the previous SDoE-based test campaign executed at NCCC [5,6]. As the ability of the SDoE methodology to reduce parametric uncertainty in a process model for an aqueous MEA system has been demonstrated in multiple campaigns, it may be considered a promising technique for designing future test campaigns to effectively increase fundamental understanding of novel CO_2 capture systems.

4. Conclusions and Future Work

In summary, a sequential design of experiments methodology was implemented for executing a test campaign for aqueous MEA at TCM, guiding collection of process data to refine the parameter distributions in the stochastic process model. This resulted in an average reduction of around 58% in the uncertainty in the prediction of CO_2 capture percentage. The deterministic model, or the model without parameter uncertainty, also predicted the plant performance accurately, with an average error in percentage of CO_2 capture of -2.74 ± 4.47% for the first three phases and an average error of -8.52 ± 14.85% for the reboiler steam requirement. An exception to the accurate performance of the model is for data collected under impractical operating conditions (low solvent circulation rate, in which solvent maldistribution in the stripper column was noted). For data collected when the system was operated with rich solvent flowrate below 90,000 kg/hr, the percent error in the reboiler steam prediction was -23.92 ± 15.70%. However, the percentage error in the steam prediction is -1.17 ± 6.65% for data collected when the rich solvent flowrate was above 90,000 kg/hr. The insights gained during the execution of SDoE guided the development of a new SDoE module with capability for straightforward implementation of the aims used in this experiment [16] that has been implemented in the Framework for Optimization, Quantification of Uncertainty, and Surrogates (FOQUS). This is available as part of the aforementioned CCSI Toolset and will enable the SDoE process to be implemented in a more streamlined manner in future applications. In planned future work, the CCSI^2 team will apply the SDoE methodology to novel CO_2 capture technologies with the primary goal of refining initial process models by reducing their uncertainty, and thus the inherent risk associated with preliminary models of new processes, through guided data collection.

Disclaimer

This project was funded by the United States Department of Energy, National Energy Technology Laboratory, in part, through a site support contract. Neither the United States Government nor any agency thereof, nor any of their employees, nor the support contractor, nor any of their employees, makes any warranty, express or implied, or assumes any legal liability or responsibility for the accuracy, completeness, or usefulness of any information, apparatus, product, or process disclosed, or represents that its use would not infringe privately owned rights. Reference herein to any specific commercial product, process, or service by trade name, trademark, manufacturer, or otherwise does not necessarily constitute or imply its endorsement, recommendation, or favoring by the United States Government or any agency thereof. The views and opinions of authors expressed herein do not necessarily state or reflect those of the United States Government or any agency thereof.

Acknowledgement

The authors gratefully acknowledge the staff of TCM DA, Gassnova, Equinor, Shell and Total for their contribution and work at the TCM DA facility. The authors also gratefully acknowledge Gassnova, Equinor, Shell, and Total as the owners of TCM DA for their financial support and contributions.

References

[1] Morgan JC, Bhattacharyya D, Tong C, Miller DC. Uncertainty quantification of property models: methodology and its application to CO_2-loaded aqueous MEA solutions. AIChE J 2015;61(6):1822-39.

[2] Morgan JC, Chinen AS, Omell B, Bhattacharyya D, Tong C, Miller DC. Thermodynamic modeling and uncertainty quantification of CO2-loaded aqueous MEA solutions. Chem Eng Sci 2017;168:309-24.

[3] Chinen AS, Morgan JC, Omell B, Bhattacharyya D, Tong C, Miller DC. Development of a rigorous modeling framework for solvent-based CO_2 capture. Part 1: hydraulic and mass transfer models and their uncertainty quantification. Ind Eng Chem Res 2018;57:10448-63.

[4] Morgan JC, Chinen AS, Omell B, Bhattacharyya D, Tong C, Miller DC. Development of a rigorous modeling framework for solvent-based CO_2 capture. Part 2: steady-state validation and uncertainty quantification with pilot plant data. Ind Eng Chem Res 2018;57:10464-81.
[5] Soepyan B, Anderson-Cook CM, Morgan JC, Tong CH, Bhattacharyya D, Omell BP, Matuszewski MS, Bhat KS, Zamarripa MA, Eslick JC, Kress JD, Gattiker JR, Russell CS, Ng B, Ou JC, Miller DC. Sequential design of experiments to maximize learning from carbon capture pilot plant testing. Comput Aided Chem Eng 2018;44:283-8.
[6] Morgan JC, Chinen AS, Anderson-Cook C, Tong C, Carroll J, Saha C, Omell B, Bhattacharyya D, Matuszewski M, Bhat KS, Miller DC. Development of a framework for sequential Bayesian design of experiments: application to a pilot-scale solvent-based CO_2 capture process. App Energy 2020;262:114533.
[7] Brigman N, Shah MI, Falk-Pedersen O, Cents T, Smith V, De Cazenove T, Morken AK, Hvidsten OA, Chhaganlal M, Feste JK, Lombardo G, Bade OM, Knudsen J, Subramoney SC, Fostås BF, de Koeijer G, Hamborg ES. Results of amine plant operations from 30 wt% to 40 wt% aqueous MEA testing at the CO_2 Technology Centre Mongstad. Energy Procedia 2014;63:6012-22.
[8] Gjernes E, Pedersen S, Cents T, Watson G, Fostås BF, Shah MI, Lombardo G, Desvignes C, Flø NE, Morken AK, De Cazenove T, Faramarzi L, Hamborg ES. Results from 30 wt% MEA performance testing at the CO_2 Technology Centre Mongstad. Energy Procedia 2017;114:1146-57.
[9] Faramarzi L, Thimsen D, Hume S, Maxon A, Watson G, Pedersen S, Gjernes E, Fostås BF, Lombardo G, Cents T, Morken AK, Shah MI, De Cazenove T, Hamborg ES. Results from MEA testing at the CO_2 Technology Centre Mongstad: verification of baseline results in 2015. Energy Procedia 2017;114:1128-45.
[10] Hamborg ES, Smith V, Cents T, Brigman N, Falk-Pedersen O, De Cazenove T, Chhaganlal M, Feste JK, Ullestad Ø, Ulvatn H, Gorset O, Askestad I, Gram LK, Fostås BF, Shah MI, Maxson A, Thimsen D. Results from MEA testing at CO_2 Technology Centre Mongstad. Part II: Verification of baseline results. Energy Procedia 2014;63:5994-6011.
[11] Montañés RM, Flø NE, Nord LO. Dynamic process model validation and control of the amine plant at CO_2 Technology Centre Mongstad. Energies 2017;10:1527.
[12] Bui M, Flø NE, De Cazenove T, Mac Dowell N. Demonstrating flexible operation of the Technology Centre Mongstad (TCM) CO_2 capture plant. Int J Greenh Gas Con 2020;262:114533.
[13] Myers RH, Montgomery DC, Anderson-Cook CM. Practical design optimality. In: Response surface methodology: process and product optimization using design experiments. 4th ed. New York: Wiley Plus; 2016. p. 467-74.
[14] Myers RH, Montgomery DC, Anderson-Cook CM. The one-half fraction of the 2^k design. In: Response surface methodology: process and product optimization using designed experiments. 4th ed. New York: Wiley Plus; 2016. p. 162-174.
[15] Johnson ME, Moore LM, Ylvisaker D. Minimax and maximin distance designs. J Stat Plan Infer 1990;26:131-48.
[16] Lu L, Anderson-Cook CM, Ahmed T. Non-uniform space-filling designs. J Qual Tech 2021; to appear.

CATCHING OUR FUTURE

Cost Reduction Study for MEA based CCGT Post-Combustion CO_2 Capture at Technology Center Mongstad

(2021)

15th International Conference on Greenhouse Gas Control Technologies, GHGT-15

15th 18th March 2021 Abu Dhabi, UAE

Cost Reduction Study for MEA based CCGT Post-Combustion CO_2 Capture at Technology Center Mongstad

Muhammad Ismail Shah[a], Eirik Falck da Silva[b,*], Erik Gjernes[c] and Knut Ingvar Åsen[d]

[a]*Technology Centre Mongstad, 5954 Mongstad, Norway*
[b]*Stavanger Research Center, TOTAL EP Norge AS, 4029 Stavanger, Norway*
[c]*Gassnova SF, Dokkvegen 10, 3920 Porsgrunn, Norway*
[d]*Equinor ASA, PO Box 8500, 4035 Stavanger, Norway*

Abstract

A campaign was carried out by Technology Center Mongstad (TCM) and its owners in the amine capture plant to study various cost saving operating options relevant for combined cycle gas turbine plants. The owners chose MEA as solvent for this test because it is a well-studied solvent system with no commercial constraints regarding sharing of data. Learnings obtained from MEA studies are also expected to be of relevance for other solvent systems.

During this campaign the main focus was on thermal energy optimization at different flue gas flow rates through the absorber column and MEA emissions, with target for reduced CAPEX and OPEX. During the campaign, new options such as a rich solvent bypass to stripper overhead and higher concentration of MEA (up to 38wt%) were tested. Tests were carried out to identify plant configurations and process parameters with the potential for CAPEX and OPEX reduction in a post-combustion carbon capture plant. Significant cost of CO_2 avoided reductions were achieved compared to the previous TCM campaigns for MEA.

Keywords: CO_2 Absorption; Cost Reduction; MEA

1. Introduction

TCM is located next to the Equinor refinery in Mongstad (outside Bergen, Norway) which is the source of the two types of flue gases supplied to TCM. These sources are the combined cycle gas turbine (CCGT) based heat and power plant (CHP) and residual fluid catalytic cracker (RFCC). The owners of TCM started their third monoethanolamine (MEA) test campaign (MEA-3) in June 2017 and continued with MEA-4 and MEA-5 that lasted until October 2018. MEA-3, MEA-4 and MEA-5 have been the most significant collaboration campaigns that TCM has conducted since its inauguration in 2012. The large number of industrial, research and academic participants involved in these campaigns have enriched the projects and ensured that the results will serve a broad range of audiences.

A sub-campaign on cost reduction during MEA-5 was carried out by TCM owners in this capture plant to study various cost saving options. MEA was chosen as solvent for this test because it is a well-studied solvent system with

* Corresponding author. Tel: +47 948 45 691, *E-mail address:* eirik.silva@total.com

no commercial constraints regarding sharing of data. This work follows previous work carried out on the same subject at TCM [1].

2. Test Campaign and Results

The TCM amine plant is shown in Figure 1. The plant has been in operation since 2012 carrying out tests on a number of proprietary and non-proprietary solvent systems. A recent modification to the plant is the addition of a rich solvent partial-bypass upstream of the lean-rich amine heat exchanger to the stripper top. This is intended to improve the energy performance of the plant. A noteworthy feature of the plant is that there are three different feed locations for the lean solvent to the absorber. This allows for testing at different packing height for CO_2 absorption (12m, 18m, and 24m), as shown in yellow in the Figure. Another important feature is that the plant has two strippers with dedicated reboilers, the Combined Heat and Power (CHP) stripper suited for stripping of lower amounts of CO_2 and the Residual Fluidized Catalytic Cracker (RFCC) stripper suited for larger volumes of CO_2. Only CHP flue gas was utilized in the present campaign.

The purpose of the present campaign has been to explore different modes of operation with cost reduction potential. Such as higher flue gas throughput, lower packing height, more concentrated solvent and higher capture rate. Simple configurations such as operating with only one water wash section and higher flue gas inlet temperatures were also investigated. Table 1 summarizes the phases A to F of the test campaign.

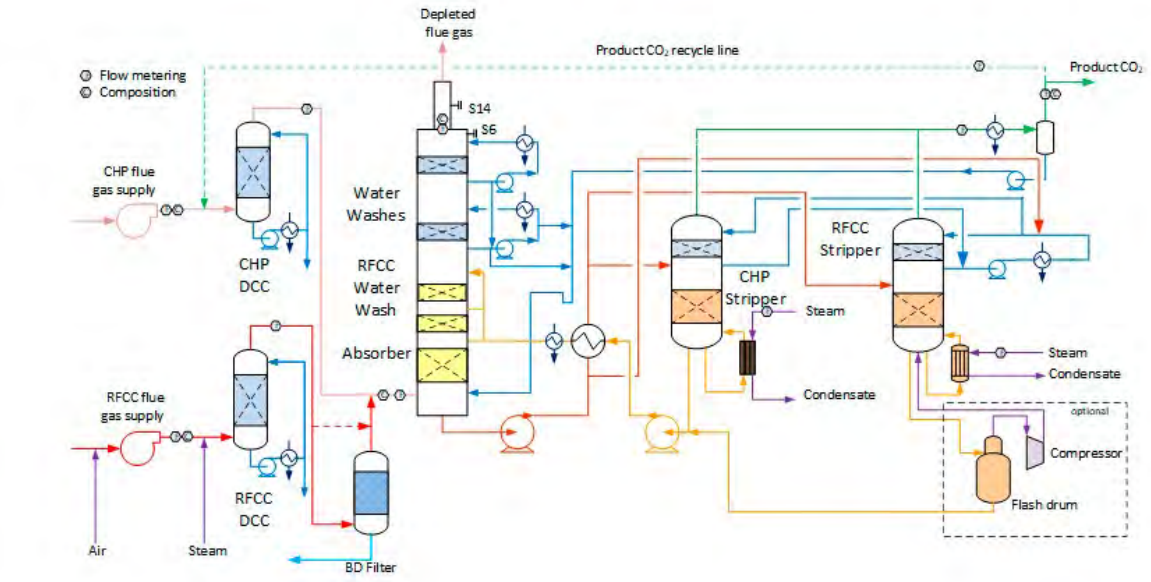

Fig. 1. A process flow diagram of the TCM Amine plant. The diagram illustrates the two different flue gas configurations (CHP and RFCC) as well as the available strippers. The CHP flue gas can be further enriched with CO_2 from a CO_2 recycle line, and the RFCC flue gas can be diluted with air to reach a target CO_2 concentration.

Table 1. Phases of the campaign.

Condition	Phase A	Phase B	Phase C	Phase D	Phase E	Phase F
Flue gas flow [Sm^3/h]	40-47,000	50,000	50,000	67,000	67,000	59,000
Absorber packing height [m]	18	18	18	24	24	18
Stripper	CHP	CHP	CHP	RFCC	RFCC	RFCC
CO_2 capture rate [%][1]	85 - 96	90 - 91	89 - 93	95 - 99	98 - 99	90-91
Optimal SRD [GJ/ton CO_2][2]	**3.8** (85)	**3.6** (91)	**3.6** (91)	**3.7** (97)	**4.0** (98)	**3.7** (91)
MEA [wt%]	32	37	34 - 37	35 -36	35 -37	36 -38
CO_2 conc, wet [vol %]	3.6 - 4.2	4.0 – 4.2	3.8 – 4.2	4.0 – 4.2	3.9 – 4.2	4.1 – 4.2
Absorber water wash stages	2	1	1	1/2[3]	1	1
L/G [kg/Sm^3][4]	0.97 - 1.14	0.92 - 1.54	1.13 – 1.74	0.95 – 1.88	1.10 – 1,54	1.12 – 1.47
Flue gas temp [°C]	30	30	45	30	45	30
Rich solvent bypass [%]	0	20	20	20	20	20
Lean solvent temp [°C]	41.2	54.9	54.5	45.0	40.0	44.4
MEA emission [ppmv]	<1	<1	0.6	1.5	2.1	1.1

1: Capture rate is based on method 4 as described in the text. 2: SRD is Specific Reboiler Duty 3 as described in the text. Associated capture rate in parenthesis. 3: Second water wash stage was partially operated to manage emissions. 4: L/G is the ratio of lean solvent flow to flue gas flow into the absorber.

The rich solvent bypass was in operation during all phases of the campaign except phase A. Flue gas CO_2 concentrations varied between 3.6 % and 4.2% during the campaign. The variations in CO_2 concentration were achieved by use of a recycle. Phase A was operated at 32 wt% MEA and was investigating effect of CO_2 concentration and flue gas flow.

Phase A was mainly intended to validate previous work and will not be discussed further. The rest of the cases were operated at MEA concentration up to 38 wt% and with the target of having only the lower absorber water wash section in operation.

Phase B and C were operated at 50,000 Sm^3/h, 18-meter absorber packing, CHP stripper and with flue gas temperature out the absorber of 30 and 45°C, respectively. Operating with higher flue gas temperature could offer potential savings since this will enable the use of a smaller Direct Contact Cooler.

During Phase D and E this temperature variation was intended to be repeated at flue gas flow of 67,000 Sm^3/h, 24-meter absorber packing and RFCC stripper in operation. The flue gas flow of 67,000 Sm^3/h rate is the highest practically possible operating point at TCM and represents 113% of design capacity.

Finally, Phase F was operated at 18-meter absorber packing and 59,000 Sm^3/h flue gas flow at 36-38wt% MEA.

The energy efficiency of the capture process is given by the Specific reboiler duty (SRD), this is defined as the heat delivered to the reboiler from the steam system divided by the amount of captured CO_2:

$$SRD = \frac{\Delta H m_{steam}}{m_{CO2\ cap}} \quad (1)$$

where m_{steam} is the steam flow to the reboiler heat exchanger. ΔH is the enthalpy difference between steam and condensate calculated from measured temperature and pressure, see also reboiler, steam and condensate in Figure 1. Steam pressure is typical around 2.5 barg and up to 160 °C for the tests reported in this paper. CO_2 capture rate is the mass fraction of CO_2 being captured out of the amount of CO_2 flowing into the absorber. The amount of captured CO_2 can be derived from the CO_2 product flow out of the stripper or from difference in CO_2 flow in and out of the absorber. SRD and capture rate are presented utilizing both methods below, while the economical assessment is based on difference in and out of the absorber such that the results can be compared to previous work [1]. This method is in the present paper referred to as "SRD 3". SRD based on the product flow out of the stripper is referred to as "SRD 1". The reported results are two-hour averages within a test slot that lasts more than 6 hours. Typically, one liquid solvent sample is taken for each test point.

In the present paper we report CO_2 capture rates based on two methods, Capture Method 1 and Capture Method 4. Method 1 is based on the ratio between the stripper product flow and the absorber inlet flow, while Method 4 is based on the mass balance over the absorber [2].

TCM is equipped with multiple flue gas analyzers and flow meters for each of the main three gas streams. Table 2 shows the ones selected for the current analysis. Water is calculated assuming saturated conditions based on pressure and temperature. Flow out of the absorber is calculated from measured flow into the absorber assuming conservation of all components in and out of the absorber except water and CO_2. Finally, it is assumed that product gas out of the stripper is only CO_2 and water.

Table 2. Measurement of gas flows.

Unit	Property	Method/Principle
Absorber in	H_2O	Calculated from p and T
	CO_2	Infrared spectroscopy (IR)
	Flow	Ultrasonic flow meter
Absorber out	H_2O	Calculated from p and T
	CO_2	Infrared spectroscopy (IR)
	Flow	Calculated from absorber in flow and composition in and out of absorber
Product flow	H_2O	Calculated from p and T
	CO_2	Calculated as: 100 - H_2O
	Flow	Coriolis flow meter

In Figure 2 SRD and capture rate vs. L/G for phase B is shown. At TCM optimum SRD is obtained by varying the lean flow rate (and thereby the L/G) and adjusting the reboiler duty at each solvent circulation point to maintain the required/targeted capture rate. The optimum SRD achieved here was 3.6 GJ/ton CO_2 (based on SRD 3).

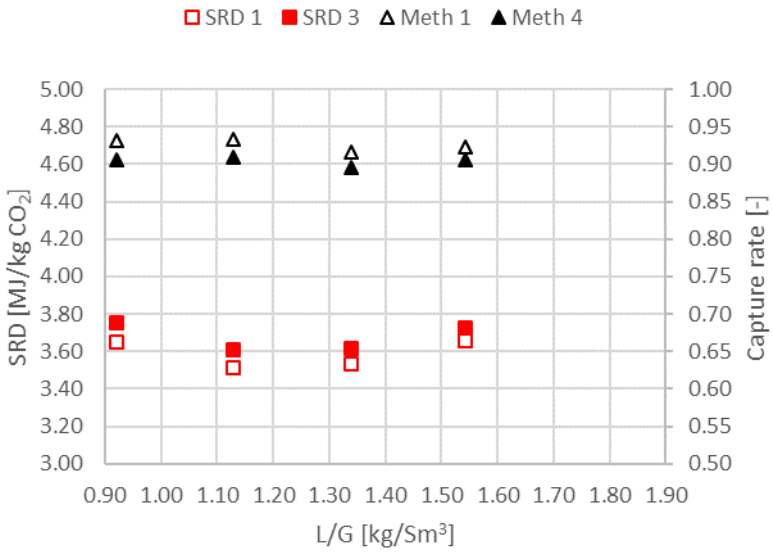

Fig. 2 SRD (left y-axis) and capture rate (right y-axis) for phase B as function of liquid to flue gas ratio (flue gas 50,000 Sm3/h).

One of the best cases demonstrated is "B3-rep" (at L/G of 1.13). The capture rate for this case is a bit above 90%, with SRD of 3.6 GJ/tCO_2 with 18m packing height, 37 wt% MEA, one water wash and MEA emissions below 1 ppm. Flue gas flow is 50,000 Sm^3/h and liquid to gas ratio (L/G) for "B3-rep" is about 1.13 kg solvent/Sm^3 of flue gas. This can result in significant reduction of CAPEX and OPEX, compared to the MEA baseline.

In Figure 3 SRD and capture vs. L/G for phase D is shown. During Phase D 97% CO_2 capture at an SRD of 3.7 GJ/ton CO_2 were achieved. This SRD is perhaps lower than that would have been expected for a very high capture rate. The point at L/G of 1.38 has a high SRD, this is due to high levels of steam being utilized to achieve high capture rates. With Method 4 the capture rate was 99%, with Method 1 it was slightly over a 100% (due to accuracy limitations in calculation). Since the number is over 100% it is not visible in the plot.

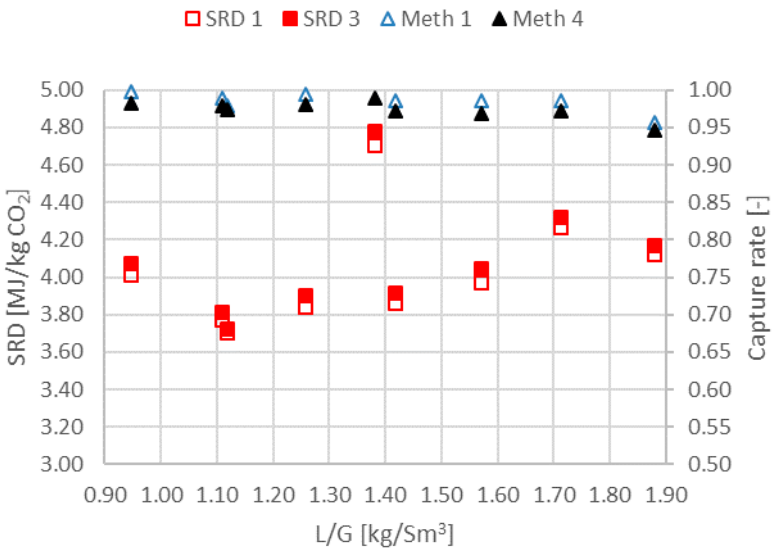

Fig. 3. SRD (left y-axis) and capture rate (right y-axis) for phase D as function of liquid to flue gas ratio (flue gas 67,000 Sm3/h).

Higher flue gas capacity tests at 67,000 Sm^3/h resulted in high amine emission, which is partly due to mechanical entrainment and partly due to only one water wash section being in operation. However high solvent entrainment can be potentially reduced by improving the absorber design by installing a more efficient demister at appropriate location in the absorber. Very high CO_2 capture rate of almost 99% was demonstrated with SRD of 3.8 GJ/tCO_2 with 24 m absorption bed and 67,000 Sm3/h of flue gas capacity. The increase in SRD is about 6% when the capture rate increases from 90% to 99%, however the comparison is not fair as the plant capacity and configuration is not similar in the two cases.

During phase E higher flue gas capacity tests at 67,000 Sm^3/h and flue gas temperature of 45°C resulted in a relatively high SRD and most importantly higher MEA emission as expected.

SRD and capture results from Phase F are shown in Figure 4. Case F2 with 3.8 GJ/ton CO_2 and 90% capture rate was selected for further assessment in the next section.

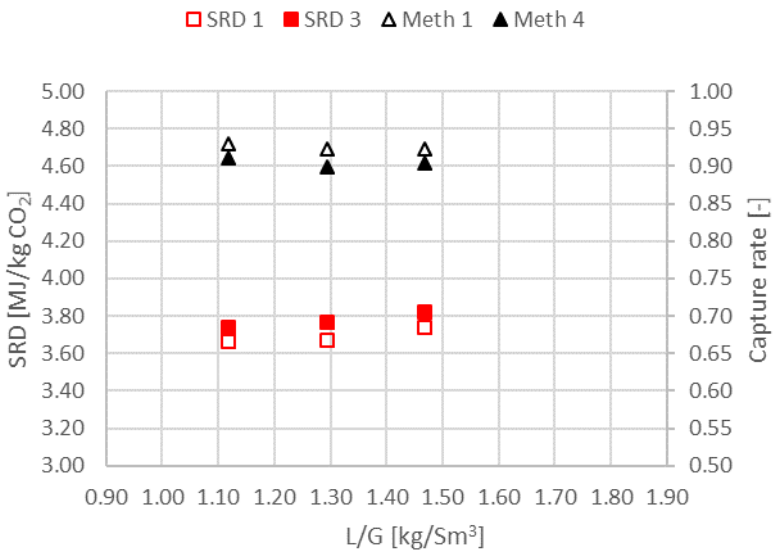

Fig. 4. SRD (left y-axis) and capture rate (right y-axis) for phase F as function of liquid to flue gas ratio (flue gas 59,000 Sm3/h).

In the present campaign the plant was mostly operated with 37 wt% MEA. There have been some relatively short campaigns at TCM in the past where the plant has operated with a concentration slightly higher than 40 wt% MEA [1]. From an energy performance perspective 40 wt% is expected to give better results. There is however a concern that solvent degradation will be more severe for 40 wt% MEA. Degradation can besides being a problem in itself also impact corrosion in the plant. 35 wt% MEA is what TCM is currently comfortable with operating, however long-term continuous test with 37-38 wt% MEA needs to be conducted to better understand degradation, emission and energy performance of the solvent.

Table 3 summarizes the selected cases for economical evaluation along with the reference case named MEA 3 (9-4) [1]. Stripper pressures were maintained at 0.9 barg for all cases. The MEA-3 and B3-rep were operated with CHP stripper while F2 and D3-rep utilized the RFCC stripper. Liquid sample for case D3-rep is taken about 1 hour outside the 2 hours being averaged, but still within the test period.

Table 3. Selected cases for economical evaluation [1-3]

#	Abs. pack [m]	MEA[1] [wt%]	Flue gas × 1000 [Sm^3/h]	L/G [kg/Sm^3]	Anti-foam [-]	Stripper bottom temp [°C]	Lean loading [mol/mol]	SRD [GJ/ton CO_2]	CO_2 Capture [%]
MEA-1	24	~ 30	47	1.17	No	119.3	0.23	4.1	~ 85
MEA-2	24	31/30	59	1	Yes	121.0	0.21	3.6	86
MEA-3	18	43/40	51.0	0.98	No	121.7	0.25	3.6	86
F2	18	36/34	59.0	1.29	No	121.0	0.26	3.8	90
B3-rep	18	37/35	50.0	1.13	No	121.4	0.24	3.6	91
D3-rep	24	36/34	67.0	1.12	No	122.5	0.21	3.7	97

1: Number given first is on MEA-water basis, second number is on MEA-water-CO_2 basis.

3. Economic Evaluation

The economic evaluations of power and capture plants in this paper is based on standard "Cost of Electricity" (COE) and "Cost of CO_2 avoided" metrics. These calculations are based on aligned and standardized estimates and assumptions on technology process performance such as energy efficiency, CO_2 generation and capture rates, see e.g. [4]. Cost estimates include CAPEX, operations and maintenance (O&M) including fuel and a set of general price and rate of return assumptions. For each case below, a complete sized capture plant equipment list is established. Aspen In-Plant Cost Estimator (IPCE) V9 is used to estimate equipment cost. Equipment installation factors are then used to estimate total installed costs. Aligned with known projects, including contingency, 30% added to the Aspen Equipment cost and average installation factor of around 5.5. The OPEX can be split in annual cost (of CAPEX), power loss, maintenance, chemicals and fixed operating costs. The gas fired power plant specific cost and performance is based on GTPro simulation of a GE 9HA CCGT plant. 25% contingency is added to the estimated GTPro CCGT CAPEX number. All calculations are furthermore carried out at:

- normalized, per unit (kWh) output from the base industrial (power) plant
- pretax, pre-financing basis
- annual cost basis, applying a capital charge factor corresponding to a standard discount factor and project time horizon

Cost of CO_2 avoided ($/ton CO_2) is calculated according to Equation below and is based on cost of electricity (COE) and CO_2 emission per kWh (CO_2 emission) for a power plant with capture (cap) and without CO_2 capture (no cap).

$$Cost\ of\ CO_2\ avoided = \frac{COE_{cap} - COE_{no\ cap}}{CO_2\ emission_{no\ cap} - CO_2\ emission_{cap}} \quad (2)$$

The calculated cost of CO_2 avoided implicitly accounts for the capture systems' own energy demand and its inherent CO_2 emissions. The following economic assumptions are applied:

- Fuel gas price: 0.1875 US $/Sm^3$

• On-stream hours: 7884 (90 %)
• Discount rate: 5 % real (pretax)
• Time horizon: 30 years

These were chosen to be consistent with a previous economical study [1].

This paper will only report percentage cost reduction and no absolute cost numbers. The main reasons are that the absolute numbers are not useful for the purpose of this work and are partially confidential. In this work one consistent method and one consistent set of assumptions are used for calculating the cost, which is important for a fair comparison.

The experiments targeted lowest possible absorber packing height, lowest possible L/G and SRD while maximizing the captured CO_2 and capture rate. In Table 4 below the experimental data for the selected cases are scaled to a full-scale design at a fixed inlet CO_2 flow of 150 tonnes CO_2/h and measured capture rate case by case.

In order to compare on the same basis in the cost assessment, the CO_2 inlet concentrations for all cases are adjusted to 4.2 % (wet) since the tests was done with close to 4.2 % (wet) CO_2 in the flue gas. Typically, an H class gas-turbine will produce flue gas with at least 4.5% CO_2 which will reduce the CO_2 capture cost further. An increased CO_2 content will impact all the cases in this paper equally (see discussion in previous paper [1]).

The adjusted/scaled absorber packing height and the most important cost parameter, the packing volume, are calculated from the experimental data for the cases selected in the test campaign. The scaled-up absorber volume is based on packing height utilized for each TCM test case and a scaled up cross sectional area. The latter is calculated based on TCM cross sectional area and the ratio of full-scale (150 tonnes CO_2/h, corresponding to 700 MW_{lhv} fuel input) to TCM (case by case) CO_2 inlet flow.

For all scaled up cases the cross-sectional areas are adjusted to fit with a superficial velocity of 2 m/s (at 0 °C, 1 atm). This will secure less differences in pressure drop between the cases and less impact on the flue gas fan duty in a full-scale plant. This means that it is assumed that the CO_2 capture rate depends mainly on the total packing volume and less on the differences in flue gas velocity through the absorber.

Thus, packing height, see Table 4, is adjusted in order to maintain the scaled-up absorber packing volume. The packing volume per captured CO_2 will be equal for each TCM case and corresponding scaled up case. The data are shown in Table 4 including lean solvent flow rate, specific packing volume, amount of captured CO_2 and CO_2 capture rate.

Packing volume is a significant CAPEX element and the most cost-effective packing volume demonstrated in this campaign was 34 m^3/tonne CO_2 capture per hour for the current test conditions. In Case B3-rep and D3-rep a significantly larger stripper (RFCC) was used removing any limits in the stripper process. This had a positive effect in allowing operating with a lower inlet lean loading at an increased solvent flow rate to the absorber (i.e. keeping an optimal L/G) increasing the absorber CO_2 capture capacity and significantly increasing the CO_2 capture rate.

Table 4. Key cost parameters

	Adjusted abs. Pack [m]	Lean solvent flow [kg/kg CO_2 in]	Spec. packing volume [m^3/t CO_2, h]	Captured CO_2 [t/h]	CO_2 capture [%]
MEA-1[1]	~28	~16	~55	128	85
MEA-2[1]	25.5	14.5	50	128	86
MEA-3[1]	18.9	12.5	37	129	86
F2	16.6	17.5	37	135	90
B3-rep	19.5	14.5	36	136	91
D3-rep	19.6	15.5	34	146	97

1: Reference [1].

The section above introduced the economic evaluation and cost of CO_2 avoided. In Figure 5 the demonstrated cost reduction for the selected three test cases are compared with the best result from the MEA-3, 2 and 1 campaign [1]. The previous assessment [1] has been revisited and the presented relative cost of CO_2 avoided are updated based a newer gas turbine (H class).

Case D3-rep demonstrates the largest cost reduction contribution, i.e. 4.8 % down relative to MEA-3 and close to 20% relative to MEA 1 The trend is a reduction in CO_2 capture cost with increasing CO_2 capture rate. Since more CO_2 is being captured for a given flue gas stream the total cost (CAPEX) of CO_2 handling will increase somewhat also increasing cost of electricity. For case D3-rep this represents an increased cost of electricity with 3-4% compared to the MEA-3 case. Due to the significantly higher amount of CO_2 captured, the avoided CO_2 cost will still be reduced as shown in Figure 5 below. The cost estimation was done with two water wash stages for the case D3-rep. Results from the campaign did suggest that one stage could have been sufficient, resulting in some additional savings.

Since the cost reduction potential of these measures is experimentally verified in one of the world's largest demonstration plants, the cost reduction should be highly accurate, and hence relevant for future post-combustion plants.

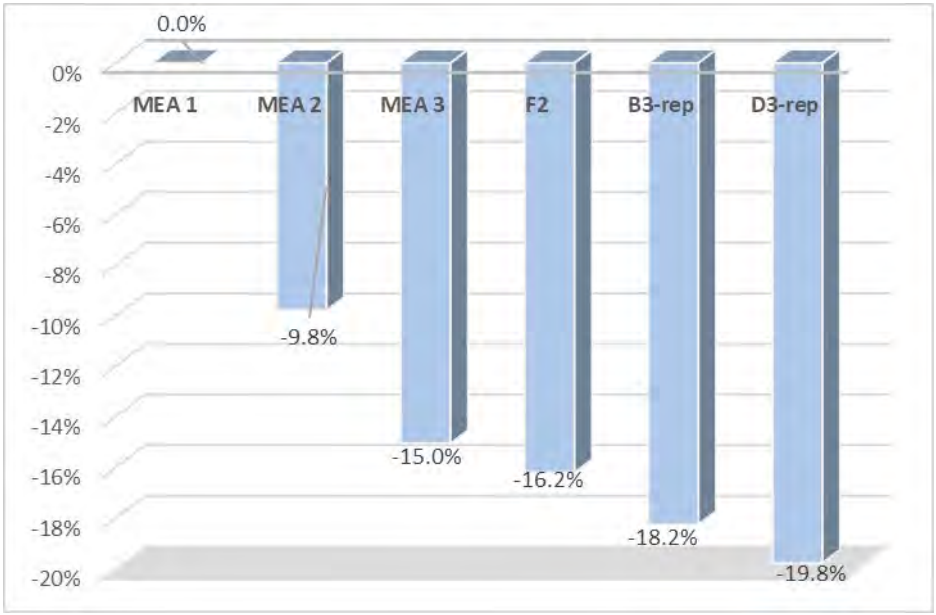

Fig. 5. Demonstrated reduction in cost of CO_2 avoided for the selected cases compared with the earlier MEA campaigns.

4. Conclusions

The results show encouraging cost reduction potential such as lower energy numbers for a more concentrated (35 wt%) MEA solvent and more cost-efficient design of the capture plant. Cost improvements of 4.8% were achieved compared to the previous TCM benchmark (MEA 3) and close to 20% compared to the first campaigns. These results can be viewed as a form of debottlenecking of the amine plant, optimizing its throughput. However, the impact of working with a more concentrated solvent on corrosion, solvent degradation and emissions is something that must be explored further.

It is important to notice that these results are generated at one of the world's largest capture demonstration units, and that it is one of the first times such a structured campaign is executed. Similar testing can be carried out with different amine-based solvents. Therefore, these results at TCM scale represent a very relevant basis for scale up and industrial design of amine solvent capture technologies.

Acknowledgements

The authors gratefully acknowledge the staff of TCM DA, Gassnova, Equinor, Shell and Total for their contribution and work at the TCM DA facility. The authors also gratefully acknowledge Gassnova, Equinor, Shell, and Total as the owners of TCM DA for their financial support and contributions.

References

[1] Gjernes E, Pedersen S, Jain D, Åsen KI, Hvidsten OA, de Koeijer G, Faramarzi L, de Cazenove T. Documenting modes of operation with cost saving potential at the Technology Centre Mongstad. GHGT-14, 21st-25th October 2018, Melbourne, Australia

[2] Faramarzi F, Thimsen D, Hume S, Maxon A, Watson G, Pedersen S, Gjernes E, Fostås BF, Lombardo G, Cents T, Morken AK, Shah MI, Cazenove Td, Hamborg ES. Results from MEA testing at the CO2 Technology Centre Mongstad: Verification of baseline results in 2015. Energy Procedia, 114, 2017, 1128-1145

[3] Hamborg ES, Smith V, Cents T, Brigman N, Falk-Pedersen O, de Cazanove T, Chhagnlal M, Feste JK, Ullestad Ø, Ulvatn H, Gorset O, Askestad I, Gram LK, Fostås BF, Shah MI, Maxson A, Thimsen D. Results from MEA testing at the CO2 Technology Centre Mongstad. Part II: Verification of baseline results. Energy Procedia 63, 2014, 5994-6011

[4] Cost and Performance Baseline for Fossil Energy Plants Volume 1a: Bituminous Coal (PC) and Natural Gas to Electricity Revision 3, July 6 2015, DOE/NETL-2015/1723

CATCHING OUR FUTURE

A Benchmark for Compact CO_2 Capture Plant Designs by Monoethanolamine Solvent Testing at Technology Centre Mongstad

(2021)

15th International Conference on Greenhouse Gas Control Technologies, GHGT-15

15th 18th March 2021 Abu Dhabi, UAE

A Benchmark for Compact CO_2 Capture Plant Designs by Monoethanolamine Solvent Testing at Technology Centre Mongstad

Gelein de Koeijer[a], Christophe Benquet[bc], Anette Knarvik[ac], Erik Gjernes[d], Steinar Pedersen[a], Odd Arne Hvidsten[ac]

[a]*Equinor ASA, P.O. Box 8500, 4035 Stavanger, Norway*
[b] *Total E&P Norge, Finnestadveien 44, Dusavik, 4029 Stavanger, Norway*
[c]*Technology Centre Mongstad, 5954 Mongstad, Norway*
[d]*Gassnova SF, Dokkvegen 10, 3920 Porsgrunn, Norway*

Abstract

Technology Centre Mongstad (TCM) is a large and flexible demonstration site for post-combustion CO_2 capture. It is located next to the Equinor refinery at Mongstad (Norway) which is the source of the flue gases supplied to TCM. It has been used for testing CO_2 capture with MEA solvent and a compact design, providing a benchmark for compact CO_2 capture technologies.. The absorber was used with its lowest possible packing height of 12m, and only one of two water washes was used (3m height). The plant was operated with a high flue gas flow rate (67,000 Sm^3/h) and 35 wt% MEA with a sensitivity down to 30 wt%. The CO_2 inlet concentration was 6% mimicking some industrial exhausts, small turbines with exhaust gas recycle or modern turbines with high turbine inlet temperatures. The tests demonstrated that such a low absorber can capture more than 80% of the CO_2 with only a slightly higher steam demand than conventional applications with higher packing heights of 18-24m. The low absorber gave 3.9 MJ/kg CO_2 for the specific reboiler duty, while previous tests at other conditions and with higher absorbers gave 3.5-3.7. Acceptable emissions were observed, while degradation was higher than earlier TCM campaigns due to the choice of running with 35 w% MEA. Overall, a benchmark has been provided for future improved compact capture technologies.

Keywords: CO_2 capture, post-combustion, compact, benchmark, demonstration, monethanolamine

1. Introduction

Technology Centre Mongstad (TCM) is a large and flexible demonstration site for post-combustion CO_2 capture. It is located next to the Equinor refinery at Mongstad (Norway) which is the source of the two types of flue gases supplied to TCM. These sources are the combined cycle gas turbine (CCGT) based heat and power plant (CHP) and residue fluid catalytic cracker (RFCC). TCM is owned by Gassnova (on behalf of the Norwegian state), Shell, Total and Equinor. Various proprietary amine solvents have been tested and matured at TCM since the start-up in 2012. In addition, various campaigns have been executed with a numbered series of open non-proprietary monoethanolamine (MEA). Most of the results have been published. The most significant campaigns were the third monoethanolamine

test campaign (MEA-3) in June 2017 and the following MEA-4 and MEA-5 that lasted until October 2018. The large number of public, industrial, research and academic participants involved in these campaigns have enabled that the results served a broad scientific audience. The main objectives of these campaigns were to gain knowledge and information that can be used to reduce the cost as well as technical, environmental and financial risks of commercial scale deployment of post-combustion capture (PCC). This includes demonstration of a model-based control system, dynamic operation of the amine plant, investigating amine aerosol emissions, establishment of residue fluid catalytic cracker (RFCC) baseline performance with MEA, and specific tests targeted at experimentally verifying measures that can reduce the cost of CO_2 avoided [1].

This paper describes a part of the MEA-5 campaign tests relevant for reducing the size of a CO_2 capture plant as the most important driver. Reduced size can be beneficial or even enable CO_2 capture in certain applications. One example is brownfield retrofit of capture on exhausts with very limited spaces, e.g. existing industry near urban areas and refineries. Another example are turbines or engines on offshore oil&gas production unit. Equinor is currently developing its 3CWI concept "CO_2 Capture with Carbonated Water Injection" for greenfield Floating Production, Storage and Offloading (FPSO) units [2]. In this concept CO_2 is captured from a gas turbine, compressed, mixed with produced and/or sea water and injected as dissolved bicarbonate ions. For these examples the main constraints is available space and equipment weight rather than the energy efficiency. As the absorber is the unit of largest mass and volume, experiments that can reduce the uncertainty at low absorber heights are of value for these applications. Not much specific research has been done yet with this motivation.

The tests in this paper are done at elevated CO_2 concentration relative to earlier CHP based campaigns at TCM. 6 vol% was chosen, which reduces the size of the absorber relative to the usual 3.5-4 vol%. The reason for this is that elevated CO_2 concentrations are likely in applications where weight and volume are restricted. One motivation for this choice is the possible use of exhaust gas recycle (EGR) both on turbines and piston engines. Another motivation is the gradual development of increasing the CO_2 content due the higher turbine inlet temperatures in modern turbines allowing for less air cooling of the expander blades. In order to achieve 6 vol% of CO_2 in the flue gas going to the capture plant, the TCM amine plant was operated with flue gas from the Mongstad CCGT plant and with recycling a portion of the captured CO_2.

The absorber packing height was set at 12m, which is the lowest possible at TCM's amine unit. Moreover, one of the two water washes was disabled. This combination simulates the lowest absorber setting possible at TCM, but has significant dry bed height in between. The results will be used for discussing the viability of making post-combustion capture more compact. It is acknowledged that the amine unit at TCM is not specifically designed for testing compact capture. Consequently, the result may not be representative for commercial use as the unit will operate outside the operational window TCM's amine unit is designed for. The data can be utilized as a source for insight, comparison and for benchmarking commercial compact capture technologies.

2. System

TCM's amine unit was used (see e.g. [4][5][6]) and its flexibility was utilized to collect data relevant for a compact capture plant design. This means that the absorber was operated with only the lower packing section (12 m) and with one water wash bed (3 m, Lower (L) in operation, Upper (U) is idle) in service. This is the smallest total amount of packing possible at TCM without modifications. The set-up is illustrated and compared to the full amine plant set-up in Figure 1.

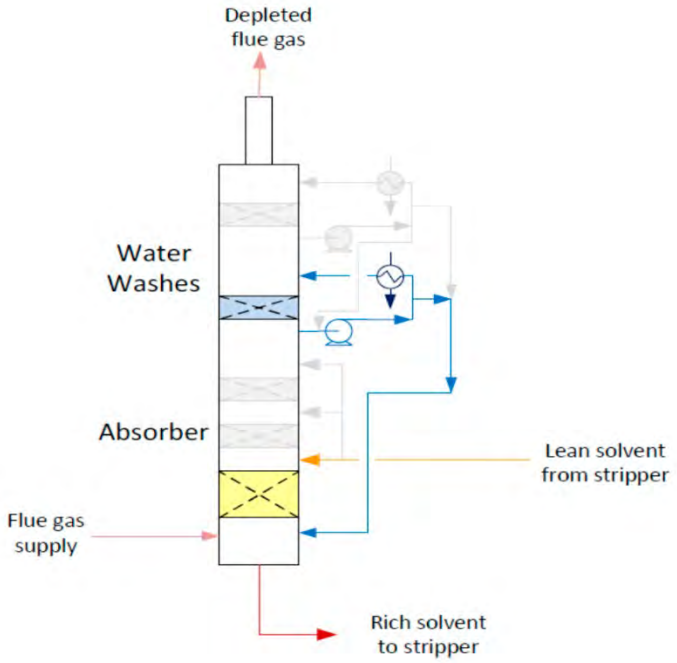

Figure 1. Illustration of the compact flue gas absorber set-up.

The flue gas flow rate was adjusted to its highest practically possible operating point (67,000 Sm^3/h, 113% of design capacity). To mimic higher capacity solvent types, the MEA concentration was increased to 35 wt% from the normally used 30 wt%.

The amine plant has extensive instrumentation with multiple measurements on the streams required for performance assessment. Details on the CHP flue gas characteristics, the main systems in the plant and an assessment of instrumentation quality as well as calculation methods for the main parameters are described in previously published papers, see Gjernes et al [1][7].

3. Method

3.1. Strategy

For this work various test series were executed named by the first letters in the alphabet. The plant was operated with a high flue gas flow rate (67,000 Sm^3/h). An overview of the test series is given in Table 1. The strategy in this work was to start out with the highest achievable capture rate in test series A. Therefore, the steam flow rate to reboiler was maximized and the solvent flow rate was high (106-138 kg/hr). The series B to D were systematic experiments to produce steam demand optimum curves (so-called U-curves) for identifying the lowest specific reboiler duty (SRD) for each series over a selected range of target capture rates (~ 83 to 72 %). In the E and F-series the flue gas temperature into the absorber was higher (45 instead of 30 °C), for assessing potential reduction in the cooling requirement and the equipment size of the direct contact cooler (DCC). As in the A series, the E cases were maximizing the steam flow rate to achieve a high capture rate and the F series was systematic experiments to find the energy optimum. The E case consists only of one test. All these series were run with around 35 w% MEA. Next, some tests were added to put the series A-F in a wider perspective. The cases named B5-1 and B5-2 are two reference runs with MEA at 30 wt% and with lower and upper water wash in operation, respectively. The motivation was to see whether there are differences between the upper and lower water washes. The case named 15-3 is included in the results section to have a comparison against the most compact absorber line-up used in the previous TCM study on modes of operation with cost saving potential back in 2018 [1]. The objectives for the experimental work were to investigate capture rates and specific

reboiler duty during parameter testing. Steam flow to reboiler and solvent flow rates were the main variables, while flue gas flow and CO_2 inlet concentration were kept constant.

Table 1. Overview of the tests.

Series	MEA [%]	Flue gas temperature [°C]	Lean x 1000 [kg/h]	Water wash
A	35	30	106-138	L+U
B	35	30	138-98	L
C	35	30	139-83	L
D	35	30	120-72	L
E	35	45	107	L
F	35	45	128-77	L
B5-1	30	30	128	L
B5-2	30	30	128	U

With this strategy, it was the intention to inspire, and stretch the targets for new technology developments of compact and low weight CO_2 capture plants. With more advanced solvents and optimized systems, it is expected that significant improvements beyond what TCM demonstrates here are possible.

The so-called U-curves were produced by variations in the lean amine to gas flow rate ratio (L/G). The cold rich by-pass of the lean rich heat exchanger (17% by-pass) was in operation during all test runs. This variable was left unchanged. It is acknowledged varying it could provide somewhat lower steam demand or higher capture rate, but not significant.

3.2. Measurements

The combination of methods used in the current work is shown in Table 2. The flow out of absorber is based on flow into the absorber assuming all components except water and CO_2 are conserved. Moisture is calculated from temperature and pressure. The product flow is assumed to be CO_2 and moisture only.

Table 2. Selected methods for test performance assessment.

Location	Property	Method
Absorber in	H_2O	Calculated from p and T
	CO_2	Infrared Spectroscopy (IR)
	Flow	Ultrasonic
Absorber out	H_2O	Calculated from p and T
	CO_2	Infrared Spectroscopy (IR)
	Flow	Calculated from absorber in flow and composition
Product flow	H_2O	Calculated from p and T
	CO_2	Calculated as: 100 - H_2O
	Flow	Coriolis

In each test run the plant is first allowed to stabilize over several hours. A set of key performance indicators is used to assess the quality of data. A two-hour stable period is selected for data extraction. Liquid sampling is conducted within this period. All properties except liquid samples (amine concentration and loading) are averaged over the two-

hour period. Thus, reported data are based on stable operation with respect to all streams. The total and CO_2 mass balances should be within 100 ± 2%. This procedure allows normally not more than two single test runs per day (24 hours). To make comparisons between the test runs, it is important to maintain stable MEA concentration (35 wt%, CO_2 free) and the absorber inlet CO_2 concentration (6 vol%, dry). MEA concentration, lean and rich loading are calculated from laboratory analysis of the liquid samples. In case there is a missing liquid sample, the lean loading is extrapolated using amine density (only for the following tests: B6-opt, C2, D4 and F2).

The solvent loading is calculated from total inorganic carbon (mole CO_2/kg solvent) and total alkalinity (mole amine/kg solvent):

$$Loading = \frac{total\ inorganic\ carbon}{total\ alkalinity} \tag{1}$$

The specific reboiler duty (SRD) is the heat delivered to the reboiler from the steam flow divided by the amount of captured CO_2:

$$SRD = \frac{\Delta H\ \dot{m}_{steam}}{\dot{m}_{CO2}} \tag{2}$$

In this work the captured CO_2 ($\dot{m}_{CO2}$) is based on the difference in mass flow of CO_2 over the absorber ($\dot{m}_{CO2}$abs, in – $\dot{m}_{CO2}$abs, out). This is chosen in order to aligned with earlier published results (e.g. [1]). Captured CO_2 ($\dot{m}_{CO2}$) based on product flow from stripper will for the present cases result in a lower CO_2 product flow. The steam pressure and temperature are typically around 2.5 barg and 160 °C in this work.

The capture rate is the mass fraction of captured CO_2 and the amount of CO_2 flowing into the absorber.

$$Capture\ rate = \frac{\dot{m}_{CO2,abs\ in} - \dot{m}_{CO2,abs\ out}}{\dot{m}_{CO2,abs\ in}} x100\% \tag{3}$$

The absorber packing volume and thus the absorber size are major CAPEX elements. The absorber packing volume (m^3/ton CO_2, h) was calculated for the cases with highest CO_2 product flow and compared with the previous test case 15-3. The parameter is one metric used for assessing compact absorber designs. The TCM absorber cross section is 7.2 m^2 and packing height applied is 12 m.

The emissions of amine and ammonia were monitored during all test runs. As higher MEA concentration is associated with increased solvent degradation [3] and plant corrosion, degradation and metal content in the solvent were closely monitored. However longer-term testing is expected to be needed to assess the solvent management aspects of higher MEA concentrations. Moreover, the solvent composition was measured before and after for estimating the cumulative degradation.

4. Results and discussion

4.1. Capture rate and steam demand

The observed relation between SRD and capture rate is shown in Figure 2 for all the series A-F and the B5-2 and B5-1 with 30 w% MEA. The lowest SRD value in the U-curves achieved within each test series is shown as transparent squares along with a dashed trend line based on the five selected optimum points. The trend line shows a corresponding decrease in capture rate and SRD from 87% and 4.3 MJ/kg CO_2 down to 73% and 3.7 MJ/kg CO_2. Within each series the capture rates were quite well controlled within the target. The trend line gives a good indication of what is achievable with a compact plant configuration. The results from the F-series (82% capture rate) shows promise also for reducing cooling need and size of the DCC. It is also seen that the SRD is significantly higher for the two test runs with MEA 30wt% (B5-2 and B5-1). The uncertainty at TCM is discussed in other papers [4][5][6] and is assumed not to be significant different in this campaign.

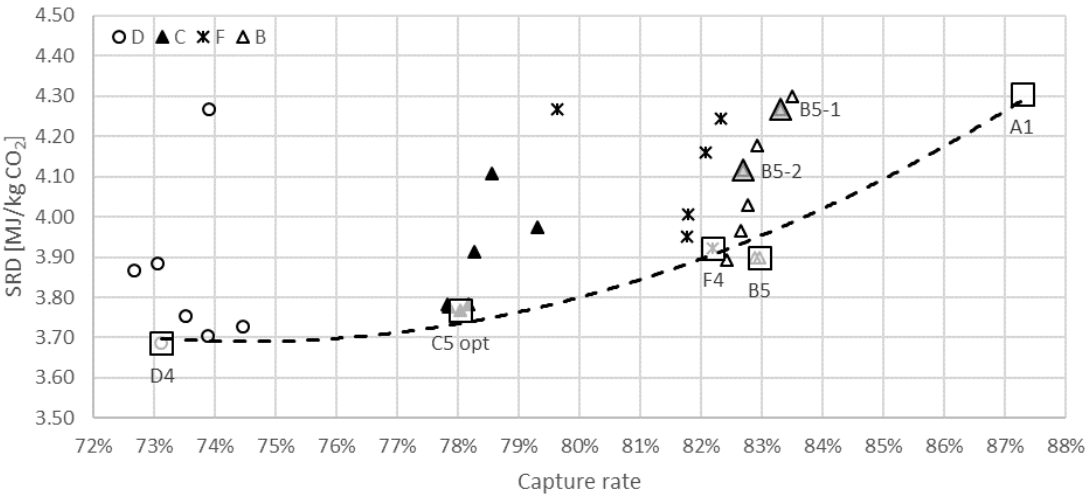

Figure 2. SRD and capture rate for the test series. Optimum points for each series are shown as transparent squares.

As expected with the low absorber height the SRD become higher than TCM has reported earlier for higher absorber heights. For 30 w% MEA Gjernes et al.[1] reports down to 3.6 MJ/kg CO_2 at 86% capture with 3.6 vol% CO_2 in the inlet, while this work shows around 4.0-4.2 MJ/kg CO_2 at 87% capture with 6 vol% CO_2 in the inlet. This increase may not be unacceptable high in situations where energy ample cheap heat is available. Figure 2 also shows that a similar low SRD of around 3.6-3.8 is achievable with a lower capture rate of 70-80%. This decrease may neither be unacceptable in the mentioned applications where space and weight are the limiting factors.

The MEA and wet CO_2 inlet concentrations were aimed to be kept constant for all tests, and the achieved results are shown in Figure 3. There are small variations between the test series and the comparison between the series are representative. There is also good agreement between the two CO_2 measurement methods. The figure also shows MEA concentration close to 31 wt% for the B5-1 and B5-2 cases and the CO_2 concentration in good agreement with the other test series. This means that any differences are likely not to be caused by variations in CO_2 inlet concentration and MEA concentration.

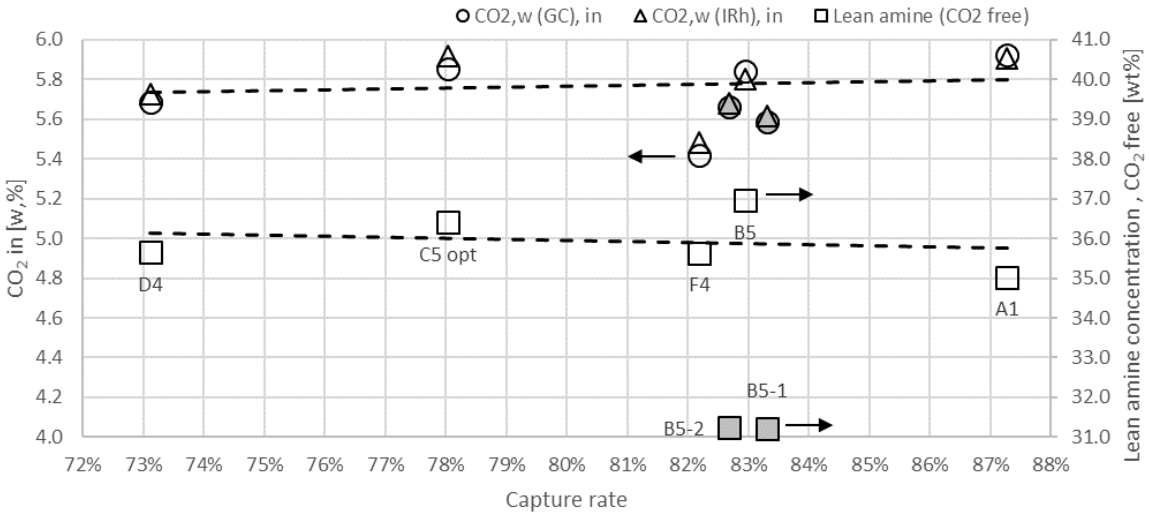

Figure 3. Wet CO_2 inlet concentration and lean amine concentration were maintained at the same level for the selected optimum cases. Grey symbols are for the B5-1 and B5-2 cases that were operated at lower amine concentration.

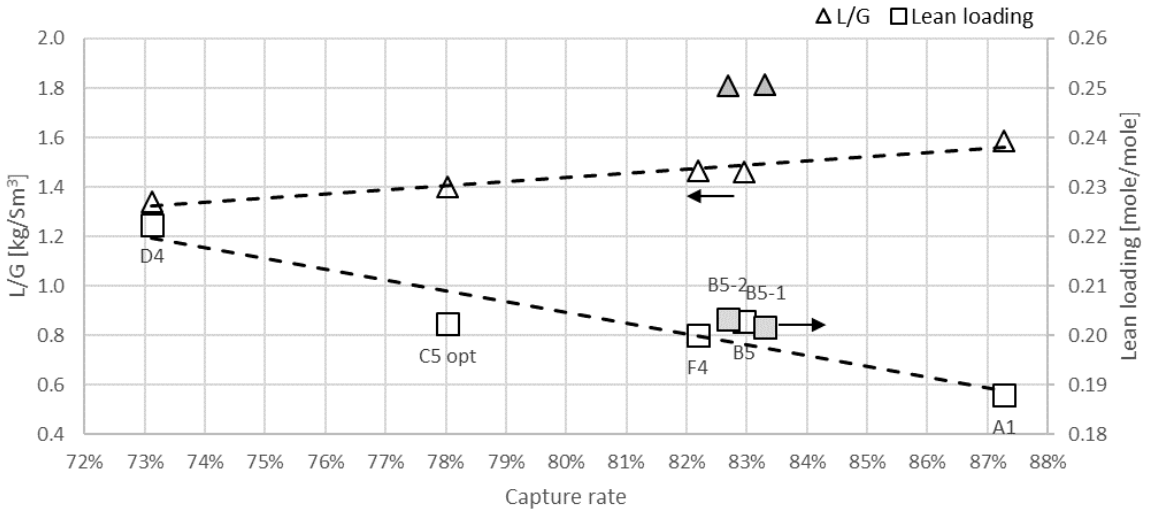

Figure 4. L/G ratio is increasing, and lean loading is decreasing for the optimum cases when plotted versus the targeted capture rate. Grey symbols are for the B5-1 and B5-2 cases that were operated at lower amine concentration.

A graph of the variations in L/G and lean loading versus capture rate is given in Figure 4. There was a wide enough experimental window with respect to lean flow and resulting loading to observe trends. A 14 percentage points higher capture rate (from 73 to 87) demands a 0.03 mole/mole lower lean loading and a 0.3 kg/Sm^3 higher L/G. It is observed that the MEA 30wt% test cases (B5-1 and B5-2) needs a significantly (0.4 kg/Sm^3) higher solvent flow rate to achieve the target capture rate of 82-83% than the results with 35% MEA, while the lean loading is not very different. As mentioned before, all cases are with 67,000 Sm^3/h flue gas flow.

A summary of results from the test series is given in Table 3. The CO_2 captured in the optimum cases shown in Figure 2 are used for calculating the absorber packing volume.

Table 3. Results summary for all test series.

Series #	L/G interval [kg/Sm^3]	Lean loading [mole/mole]	Captured CO_2 Optimum case [tonne/h]	Capture rate interval [%]	SRD interval [MJ/kg CO_2]	Absorber packing volume per tonne captured CO_2 [m^3/tonne CO_2, h]
A	1.6-2.1	0.19-0.24	6.4	84-87	4.3	13
B	1.5-2.1	0.19-0.25	6.0	83-84	3.9-4.3	14
C	1.2-2.1	0.18-0.25	5.8	78-79	3.8-4.1	15
D	1.1-1.8	0.15-0.27	5.2	73-75	3.7-4.3	16
E	1.7	0.19	5.9	87	4.3	15
F	1.2-1.9	0.16-0.24	5.6	80-82	3.9-4.3	15
B5-1/2	1.8	0.2	5.9	82	4.1-4.3	15
15-3	1.4	0.23	3.2	72	4.0	27

The new property added in this Table is the "Absorber packing volume per ton captured CO_2. This is a good property for analyzing the potential for size and weight reductions. Most interestingly, in the A-1 case the CO_2 produced is 6,427 kg/h and the absorber packing volume parameter is 13. The result for the 15-3 case from earlier TCM publication [1] was 27. This shows that there are significant differences in this property and that this campaign had low number ranging from 13-16. The difference with 15-3 up to 27 shows that there should be a significant opportunity for more

compact absorber designs and corresponding cost saving for this largest equipment item in post-combustion capture. It is recommended to use this new property in future work for comparison.

A final observation is that no large differences were observed between B5-1 and B5-2. This means that there are likely no big differences between upper and lower water wash (as expected) that can explain any variation or invalidate any conclusions.

4.2. Emissions to air

When changing design of amine based post-combustion one must always keep control of the emissions since these pose of the main HSE risks [8]. Table 4 gives an overview of the measured emissions to air at moments or intervals the results were regarded as reliable and representative. The letter gives which series the measurement is taken from while the number gives which test it is (not reported in detail in this work). Two measurements were done in the C5 test. The online data were 5 min averaged data over an analyzed period of 2 hours.

Table 4 Overview of isokinetic sampling during the period. Note that FTIR values are reported for time slots where isokinetic samplings were not available. In addition to optimum cases, emission results are included from B4, C3 rep, E1 and F3. The FTIR was out of service during case D4 and F4.

Series/Test	Water wash	MEA [ppm]	NH_3 [ppm]	Emission result type
A1	L+U	0.12	9.3	Online (FTIR)
B4	L	0.13	11	Isokinetic
B5	L	0.00	12	Online (FTIR)
C3 rep	L	0.059	9.0	Isokinetic
C5	L	0.047	14	Isokinetic
C5 opt	L	0.37	22	Isokinetic
C5 opt	L	0.52	30	Online (FTIR)
D4	L	-	-	Online (FTIR)
E1	L	5.7	24	Isokinetic
F3	L+U	3.5	26	Isokinetic
F4	L+U	-	-	Online (FTIR)

Except for E1 and F3 the emissions to air were not significantly higher than the ones published earlier on industrially representative operation [9]. In E and F especially the MEA emissions are high, probably higher than most future emission permits will allow. The reason is that the inlet temperature was increased from 30 to 45 °C. So, this seems not to be a favourable measure for compact capture. This indicates that two water washes are likely needed for compact capture if high inlet temperature is unavoidable.

The numbers presented here have a somewhat higher uncertainty than TCM presents in dedicated emission papers, e.g. Morken et al [9]. Some numbers may be somewhat higher than if the plant was operated stable for longer time. Build-up of MEA in water wash can occur. On the other hand, some numbers may be low since they can be impacted by the large amount of dry packing bed above the absorption bed. It must be noted that the quantification limit for the FTIR is 0.5 ppm due to increased instrument noise at low levels. However these uncertainties do not impact the conclusion on the overall low enough levels with 30 °C inlet and the overall too high levels at 45 °C inlet temperature.

4.3. Solvent degradation

When changing design of amine based post-combustion one must also always keep control of the degradation since it can be important for the OPEX and HSE risk. Table 5 gives an overview of metal and heat stable salt (HSS) in the solvent. The compact campaign was done after another campaign of 905 hours. So, the amine was already partly

degraded at the start.

Table 5. Overview of metal and heat stable salt (HSS) concentrations after reclaiming and at the beginning and end of the campaign discussed in this paper. All concentrations are mg/kg solvent. Components below the detection limit are marked with "<".

Component	After Reclaiming	Beginning	End
Sum operational hours	0	905	1,230
Sum tons CO_2 captured	0	5,830	7,702
Cr	<0.1	0.30	1.3
Fe	0.2	1.60	11
Ni	0.2	0.5	1.7
Mo	<0.1	<0.1	<0.1
Na	0.9	1.9	4.5
V	<0.1	<0.1	<0.1
Zn	<0.1	<0.1	<0.1
Cu	<0.1	<0.1	<0.1
Sum metals	1.3 - 1.7	4.3 - 4.7	18.5 - 18.9
Formic acid	41.8	285	645
Glycolic acid	<20	54	79
Oxalic acid	<20	84	213
Acetic acid	<20	74	165
Nitrate	37.3	246	510
Nitrite	<30	<35	<35
Sulfate	<35	92	114
Sulfite	<30	<35	<35
Sum HSS	79.1 - 234.1	835 - 905	1,726 – 1,796

The degradation products increase as expected. When deciding to run this campaign with 35wt% a risk of excessive degradation was taken. This risk was mitigated by only running a relative short time of 325 hours. From all the measured concentrations the main discussion in literature focuses on the iron concentration. TCM's own guideline [10] recommends keeping the iron concentration below 5 mg/kg solvent. In the compact campaign it increased from from 1.6 to 11 crossing the recommended value. However, Moser [11] has observed long periods of low degradation above the 5 mg/kg iron. It seems anyhow recommended to have more mitigation actions in place for keeping the degradation under control for using 35 w%. Examples are continuous reclaiming or use any of the new O_2 and/or iron removal technologies.

4.4. Comparison with previous results

Over the years various campaigns have been executed at TCM with MEA on CCGT flue gas, of which the compact campaign in this paper is the latest. From each campaign one representative result was chosen that has most industrial relevance. Table 6 below gives an overview of these representative results enabling a comparison and perspective of what TCM has been achieved at TCM.

Table 6. Comparison of representative results from all MEA campaigns at TCM.

Campaign (literature reference)	CO_2 inlet [vol%]	Gas velocity [m/s]	Absorber packing [m]	MEA [w%]	L/G [kg/Sm^3]	Capture rate [%]	SRD [MJ/kg]	MEA emissions [ppmv]
MEA2 [1]	3.6	2.3	24	30	1.0	86	3.6	< 1
MEA3 [1]	4.2	2.0	18	40	0.98	86	3.6	< 1
MEA5 (B5 this paper)	6	2.7	12	35	1.46	83	3.9	< 1

The results from this compact campaign has as expected the largest SRD as well as the lowest capture rate. The differences with the other cases on variables that are important for cost and HSE are not very large. Hence, we can conclude that the amine unit at TCM can be used to study compact capture, although it is not specifically designed for it. Another result from this Table is a set of data that can be used to tune any overall MEA model. The data give a large enough specter to serve this purpose.

4.5. Discussion on compact capture

The results in this paper give a benchmark for any compact capture technology. Many new ideas and improvements on reducing weight and size can use this work for comparison. Preferably, these should perform better on most variables that are important for cost and HSE. Examples of such more compact but less mature technologies are rotating absorption&desorption, membrane contactors and CO_2 selective gas-gas membranes.

But better results could also be obtained at TCM in the future. One improvement idea for TCM is to use another better solvent. This work already shows that increasing the MEA concentration from 30 to 35% makes compact capture design more attractive. TCM has already tested the solvent CESAR-1 for other motivations [12]. Testing this solvent on compact design like done in this work is a logic next step.

Another idea for TCM is to study in more detail metal build-up and degradation rates in compact design. This work provides a good indication but had not enough hours for industrially relevant conclusions. A final idea is further testing at 45°C and two water washes could also be interesting to be able to find the balance with the size of the direct contact cooler (DCC) upstream the absorber and the lean amine cooler.

5. Conclusions

The amine unit at TCM has been used for testing compact capture for providing a benchmark. The absorber was used with its lowest possible packing height of 12m, and only one of two water washes was used (3m height). The plant was operated with a high flue gas flow rate (67,000 Sm^3/h) and 35 wt% MEA with a sensitivity down to 30 wt%. The CO_2 inlet concentration was 6% mimicking some industrial exhausts, small turbines with exhaust gas recycle or modern turbines with high turbine inlet temperatures. The tests demonstrated that such a low absorber can capture more than 80% of the CO_2 with only a slightly higher steam demand than conventional applications with higher packing heights of 18-24m. The low absorber gave 3.9 MJ/kg for the specific reboiler duty for the low absorber, while the higher absorbers gave 3.5-3.7. Acceptable emissions were observed, while degradation was high due to the choice of running with 35 w% MEA. Overall, a benchmark has been provided for future improved compact capture technologies.

Acknowledgements

The authors gratefully acknowledge the staff of TCM DA, Gassnova, Equinor, Shell and Total for their contribution and work at the TCM DA facility. The authors also gratefully acknowledge Gassnova, Equinor, Shell, and Total as the owners of TCM DA for their financial support and contributions.

References

[1] Gjernes E, Pedersen S, Jain D, Åsen KI, Hvidsten OA, de Koeijer G, Faramarzi L, de Cazenove T, Documenting modes of operation with cost saving potential at the Technology Mongstad, Energy Procedia, 14th Greenhouse Gas Control Technologies Conference Melbourne 21-26 October 2018 (GHGT-14)

[2] Pettersen J, Nilssen OR, De Koeijer G, Approaching Zero CO_2 Emissions for Future Oil and Gas Production Offshore, Abstract and presentation to TCCS-10 conference, June 2019, Trondheim, Norway

[3] Supap T, Idem R, Veawab A, Aroonwilas A, Tontiwachwuthikul P, Chakma A, and Kybett BD, Kinetics of the Oxidative Degradation of Aqueous Monoethanolamine in a Flue Gas Treating Unit, Ind. Eng. Chem. Res. 2001, 40, 16, 3445–3450

[4] Thimsen D, Maxson A, Smith V, Cents T, Falk-Pedersen O, Gorset O, Hamborg ES, Results from MEA testing at the CO_2 Technology Centre Mongstad. Part I: Post-Combustion CO_2 capture testing methodology, Energy Procedia, 63, 2014, 5938-5958,

[5] Hamborg ES, Smith V, Cents T, Brigman N, Falk-Pedersen O, de Cazanove T, Chhagnlal M, Feste JK, Ullestad Ø, Ulvatn H, Gorset O, Askestad I, Gram LK, Fostås BF, Shah MI, Maxson A, Thimsen D, Results from MEA testing at the CO2 Technology Centre Mongstad. Part II: Verification of baseline results, Energy Procedia, 63, 2014, 5994-6011

[6] Faramarzi L, Thimsen D, Hume S, Maxon A, Watson G, Pedersen S, Gjernes E, Fostås BF, Lombardo G, Cents T, Morken AK, Shah MI, de Cazenove T, Hamborg ES, Results from MEA Testing at the CO_2 Technology Centre Mongstad: Verification of Baseline Results in 2015. Energy Procedia, Volume 114, 2017, p 1128-1145.

[7] Gjernes E, Pedersen S, Cents T, Watson G, Fostås BF, Shah MI, Lombardo G, Desvignes C, Flø NE, Morken AK, de Cazenove T, Faramarzi L, Hamborg ES, Results from 30 wt% MEA performance testing at the CO_2 Technology Centre Mongstad, Energy Procedia, Volume 114, 2017, 1146-1157

[8] De Koeijer G, Talstad VR, Nepstad S, Tønnessen D, Falk-Pedersen O, Maree Y, Nielsen C. Health risk analysis for emissions to air from CO2Technology Centre Mongstad, International Journal of Greenhouse Gas Control, 18, 2013, 200–207.

[9] Morken AK, Pedersen S, Kleppe ER, Wisthaler A, Vernstad K, Ullestad Ø, Flø NE, Faramarzi L, Hamborg ES, Degradation and Emission Results of Amine Plant Operations from MEA Testing at the CO2 Technology Centre Mongstad, Energy Procedia, 114, 2017, 1245- 1262

[10] Morken AK, Pedersen S, Nesse SO, Flø NE, Johnsen K, Feste JK, de Cazenove T, Faramarzi L, Vernstad K, CO_2 capture with monoethanolamine: Solvent management and environmental impacts during long term operation at the Technology Centre Mongstad (TCM), International Journal of Greenhouse Gas Control 82 (2019) 175-183.

[11] Moser P, Wiechers G, Schmidt S, Monteiro JGMS, Charalambous C, Garcia S, Fernandez ES, Results of the 18-month test with MEA at the post-combustion capture pilot plant at Niederaussem – new impetus to solvent management, emissions and dynamic behaviour, International Journal of Greenhouse Gas Control, Volume 95, 2020.

[12] Christophe Benquet C, Knarvik A, Gjernes E, Hvidsten OA, Kleppe ER, Akhter S, First Process Results and Operational Experience with CESAR1 Solvent at TCM with High Capture Rates (ALIGN-CCUS Project). To be presented at GHGT-15 Virtual Conference: 15-18 March 2021.

Documenting modes of operation with cost saving potential at the Technology Centre Mongstad

(2018)

14th International Conference on Greenhouse Gas Control Technologies, GHGT-14

21st -25th October 2018, Melbourne, Australia

Documenting modes of operation with cost saving potential at the Technology Centre Mongstad

Erik Gjernes[a]*, Steinar Pedersen[b], Divya Jain[c], Knut Ingvar Åsen[b], Odd Arne Hvidsten[b,d], Gelein de Koeijer[b], Leila Faramarzi[b,d], Thomas de Cazenove[d,e]

[a]*Gassnova SF, Dokkvegen 10, 3920 Porsgrunn, Norway*
[b]*Equinor ASA, PO Box 8500, 4035 Stavanger, Norway*
[c]*Shell Global Solutions International B.V., PO Box 663, 2501CR The Hague, The Netherlands*
[d]*Technology Centre Mongstad, 5954 Mongstad, Norway*
[e]*A/S Norske Shell, Tankveien 1, P.O.Box 40, 4098 Tananger, Norway*

Abstract

From December 2017 to February 2018 the Technology Centre Mongstad (TCM DA), operated a test campaign capturing CO_2 by use of monoethanolamine (MEA) in a 80 to 200 ton CO_2 per day demonstration unit. The primary objective was to provide experimental evidence for reducing operational as well as capital costs of CO_2 capture. For cost assessment a selection of the test cases has been used as a basis for estimating cost of full scale amine based CO_2 capture for a large combined cycle gas turbine based (CCGT) power plant. The cost of CO_2 avoided is presented for these cases and the case with the lowest cost of CO_2 avoided has been furthered investigated by a parameter study. The cost assessment is presented relative to two earlier MEA campaigns at TCM. A reduction in cost of CO_2 avoided up to 18% was justified by experiments while further improvements were made plausible theoretically.

Keywords: MEA; post-combustion capture; cost of CO_2 avoided; CO_2 Technology Centre Mongstad; TCM DA

1. Introduction

The Technology Centre Mongstad (TCM) is the world's leading facility for verifying and improving CO_2 capture technologies. TCM is located at Mongstad, one of Norway´s most complex industrial facilities. TCM has been operating since autumn 2012, providing an arena for qualification of CO_2 capture technologies on an industrial scale. In autumn 2017, Gassnova (on behalf of the Norwegian state), Equinor (formerly Statoil), Shell and Total entered into a new ownership agreement securing operations at TCM until 2020. The owners of TCM started their most recent monoethanolamine (MEA) test campaign in June 2017 where a large number of public, industrial, research and academic stakeholders were involved [1]. The campaign included demonstration of a model-based control system, dynamic operation of the amine plant, investigating amine aerosol emissions and specific tests targeted at reducing the

* Corresponding author. Tel.: +47 40 00 59 08.
E-mail address: postmottak@gassnova.no

cost of CO_2 avoided. Through the testing, both flue gas sources currently available at TCM were used. These sources are the combined cycle gas turbine (CCGT) based heat and power plant (CHP) and the residual fluidized catalytic cracker (RFCC). They provide flue gases with a wide range of properties and a CO_2 content from 3.6 to 14 %. TCM is located next to the Equinor refinery in Mongstad. The Mongstad refinery is the source of both flue gases supplied to TCM.

The part of the test campaign addressing cost of CO_2 avoided will be reported in the current paper where the aim is to estimate the potential for cost reduction of some known measures based on experimental data from TCM's amine unit. This means that these estimates will be experimentally verified. It is the first time such a structured cost reduction test campaign has been executed on such a large test unit. Hence the results are expected to be useful for large scale plants. Besides an experimental verification of known measures, this paper will also use this methodology to estimate other cost reduction measures on a theoretical basis using extrapolation of the verified results.

The performance of TCM's amine plant was presented in 2014 [2] along with an independent verification protocol developed by Electric Power Research Institute (Epri) [3]. The performance was reported with a specific reboiler duty (SRD) of 4.1 GJ/ton CO_2 for a case with 47,000 Sm^3/h flue gas flow at 3.7 % CO_2 and a capture rate around 85 %. CO_2 concentration in the flow in and out of the absorber as well as in the product flow was measured by use of one FTIR unit that cycled between the three flows. One cycle lasted more than one hour, thus simultaneous gas composition measurements could not be presented. In 2015 performance was revisited after a major upgrade of the gas phase measuring system. The upgrade included multiple gas phase analyzers at each of the three flows, i.e. in and out of the absorber and out of the stripper. The use of anti-foam significantly improved the performance and resulted in an SRD of 3.6 GJ/ton CO_2 [4] for operation at 59,0000 Sm^3/h flue gas flow with 3.6 % CO_2. The 47,000 Sm^3/h case was also revisited in 2015 [5] with a test program for energy optimization based on maintaining 85 % capture rate for various combinations of stripper bottom temperature and corresponding lean CO_2 loading (mole CO_2 per mole amine). This resulted in SRDs for the cases without and with the use of anti-foam of 3.9 and 3.6 GJ/ton CO_2, respectively. These results were used for establishing a baseline. This work takes the next step: how can the cost of capture based on this baseline be reduced through a structured test campaign?

Nomenclature

Abs. pack	Absorber packing height
CAPEX	Capital expenditure
CCGT	Combined cycle gas turbine
CHP	Combined heat and power plant
L/G	Liquid to gas ration, i.e. ratio of solvent flow and flue gas flow
MEA	Monoethanolamine
MEA-1	Test campaign at TCM on MEA (2013-2014)
MEA-2	Test campaign at TCM on MEA (2015)
MEA-3	Test campaign at TCM on MEA (2017-2018)
OPEX	Operational expenditure
RFCC	Residual fluidized catalytic cracker
Sm^3/h	Standard cubic meter per hour at 15 °C and 101.325 kPa
SRD	Specific reboiler duty
ton	1,000 kg,
TCM	Technology Centre Mongstad
wt%	Concentration on weight basis

2. Overview of the tests program

The test program that is reported in this paper was executed at TCM from December 2017 to February 2018. The main elements investigated were:

- Absorber configurations with packing heights at 24, 18 and 12 meter
- Solvent concentration with MEA at 30 and 40 wt%

In addition to this, most of the tests were operated at slightly elevated CO_2 concentration in the flue gas to be treated, i.e. from 3.6 to 4.2 % CO_2 (wet), and during last part of the campaign anti-foam was injected based on experience from the test program in 2015 [5]. The test program contains 18 test series and the main operational parameters are listed in Appendix A.

The operation in December 2017 was stopped due to signs of corrosion i.e. increasing iron content in the solvent and high levels of ammonia emissions to air. Results from corrosion monitoring at TCM is reported in e.g. [6]. After inspection and a comprehensive plant washing operation, the test program was started up again week 3, 2018. The following two months different modes of operation were investigated. Before presenting the experimental results and cost assessments, the definitions of specific reboiler duty, capture rate and CO_2 loading will be discussed.

Figure 1 shows the TCM amine plant in CHP mode. It is a flexible plant that enables testing of CO_2 capture in several configurations and offers a wide range of flue gas flow rates as well as flue gas compositions [2 to 5]. In the current campaign injection of lean amine is made at three different heights in the absorber and thus utilising 24, 18 and 12 meter absorber packing (yellow boxes in figure), respectively. The CO_2 recycle line has been in operation for most of the campaign in order to maintain a CO_2 level of 4.2 % (wet) in the flue gas into the absorber.

Specific reboiler duty (SRD) is defined as the heat delivered to the reboiler from the steam system divided by the amount of captured CO_2:

$$SRD = \frac{\Delta H\, \dot{m}_{steam}}{\dot{m}_{CO_2 cap}} \tag{1}$$

where $\dot{m}_{steam}$ is the steam flow to the reboiler heat exchanger. ΔH is the enthalpy difference between steam and condensate calculated from measured temperature and pressure, see also reboiler, steam and condensate in Figure 1. Steam pressure is typical around 2.5 barg and up to 160 °C for the tests reported in this paper.

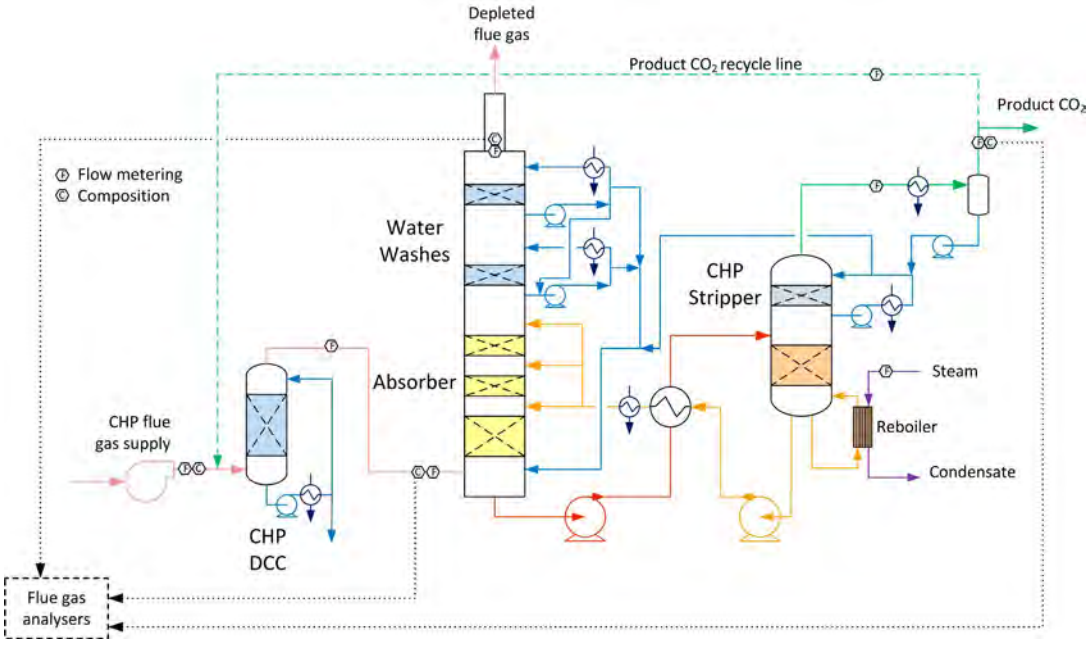

Figure 1. The TCM amine plant in CHP mode (up to 80 ton CO_2 per day). Flow meters and flue gas analysers are located at absorber inlet, outlet/depleted flue gas and product flow. Captured CO_2 can be recycled, see green dotted line, to increase the CO_2 concentration in the flue gas flow into the absorber.

CO_2 capture rate is the mass fraction of CO_2 being captured out of the amount of CO_2 flowing into the absorber:

$$\varepsilon = \frac{\dot{m}_{CO_2 cap}}{\dot{m}_{CO_2\,in}} \tag{2}$$

Captured CO_2 ($\dot{m}_{CO_2 cap}$) in (1) and (2) can be based on CO_2 in product flow ($\dot{m}_{CO2,prod}$) leaving the stripper or on difference in mass flow of CO_2 over the absorber ($\dot{m}_{CO_2 abs,in} - \dot{m}_{CO_2 abs,out}$). There are several ways of calculating CO_2 capture rate [4]. In addition to this and as outlined in more details in [4,5] TCM is equipped with multiple flue gas analysers for measuring composition in and out of the absorber and out of the stripper, see Figure 1. This also includes moisture which alternatively can be calculated based on thermodynamics using temperature and pressure of the gases in question. The flow meter at the absorber outlet is unreliable and flow out of absorber is calculated from flow into the absorber assuming that all components except moisture and CO_2 are conserved. The current analysis will be based on the selection of composition analysers, flow meters and calculation methods presented in Appendix B.

Lean and rich solvent loading (mole CO_2/mole amine) are calculated from laboratory analysis of liquid solvent samples that provide total inorganic carbon (mole CO_2/kg solvent) and total alkalinity (mole amine/kg solvent):

$$loading = \frac{Total\ inorganic\ carbon}{Total\ alkalinity} \tag{3}$$

3. Optimising performance: energy

Most of the MEA-3 program was conducted with CO_2 concentration at 4.2 % (wet) in the flue gas into the absorber. This was maintained by recycling captured CO_2 back to the absorber inlet. This secured stable CO_2 concentration in the flue gas since recycled CO_2 could top the initial CO_2 concentration of 3.5 to 3.9 % up to 4.2 % (wet). This CO_2 level is typical for state of the art CCGT plants. Selected test series that will be discussed below are presented in Table 1.

Figure 2 shows to the left the MEA-3 test series 3 with black filled symbols and series 11 with black open symbols. These two series were operated at 47,000 Sm^3/h, 24 meter absorber packing and without use of anti-foam. Compared to results from the MEA-2 campaign in 2015 [5] these two new test series resulted in a lower optimum SRD, but this may be due to several aspects and in addition the CO_2 concentration in the flue gas into absorber was higher. However, during this part of the campaign the amine plant could be operated at rather high stripper bottom temperature and corresponding low lean solvent CO_2 loading without the use of antifoam. Thus, the resulting optimum point was found at a higher stripper bottom temperature and lower lean CO_2 loading compared to MEA-2 results, i.e. 118.1 °C /0.29 mole/mole for MEA-2 versus 121.0 °C/0.21 mole/mole for MEA-3. Results down to 3.6 GJ/ton CO_2 was not achieved at 24 meter absorber packing when operated without the use of anti-foam and as will be presented below the effect anti-foam was not at all as pronounced as in the MEA-2 campaign. We acknowledge this difference in performance which could be due to several factors, however, this has not yet been concluded.

Table 1. Selected test series from MEA-3 campaign at 24 and 18 meter absorber packing, the latter operated at 30 and 40 wt% MEA. The liquid-to gas ratio (L/G) is the ratio of lean amine- to flue gas flow. SRD is based on thermal energy, see equation 1.

#	Abs. pack [m]	MEA [wt%]	Flue gas × 1000 [Sm^3/h]	Anti-foam [-]	Lean × 1000 [kg/h]	L/G [kg/Sm^3]	Stripper bottom temp [°C]	SRD [GJ/ton CO_2]	CO_2 capture [%]
3	24	30	47.0	No	42.0–55.0	0.89–1.17	119.8–121.5	3.8-4.4	86
11	24	30	47.0	No	45.0–60.0	0.96–1.28	119.7–121.4	3.8-4.4	83-86
13	18	30	47.0	Yes	47.5–55.0	1.01–1.17	120.6–121.4	3.9-4.1	84-86
17	18	30	47.0	Yes	52.2–55.1	1.11–1.17	121.5–121.9	3.8-3.9	85-89
B	18	30	47.1-47.2	No[1]	52.5–52.7	1.11–1.12	120.8–120.9	3.8-3.9	87
9	18	40	51.0	No	44.8–55.0	0.88–1.08	121.0–122.8	3.6	82-86

[1]Test series B is made after reclaiming and with no use of anti-foam.

All SRDs and capture rates presented in Figure 2, Table 1 and Table 2 are calculated based on that captured CO_2 ($\dot{m}_{CO_2cap}$) in equation (1) is derived from the difference in mass flow of CO_2 over the absorber. Earlier reported data from MEA-2 campaign [5] was based on measured product mass flow of out of stripper. The discussion below is based on a reassessment of these data using mass flow of CO_2 over the absorber. The data points presented are made from averaging process data over a two hour time slot. This time slot also includes liquid solvent samples such that solvent CO_2 loading can be calculated according to equation (3).

Performance at 18 meter absorber packing height was investigated at both 30 and 40 wt% MEA. Figure 2 shows to the right the MEA-3 test series 13 and 17 with filled and open brown symbols, respectively. The blue filled symbols are test series B without anti-foam that was executed after solvent reclaiming. The best SRDs were obtained around 3.8 GJ/ton CO_2 for test series 17 which is a bit below the 24 meter tests in MEA-2 without anti-foam. The red filled symbols in Figure 2 right hand side shows MEA-3 series 9 which was operated with 51,000 Sm^3/h flue gas flow, 40 wt% MEA and without the use of anti-foam. The optimum SRD is similar as the best performance from MEA-2, however, the absorber packing required was reduced from 24 meter (MEA-2) to 18 meter (MEA-3) and no use of anti-foam. Test series 9 was stopped before completion due to increasing ammonia emission and signs of corrosion i.e. increasing iron content in solvent. Thus only a limited number of parameter variations was conducted during operation at 40 wt% MEA and there might still be a potential for obtaining even lower SRDs. Another observation was that the use of anti-foam had limited effect on performance which can be seen from the brown (with anti-foam) and the blue symbols (without anti-foam) in Figure 2 to the right. Case 9-4 that was operated at 40 wt% MEA without the use of anti-foam resulted in the lowest SRD in this campaign.

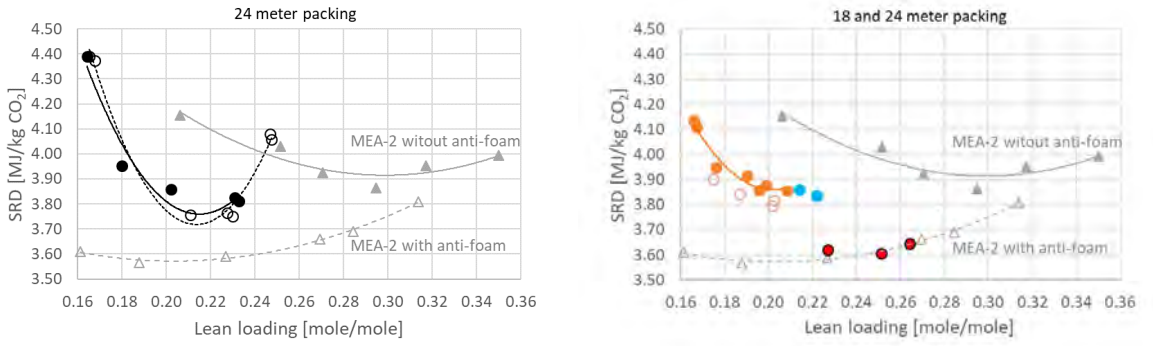

Figure 2. To the left SRD for tests utilising 24 meter absorber packing compared to results from MEA-2 in 2015 (grey symbols and lines). MEA-3 series 3 is with black filled symbols and series 11 is with black open symbols. To the right SRD for tests at 18 meter absorber packing compared to the same results from MEA-2 in 2015 (grey symbols and lines). Series 13 is with brown filled symbols, series 17 with brown open symbols, series B with blue symbols and series 9 which is with 40 wt% MEA, is with red symbols. SRDs are calculated based on difference in mass flow of CO_2 over the absorber. All plots except series 9 are with 30 wt% MEA. The right and left figure present the same MEA-2 results utilising 24 meter absorber packing. Table 1 and Table 2 provide more information about the test series.

Table 2. With ref to Figure 2 operational data, SRD and capture rate for the three cases at lowest SRD values during MEA-3. SRD is based on thermal energy, see equation 1.

#	Abs. pack [m]	MEA [wt%]	Flue gas × 1000 [Sm^3/h]	L/G [-]	Anti-foam [-]	Stripper bottom temp [°C]	Lean loading [mole/mole]	SRD [GJ/ton CO_2]	CO_2 Capture [%]
11-1	24	30	47.0	1.07	No	121.0	0.21	3.8	85
17-5	18	30	47.0	1.11	Yes	121.6	0.20	3.8	88
9-4	18	40	51.0	0.98	No	121.7	0.25	3.6	87

4. Modes of operation

Based on previous work [4,5] it was interesting to further investigate the trade-off between capital expenditure (CAPEX) and operational expenditure (OPEX) parameters for operating conditions relevant for various CCGT- and exhaust gas recycling systems with the aim of providing experimental evidence on how total capture cost can be minimized.

The flexibility of the TCM amine plant was utilized in test series with large variations in absorber packing height, flue gas flow rate, liquid- to gas flow ratio (L/G), solvent CO_2 loading and inlet CO_2 concentration. This experimental set-up covered a range of operating modes. Data collection and performance results such as mass balance, CO_2 recovery, capture rate and SRD are according to methods described in section 2 above. Table 3 gives operational parameters and performance results for selected cases used in the cost evaluation described in section 6 below. Data from previous campaigns, MEA-1 and MEA-2 [2,4], are also included in the table for comparison.

Table 3. Test cases selected for further investigation. Case 11-1 and 9-4 are optimum modes of operation selected from Figure 2. The liquid- to gas ratio (L/G) is the ratio of lean amine- to flue gas flow. SRD is based on thermal energy, see equation 1.

#	Abs. pack [m]	MEA [wt%]	Flue gas × 1000 [Sm^3/h]	CO_2 wet [%]	L/G [-]	Lean loading [mole/mole]	SRD [GJ/ton CO_2]	$\dot{m}_{CO_2 cap}$ [kg/h]	CO_2 capture [%]
11-1	24	30	47.0	4.2	1.07	0.21	3.8	3,160	85
5-1	24	30	59.0	4.1	0.92	0.20	4.0	3,480	77
8-1	18	30	51.0	4.3	1.07	0.21	3.9	3,360	82
9-4	18	40	51.0	4.2	0.98	0.25	3.6	3,430	86
13-2	18	30	47.0	4.3	1.12	0.20	3.9	3,180	84
15-0	12	30	47.0	4.2	1.18	-	4.1	2,700	73
15-3	12	30	47.0	5.0	1.38	0.23	4.0	3,170	72
MEA-1	24	30	47.0	3.7	1.17	0.23	4.1	2,750	~ 85
MEA-2	24	30	59.0	3.6	1.00	0.21	3.6	3,390	86

The initial learning at TCM during the years 2013 and 2014 are represented by the test case MEA-1. At that time the operation was mainly with 24 meter absorber packing height and flue gas flow at 47,000 Sm^3/h (80 % of design flow capacity). For capture rates between 85 to 90 % the specific reboiler duty was measured to 4.1 GJ/ton CO_2.

In the MEA-2 campaign in 2015 learning from several test campaigns were implemented in the test plan. Addition of anti-foam improved especially the stripper performance. This allowed operation with full flue gas load and achievement of both high capture rates and significantly lower SRD values.

In the current MEA-3 campaign, the cases 11-1 and 5-1 are utilizing 24 meter absorber packing height and were run at 47,000 and 59,000 Sm^3/h flue gas flow, respectively. The stripper performance constrained the maximum possible CO_2 capture to 3,480 kg/h in the case with highest flue gas flow. The corresponding capture rate was 77%. However, during the current campaign no energy optimisation was made at 59,000 Sm^3/h flue gas flow and this test was done without the use of anti-foam.

From the three cases run at 18 meter absorber packing height (cases 8-1, 9-4 and 13-2) it is seen that the benefit of 40 w% MEA is lower L/G, lower SRD and still achieving high capture rate. The low L/G and the high lean CO_2 loading indicates a further potential for capturing more CO_2 in this system.

The two cases run at 12 meter absorber packing height achieved rather low capture rates. The benefit of increasing the CO_2 concentration in the flue gas flow into absorber from 4.2 to 5.0 % (wet) is assessed based on results from these two cases.

5. Cost assessment and cost of CO_2 avoided

The economic evaluations of power and capture plants in this paper is based on standard "Cost of Electricity" (COE)- and "Cost of CO_2 avoided" metrics. These calculations are based on aligned and standardized estimates and assumptions on technology process performance such as energy efficiency, CO_2 generation and capture rates, see e.g. [7]. Cost estimates include CAPEX, operations and maintenance (O&M) including fuel and a set of general price and rate of return assumptions. For each case in section 6 below, a complete sized capture plant equipment list is established. Aspen In-Plant Cost Estimator (IPCE) V9 is used to estimate equipment cost. Equipment installation factors are then used to estimate total installed costs. The OPEX can be split in annual cost (of capex), power loss, maintenance, chemicals and fixed operating costs. The gas fired power plant specific cost is based on GTPro and a West Europe scenario. All calculations are furthermore carried out at:

- normalised, per unit (kWh) output from the base industrial (power) plant
- pretax, pre-financing basis
- annual cost basis, applying a capital charge factor corresponding to a standard discount factor and project time horizon

Cost of CO_2 avoided (\$/ton CO_2) is calculated according to (4) below and is based on cost of electricity (COE) and CO_2 emission per kWh ($CO_2\ emission$) for a power plant with capture (cap) and without CO_2 capture ($no\ cap$).

$$Cost\ of\ CO_2\ avoided = \frac{COE_{cap} - COE_{no\ cap}}{CO_2\ emission_{no\ cap} - CO_2\ emission_{cap}} \quad (4)$$

The calculated cost of CO_2 avoided implicitly accounts for the capture systems' own energy demand and its inherent CO_2 emissions. The following economic assumptions are applied:

- Fuel gas price: 0.1875 US \$/Sm^3
- On-stream hours: 7,884 (90 %)
- Discount rate: 5 % real (pretax)
- Time horizon: 30 years

This paper will only report percentage cost reduction and no absolute cost numbers. The main reasons are that the absolute numbers are not useful for the purpose of this work and are partially confidential. In this work one consistent method and one consistent set of assumptions are used for calculating the cost, which is important for a fair comparison.

6. Cost evaluation of selected cases

The experiments targeted lowest possible absorber packing height, lowest possible L/G and SRD while maximizing the captured CO_2 and capture rate. In Table 4 below the experimental data for the selected cases are scaled to a full-scale design at a fixed inlet CO_2 flow of 150 ton CO_2/h and measured capture rate case by case.

In order to compare the MEA-1 and MEA-2 to MEA-3 on the same basis in the cost assessment, the CO_2 inlet concentrations for these two cases are adjusted up to 4.2 % (wet) and the flue gas flow rates are reduced correspondingly, reducing the size and cost of flue gas blower, DCC and absorber. The superficial gas velocity is held constant in the DCC and absorber, reducing the diameter of these units.

The adjusted/scaled absorber packing height and the most important cost parameter, the packing volume, are calculated from the experimental data for the cases selected in the MEA-3 campaign. The scaled-up absorber volume is based on packing height utilised for each TCM test case and a scaled up cross sectional area. The latter is calculated based on TCM cross sectional area and the ratio of full-scale (150 ton CO_2/h) to TCM (case by case) CO_2 inlet flow. For all scaled up cases the cross sectional areas are adjusted to fit with a superficial velocity of 2 m/s (at 0 °C, 1 atm).

Thus, packing height, see Table 4, is adjusted in order to maintain the scaled-up absorber packing volume. The packing volume per captured CO_2 will be equal for each TCM and corresponding scaled up case. The data are shown in Table 4 below together with calculated lean solvent flow per kg CO_2 into absorber, CO_2 loading in lean and rich amine. The rich CO_2 loading is calculated based on solvent flow rate and captured CO_2.

Packing volume is a major CAPEX element and for operation with 30 and 40 wt% MEA the most cost-effective packing volume demonstrated at TCM was about 37 m^3/ton CO_2 capture per hour for the current test conditions. This result is however, design and site specific. In case 9-4 with 40 wt% MEA the main cost reduction parameters are reduced enthalpy to reboiler (low SRD) and reduced solvent flow rate.

The case 11-1 had more packing than needed and very little CO_2 is captured in the upper 6 m packed bed. The cases 11-1, 8-1 and 13-2 performed close to the MEA-2 results, while the case 5-1 was performing poorer. The flue gas flow rate was very high in this case resulting in high CO_2 flow into the absorber. The rich CO_2 loading was high, indicating that the solvent flow rate was too low to achieve high capture rate. Solvent flow rate was 12.02 kg solvent per kg CO_2 in comparison to at least 13.50 kg solvent per kg CO_2 into absorber for the best cases. In new campaigns some of the cases could be further improved if higher capture rates are obtained.

The cases 15-0 and 15-3 with 12 m absorber packing achieved the lowest packing volume per kg CO_2 captured. On the other hand, the capture rate was low and the solvent flow rate was higher. This resulted in higher capture cost. These cases had in fact a too low packing volume.

In MEA-1 the packing volume was slightly higher than for the 11-1 case, solvent flow was higher and the rich loading was lower. In MEA-2 with 24 meter absorber packing height, the packing volume of 50 m^3 per ton CO_2 captured is on the high side compared to the MEA-3 results.

Table 4. The test cases selected for further investigation are scaled up to 150 ton of CO_2/h in the flue gas into the absorber base on 2 m/s superficial velocity (at 0 °C, 1 atm) in the absorber. Case 11-1 and 9-4 are optimum cases in Figure 2 while rest of the tests documents different modes of operation.

#	Adjusted abs. pack [m]	Packing Volume [m^3/ton CO_2, h]	Lean solvent flow [kg/kg CO_2 in]	Lean loading [mole/mole]	Rich Loading [mole/mole]	Captured CO_2 [ton/h]	CO_2 capture [%]
11-1	27.3	54	13.48	0.21	0.51	128	85
5-1	22.4	49	12.02	0.20	0.51	115	77
8-1	18.5	38	13.31	0.21	0.51	123	82
9-4	19.0	37	12.48	0.25	0.50	129	86
13-2	20.2	40	13.94	0.20	0.50	127	84
15-0	13.7	32	15.07	0.21	0.45	110	73
15-3	13.7	27	14.74	0.23	0.47	108	72
MEA-1	~28	~55	~16	0.23	0.48	128	85
MEA-2	25.5	50	14.5	0.21	0.50	128	86

Section 5 above introduces the economic evaluation and cost of CO_2 avoided. In Figure 3 to the left the demonstrated cost reduction for the seven test cases selected from MEA-3 is presented relative to the cost of CO_2 avoided of MEA-1. The demonstrated effect of increasing the CO_2 concentration in flue gas into absorber from 4.2 to 5.0 % (wet) is shown by cases 15-0 and 15-3. When scaled to 150 ton CO_2/h the cost reduction for 15-0 to 15-3 is mainly due to the reduced resulting flow of flue gas, impacting the cost of the DCC, flue gas blower and absorber. Case 9-4 demonstrates the largest cost reduction contribution, i.e. 13.5 % down relative to MEA-1. This case is also presented in Figure 3 to the right (MEA-3) along with MEA-2 and a theoretically case based on 9-4 assuming 5 % CO_2 (wet) in the flue gas. The latter improves the case 9-4 by about 5 % points.

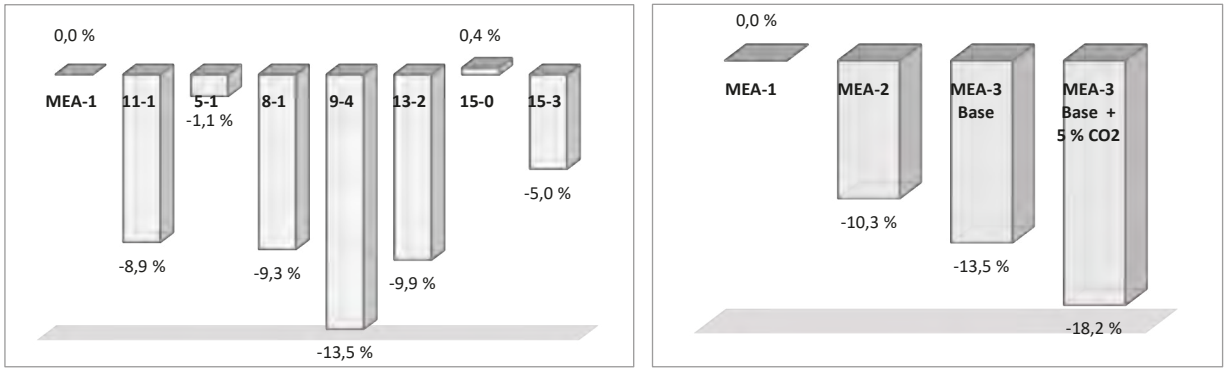

Figure 3. To the left: Demonstrated reduction in cost of CO_2 avoided for seven selected MEA-3 cases. To the right: Lowering cost of CO_2 avoided in campaigns MEA-1 to MEA-3. The MEA-3 is also presented with its theoretically potential if CO_2 content in flue gas is 5 % (MEA-3 Base + 5 % CO_2). Results are presented relative to assessment made for MEA-1 in 2014. Note that case 9-4 in the left plot is presented as "MEA-3 base" in the right plot.

The measures in Figure 3 do not represent radical new ways of operating or new technologies. They can rather be categorized as learning-by doing. They are typically measures relevant for the first few plants, also called FOAK – first of a kind. Since the cost reduction potential of these measures is experimentally verified in one of the world's largest demonstration plants, the cost reduction should be highly accurate, and hence relevant for future post-combustion plants.

Based on the experience from the test campaign other reduction measures have been studies on a theoretical basis in order to investigate future potential for reducing cost of CO_2 avoided. A theoretical parameter study has been made based on case 9-4, referred as "MEA-3 Base" in Figure 4. The following elements have been assessed:

- Reduce from 2 × 3 meter wash section to 1 × 3 meter wash section
- Reduce solvent consumption from 1.6 kg/ton CO_2 down to 0.3 kg/ton CO_2 [8,9]
- Increase CO_2 capture rate from 86 to 90 %
- Reduce steam consumption to achieve SRD of 3.1 GJ/ton CO_2 (other solvents than MEA)
- Increasing CO_2 content in flue gas from 4.2 up to 5 %

These measures are considered to be realistic. Most of the numbers are reported in the post-combustion literature and seem reasonable. In addition to these measures reduced manning is also included in the parameter study for illustration:

- Reduced manning from 4 operators per shift to 1 operator per shift

Figure 4 shows the cumulative effect for cost of CO_2 avoided from these 6 elements. Solvent and process development relates to the first five items. The assumptions on operators before and after reduction is not based on TCM experience. The second last element corresponds to state of the art CCGT plants that are expected to be operated at 5 % CO_2. The five first elements improves the "MEA-3 Base" by 17.1 % while utilizing all six elements results in 21.5 % improvement.

All in all, these initiatives will represent a reduction in cost of CO_2 avoided of the order of 30 % when compared to MEA-1. However, note that these measures are not necessary cumulative, i.e. all combinations may not be possible at the same time.

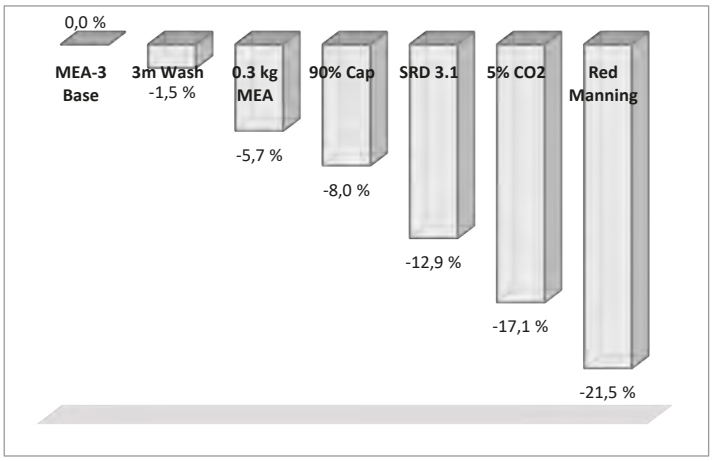

Figure 4. Relative cost of CO_2 avoided based test case 9-4 (MEA-3 Base) and a theoretical parameter study involving 6 cost reduction initiatives introduced on top of each other.

7. Conclusion

Different modes of operation with cost saving potential were executed as part of the MEA-3 campaign at TCM from December 2017 to February 2018. The target was to explore learning from five years of operation at TCM with respect to overall cost reduction potential using the relative cost of CO_2 avoided metric. The new results were therefore compared to those reported from the MEA-1 and MEA-2 campaigns. The investigation of optimum energy performance identified that SRD values below 3.6 GJ/ton CO_2 for MEA are challenging to achieve with 30 wt% MEA and a CCGT like flue gas. This performance is achieved at TCM with a conventional amine plant and may be optimized with an advance process plant. In the cost reduction part of the investigation the level of 10 % cost reduction in cost of CO_2 avoided as achieved in MEA-2 was confirmed with the new experiments. Packing volume is a major CAPEX element and the most cost-effective packing volume demonstrated based on TCM equipment, was about 37 m^3/ton CO_2 capture per hour for the current test conditions. The lowest cost of CO_2 avoided was demonstrated when using MEA at 40 wt% and 18 meter absorber packing height. Compared with MEA-1 results a cost reduction of 13.5% was demonstrated. There is likely a further cost reduction potential of 5 %-points for this case. This is based on results from tests when the flue gas CO_2 concentration was increased from 4.2 to 5.0 % (wet). Finally, a theoretical parameter variation showed a potential cost reduction of around 20 % compared with MEA-3 Base. Compared to MEA-1 this amounts to a reduction potential of the order of 30 %. However, all combinations may not be possible at the same time.

It is important to notice that these results are generated at one of the world's largest capture demonstration units, and that it is the first time that such a structured campaign is executed. Similar testing can be carried out with different amine-based solvents. Therefore, these results at TCM scale represent a very relevant basis for scale up and industrial design of amine solvent capture technologies.

Acknowledgements

The authors gratefully acknowledge the staff of TCM DA, Gassnova, Equinor, Shell and Total for their contribution and work at the TCM DA facility. The authors also gratefully acknowledge Gassnova, Equinor, Shell, and Total as the owners of TCM DA for their financial support and contributions.

Appendix A

Table A1. The test series during MEA-3, 2017-2018.

#	Abs. pack [m]	MEA [wt%]	Flue gas × 1,000 [Sm^3/h]	Anti-foam [-]	Lean × 1,000 [kg/h]	L/G [-]	Stripper bottom [°C]	Lean loading [-]	CO_2 wet %
1[1]	12-18	30	40.0-60.0	No	39.4-66.0	0.82-1.11	119.2-121.5	0.15-0.23	3.5-3.9
2	12-24	30	40.0-47.0	No	40.5-44.1	0.94-1.10	120.0-120.5	0.18-021	3.8-3.9
3	24	30	47.0	No	42.0–55.0	0.89–1.17	119.8–121.5	0.16-0.23	4.1-4.3
4	24	30	50.5-53.0	No	54.5-54.6	1.03-1.08	120.2-120.4	0.20-0.21	4.1-4.2
5	24	30	59.0	No	54.4	0.92	120.5	0.20	4.1-4.2
6	Test of max flue gas flow vs. pressure drop in the absorber								
7	24	30	51.0	No	54.8	1.07	120.8	0.21	4.1-4.2
8	18	30	51.0	No	54.1-73.9	1.06-1.45	118.5-120.6	0.21-0.28	4.2-4.3
9[2]	18	40	51.0	No	44.8–55.1	0.88–1.08	120.5–122.8	0.23-0.28	4.1-4.4
10	18	30	51.0	No	55.2-60.1	1.08-1.18	120.6-121.2	0.22-0.25	4.1-4.2
11	24	30	47.0	No	45.0–60.0	0.96–1.28	119.7–121.4	0.17-0.25	4.2-4.3
12	18	30	47.0	No	49.6-54.7	1.06-1.16	120.5-121.1	0.19-0.21	4.1-4.3
13	18	30	47.0	Yes	47.5–55.0	1.01–1.17	120.6–121.4	0.17-0.21	4.1-4.3
14	12	30	47.0	Yes	54.2-65.2	1.15-1.39	120.8-121.7	0.18-0.22	4.1-4.3
15[3]	12	30	47.0	Yes	55.3-65.0	1.18-1.38	120.5	0.23	4.2-5.0
16	12	30	40.0	Yes	35.2	1.14	121.2	0.20	4.2
17[4]	18	30	47.0	Yes	52.2–55.1	1.11–1.17	121.0–121.9	0.17-0.21	4.2
B	18	30	47.1-47.2	No	52.5–52.7	1.11–1.12	120.8–120.9	0.21-0.22	4.2-4.3

[1]Tests in week 49 and 50 2017. Rest of the test series were executed in 2018.
[2]Full range of parameters reported, but 9-1 and 9-3 were at capture rate below 80% and are not included in Table 1 (section 3).
[3]Includes test at elevated CO_2, i.e. 5% CO_2 (wet).
[4]Full range of parameters reported, but 17-1 was at capture rate below 80% and is not included in Table 1 (section 3).

Appendix B

Table B1. Selected instruments and calculation methods for analysing test data.

Unit	Property	Method	Tag/comment
Absorber in	H_2O	Calculated f(T,p)	8610-TT-2041, 8610-PT-2040
	CO_2	IR-high	8610-AI-2004A
	Flow	Ultrasonic	8610-FT-0150
Absorber out	H_2O	Calculated f(T,p)	8610-TT-2035, 8610-PT-2430
	CO_2	IR-high	8610-AI-2030A
	Flow	Calculated	Based on flow: "Absorber in"
Product flow	H_2O	Calculated f(T,p)	8615-TT-2210, 8615-PT-2213
	CO_2	Calculated	100 – f(T,p)
	Flow	Coriolis	8615-FT-2215

With ref to Table B1 the volume flow out of the absorber ($\dot{V}_{out}$) is calculated from volume flow into $(\dot{V}_{in})$ the absorber assuming all components except water (C_{H_2O}) and CO_2 (C_{CO_2}) are conserved:

$$\dot{V}_{out} = \dot{V}_{in} \frac{100 - C_{H_2O}^{in} - C_{CO_2}^{in}}{100 - C_{H_2O}^{out} - C_{CO_2}^{out}} \quad \text{(B-1)}$$

References

[1] The Open-source Centre at TCM, https://catchingourfuture.com/

[2] Hamborg ES, Smith V, Cents T, Brigman N, Falk-Pedersen O, de Cazenove T, Chhaganl M, Feste JK, Ullestad Ø, Ulvatn H, Gorset O, Askestad I, Gram LK, Fostås BF, Shah MI, Maxson A, Thimsen D. Results from MEA testing at the CO_2 Technology Centre Mongstad. Part II: Verification of baseline results. Energy Procedia, Volume 63, 2014, p. 5994-6011.

[3] Thimsen D, Maxson A, Smith V, Cents T, Falk-Pedersen O, Gorset O, Hamborg ES. Results from MEA testing at the CO_2 Technology Centre Mongstad. Part I: Post-Combustion CO_2 capture testing methodology. Energy Procedia, Volume 63, 2014, p. 5938-5958.

[4] Faramarzi L, Thimsen D, Hume S, Maxon A, Watson G, Pedersen S, Gjernes E, Fostås BF, Lombardo G, Cents T, Morken AK, Shah MI, de Cazenove T, Hamborg ES, Results from MEA Testing at the CO_2 Technology Centre Mongstad: Verification of Baseline Results in 2015. Energy Procedia, Volume 114, 2017, p 1128-1145.

[5] Gjernes E, Pedersen S, Cents T, Watson G, Fostås BF, Shah MI, Lombardo G, Desvignes C, Flø NE, Morken AK, de Cazenove T, Faramarzi L, Hamborg ES. Results from 30 wt% MEA performance testing at the CO_2 Technology Centre Mongstad. Energy Procedia, Volume 114, 2017, p 1146-1157.

[6] Flø NE, Faramarzi L, Iversen F, Kleppe ER, Graver B, Byntesen HN, Johnsen K. Assessment of material selection for the CO_2 absorption process with aqueous MEA solution based on results from corrosion monitoring at Technology Centre Mongstad. To be presented at GHGT-14, 2018, Melbourne, Australia.

[7] Cost and Performance Baseline for Fossil Energy Plants Volume 1a: Bituminous Coal (PC) and Natural Gas to Electricity Revision 3, July 6, 2015, DOE/NETL-2015/1723.

[8] Morken, AK, Pedersen S, Kleppe ER, Wisthaler A,Vernstad K, Ullestad Ø, Flø NE, Faramarzi L, Hamborg ES. Degradation and Emission Results of Amine Plant Operations from MEA Testing at the CO_2 Technology Centre Mongstad. Energy Procedia, Volume 114, 2017, p 1245-1262.

[9] Gorset O, Knudsen JN, Bade OM, Askestad I. Results from Testing of Aker Solutions Advanced Amine Solvents at CO_2 Technology Centre Mongstad. Energy Procedia, Volume 63, 2014, p 6267-6280.

Monitoring real time, in-line variations of noble gas concentrations during CO_2 capture operations by means of a portable mass spectrometer

(2018)

14th International Conference on Greenhouse Gas Control Technologies, GHGT-14

21st -25th October 2018, Melbourne, Australia

Monitoring real time, in-line variations of noble gas concentrations during CO_2 capture operations by means of a portable mass spectrometer

Anja Sundal[1]*, Ulrich W. Weber[1, 2], Matthias S. Brennwald[2], Philip Ringrose[3, 4], Nina Enaasen Flø[4, 5], Kim Johnsen[4, 5], Leila Faramarzi[4, 5], Per Aagaard[1], Rolf Kipfer[2]

[1]*Department of Geosciences, University of Oslo, Sem Saelands vei 1, 0371Oslo, Norway*
[2]*Swiss Federal Institute of Aquatic Science and Technology, Dübendorf, Switzerland*
[3]*Norwegian University of Science and Technology, Trondheim, Norway*
[4]*Equinor, Norway*
[5]*Technology Centre Mongstad, Norway*

Abstract

In the ICO2P-project the overall aim is to develop an innovative and cost-effective monitoring scheme for CO_2 capture and storage operations, implementing new methods for in situ noble gas measurements. The first step is to establish a basis for fluid source identification by recording temporal variance of noble gas composition in CO_2 product. Studies of noble gases related to CCS typically include few, single point samples. In ICO2P, a portable mass spectrometer (i.e. miniRUEDI) is utilized to directly measure real time variability of the noble gas content in CO_2 gas streams at operating CCS facilities. The first study was performed at the Technology Centre Mongstad (TCM) in Norway, a large-scale test facility for post-combustion CO_2 capture operations. During an open scientific test campaign for amine-based capture (TSA-MEA), noble gases (He, Ar, Kr) as well as CO_2, N_2, O_2 concentrations in the CO_2 product stream were recorded every 10 to 15 minutes during a 5-day period. He concentrations (<0.001ppm)were depleted post-capture and too low for temporal variation measurements in the CO_2 product line. Ar concentrations (0.15 – 0.65 ppm) were significantly higher and temporal variation was successfully recorded in the CO_2 product line. Ar was found to be sensitive to capture operations, e.g. CO_2 recycling ratio. This new approach will provide knowledge of the uniqueness and variability of inherent noble gas fingerprints and depletion/absorption during CCS operations and provide grounds for comparison between fluid origins needed in leakage detection schemes at CO_2 storage sites.

Keywords: CO_2 storage; CO_2 capture; CCS; noble gases; monitoring;

* Corresponding author. Tel.: +47 22856652
E-mail address: anja.sundal@geo.uio.no

1. Introduction

During a recent feasibility study [1], to assess the potential for real-time, semi-continuous noble gas monitoring, data were collected from CO_2 capture operations at the Technology Centre Mongstad (TCM) in Norway (Fig. 1), using a novel method for quantitative gas composition measurement. The overall aim has been to contribute towards developing innovative and cost-effective monitoring schemes for CO_2 capture and storage operations, work that is now part of an ongoing research project - the ICO$_2$P-2 project [1] during 2018-2021.

By recording temporal variance of noble gas composition in CO_2 capture products, the inherent geochemical fingerprint can be evaluated with respect to the potential for source identification at prospective storage sites (i.e. differentiation of sources at CO_2 seepage sites or natural variations in marine and terrestrial environments). Studies so far typically include only a few, single point samples, and there is a clear need for more background data on gas compositions and better sampling strategies to ensure safe storage and reliable leakage detection. The miniRuedi [2] portable mass spectrometer has the capacity to measure low concentrations (i.e. partial pressures) of He, Ar and Kr, as well as CO_2, CH_4, O_2 and other relevant chemical substances with high accuracy at sample intervals of < 15 minutes. This technology proved suitable for monitoring fluctuations in some components of the CO_2-product composition, as tested during an open scientific test campaign for post-combustion capture processes; amine-based temperature swing absorption (TSA), at TCM in summer 2017.

This data set, and further work, will provide important knowledge on absolute variability in CO_2 product from complex and mixed sources. During capture operations and before storage of CO_2 can commence, there is a need to document variability, and to evaluate the inherent compositional signature (and the potential need for adding tracers). This approach will allow for source-specific identification of fluids; differentiating injected (anthropogenic) CO_2 from natural (methanogenic / biogenic) CO_2 rich gases at potential leakage points.

Fig. 1. Technology Centre Mongstad (TCM), Norway [Photo © Equinor] DA amine plant with CHP flue gas inlet from the front, and the high absorber tower in the middle. "Captured" CO_2 product outlet and sample point towards the right.

2. Noble gases as tracers in CCS (and EOR)

Reliable monitoring is a prerequisite for safe, long-term storage and public acceptance of CCS. Terrestrial noble gases (i.e. He, Ne, Ar, Kr, Xe) appear to be suitable natural tracers for monitoring and understanding CO_2-rich gas systems [3]. They are chemically inert and non-degradable. And in contrast to several commonly applied chemical tracers (e.g. PerFluoroCarbons), inherent noble gases are not harmful to the environment and bring no additional cost. The concept of using noble gases for monitoring CO_2 projects has been demonstrated at small-scale onshore facilities, and noble gas data proved to be crucial evidence to rule out an alleged leakage incident at the Weyburn project [4].

However, there are still knowledge gaps: studies so far typically include only a few, single-point samples, and there is a clear need for better data on gas compositions and variability.

To understand large-scale reservoir dynamics and fluid mixing at CO_2 injection sites and along possible leakage paths, experience from research related to multi-phase hydrocarbon systems have to be used and adapted to the scientific case of CCS. Formation water in deep, saline aquifers will have a unique noble gas signature based on a blend of an atmospheric component (stable contents of ^{20}Ne, ^{36}Ar, ^{84}Kr), a deep mantle component (mostly supplying ^{3}He) and a crustal radiogenic component (production of ^{4}He, ^{21}Ne, ^{40}Ar). The signature is a function of time and dependent on the in-situ lithology [5]. Crustal ^{4}He is supplied from radiogenic decay of U and Th in minerals, and ^{40}Ar is produced by radioactive decay of ^{40}K. The mixing ratios of meteoric, mantle and crustal components may yield information about residence times and fluid mixing. E.g., it was found that seepage of methane causes depletion of ^{20}Ne and ^{36}Ar relative to ^{4}He by partitioning, as the heavier noble gas species are more soluble in methane than in water [5]. Exchange between groundwater and oil phase may also be detected as increased ^{20}Ne and ^{36}Ar abundance in oil, as described for the Magnus Field in the British North Sea [6]. Injected CO_2-rich fluid will also interact with formation water and/or hydrocarbon phases present in a storage reservoir. A recent tracer test at the Cranfield enhanced oil recovery (EOR) field in the US, adding Kr and Xe, showed noble gases to be stripped from formation water and into the CO_2 phase [7]. Mapping of the background noble gas abundance before injection is of utmost importance to characterize the natural gas composition and spatial distributions prior to CO_2 injection. This will improve the understanding of CO_2 trapping mechanisms and oil/water/gas partitioning in reservoirs, and form the grounds for comparison needed in leakage detection schemes.

2.1. Compositional variability in captured CO_2

Norway is currently at the forefront in developing CCS, along with Canada, Australia, USA and China. With two active storage sites and a national plan to establish another, larger-scale offshore storage site at Smeaheia, there is an imminent need to prepare reliable, cost-effective and long-term monitoring programs. Noble gas finger-printing can provide an applicable solution, but there is a significant knowledge gap concerning the inherent signature of CO_2 from various capture processes.

At the operative Sleipner and Snøhvit sites, inherent CO_2 from fossil sources (natural gas reservoirs) is captured (as part of the gas processing) and re-injected into a storage formation (saline aquifer). Such single-source storage schemes are expected to display the least degree of temporal variation in the noble gas compositions of injected gas. The noble gas signature of a given natural gas accumulation is related to long-term, slow accumulation rates of e.g. ^{3}He, ^{4}He, ^{21}Ne, ^{40}Ar in a given geological setting. Lateral or vertical compositional gradients in reservoirs related to the lithology and contact time with fluids in traps and along migration paths, may be documented as compositional changes during production. However, these changes are expectedly subtle, compared to complex mixed-source and post-combustion schemes. At the Technology Centre Mongstad (TCM) the source is mixed, and natural gas from several reservoirs are combusted before CO_2-rich flue-gas enters the capture facility. CO_2 is captured from a combination of flue gases; (1) from a combined cycle gas turbine (CCGT) based heat and power plant (CHP) or (2) the residual fluid catalytic cracker (RFCC) at the Equinor refinery at Mongstad. At the CHP plant large quantities of gases from different fossil sources are combined, but after initial mixing and combustion, the signature of the flue gases are expected to become relatively homogenous within a few days. Then, with addition of residual refinery gas, the compositional variability is expected to increase. Further, the combustion process will add an atmospheric component.

Depletion of the radiogenic/nucleogenic components of reservoir derived noble gases occurs during combustion and capture [8]. In the product line recirculation rates, addition of different solutes with given solubilities for the gases and their isotopes under varying pressure and temperature conditions will affect noble gas contents. In this study, we attempt to document temporal changes, and the next step is to interpret and decipher the relative effects of capture processes on noble gas fingerprinting. Additionally, documenting variation in the fossil gas feed is highly relevant in evaluating the traceability of mixed-source gas in future storage schemes, involving captured CO_2 also from other industries (e.g. cement, ammonia, waste incineration, biogas). E.g. the presented storage scheme for Smeaheia involves storage of CO_2 from mixed sources, after post-combustion capture.

3. Methodology

3.1. Capture processes at TCM

The Technology Centre Mongstad (TCM) is a large-scale test facility for CO_2 capture operations. This study was conducted in July 2017 during an open scientific test campaign for post-combustion capture processes, using amine-based temperature swing absorption (TSA) [e.g. 9, 10, 11]. Monoethanolamine (MEA) is used as solvent for CO_2. The combined cycle gas turbine and power plant is run with reservoir gas from different fields in the North Sea mixed with a fraction (up to 50 %) of residual gases from the nearby refinery. Flue gas is fed into the TCM plant, cooled, run through the absorber, before CO_2 is stripped off by heating the solvent and vented to a safe location in a dedicated vent stack (Fig. 2). During the test period, the capture plant was run with flue gas from the CHP plant, with a CO_2 concentration of approximately 4 vol%. In addition, recycling (i.e. return of CO_2 product back to feed gas upstream absorber) was performed, increasing the CO_2 content to mimic concentrations similar to coal combustion capture (Fig. 2).

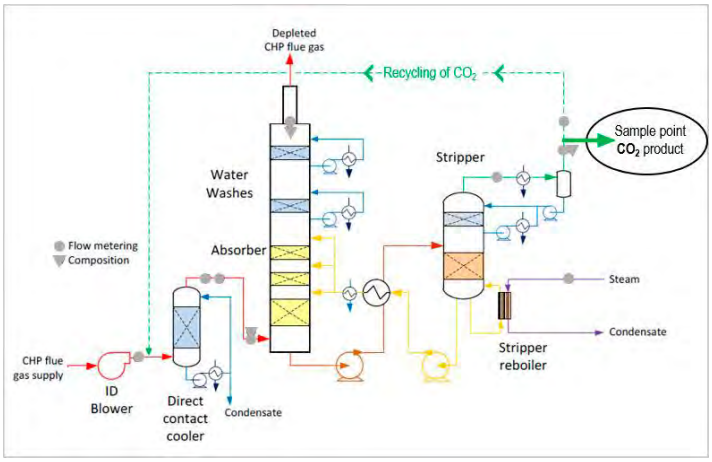

Fig. 2. Post-Combstion CO_2 capture at the Technology Centre Mongstad during TSA-MEA test campaigns. A mobile mass spectrometer was connected to the CO_2 product line. Modified from Thimsen et a. [9]

3.2. Portable mass spectrometer

The adapted mass spectrometric technology for analyzing extremely low concentrations and the isotopic fractionations of He, Ne, Kr, Xe, Ar in water and gas is available only in few laboratories worldwide, with the research laboratory at Eawag/ETH (Zürich) being one of the pioneers in this field.

The miniRuedi (Fig. 3) allows for semi-continuous gas analysis (i.e. partial pressures), and may be used to measure noble gas concentrations. It consists mainly of two vacuum pumps (DP, TP) and a quadrupole mass spectrometer (QMS) with two detectors (Faraday and Multiplier) with different sensitivities. In contrast to fixed laboratory units, no purification by e.g. cryogenics is carried out, which reduces the detection limits, but allows for on-site measurements and smaller instrument units [2]. The instrument has several inlet ports such that a standard gas for calibration and multiple samples can be measured subsequently and automatically without changing the setup. The consumption rate of sample gas is negligible low compared to passing gas streams.

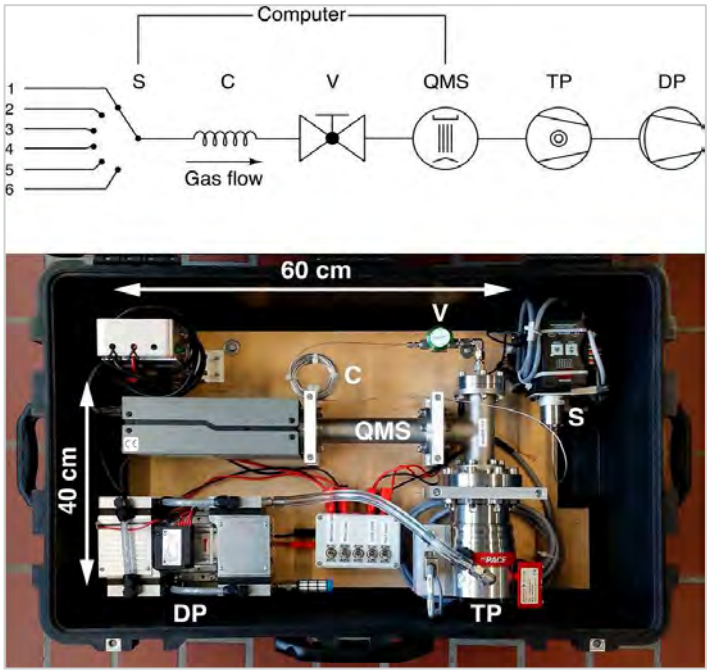

Fig. 3. The miniRuedi portable mass spectrometer (figure from Brennwald et al. [2]) set up with 6-port inlet selector valve (S), capillary (C), inlet valve (V), quadrupole masspectrometer (QMS), turbomolecular pump (TP), and diaphragm pump (DP).

3.3. Sample set-up

A miniRuedi [2] mass spectrometer was connected to the outgoing CO_2 product line, downstream the overhead condenser of the CO_2 stripper (Fig. 2). This stream is water-saturated, and the slip-stream to the instrument was passed through a dryer to avoid the risk of condensation in the instrument. A pressure regulator was mounted between the sample point and the membrane inlet to decrease the inlet pressure to atmospheric pressure. This inlet pressures were fairly constant and recorded with a pressure sensor. The instrument was mounted in less than 1 hour, and ran continuously during a 5-day test period. The analytical sequence was set to repeating cycles of one air-standard analysis block (calibration), followed by three CO_2 output stream sample analysis blocks. An ambient air sample analysis block was added intermittently to remove residual CO_2 from the ion source. The analysis blocks lasted between 10 and 15 minutes depending on the number of components measured. During the test He, H_2O, Ne, N_2, O_2, Ar, CO_2 and Kr were measured. In this way, a unique, semi-continuous data series of gas content was collected and suitable measurement routines were established. Single samples were gathered for lab analysis of noble gas isotopes.

4. Results

The instrument ran steadily throughout the sampling period. However, as this was a feasibility study, parameters such as air-calibration and sampling intervals as well as the selection of analyzed components were tweaked and tested underway. Absolute concentrations of CO_2, O_2 and N_2 were compared with measurements performed by TCM (in-line gas-chromatography). Low concentrations of noble gases throughout the measuring campaign confirm depletion during capture. Kr and Ne were excluded after initial sampling tests, as their partial pressures were below the detection limit. He was too low (< 0.001 ppm) throughout for proper quantification with the miniRuedi, as peak variation could not be deciphered from background. This was confirmed in new, preliminary data analysed after the GHGT poster presentation, and thus He plots are excluded from this final summary. Further studies of single samples and continuous measurement of pre-capture variation (source inlet) are ongoing.

Ar (150 – 650 ppm) contents were significantly higher compared to He, Kr, Ne, and was measured throughout the 5-day sampling period (Fig. 4). Some significant changes were observed (i.e. sudden increase/decrease). The

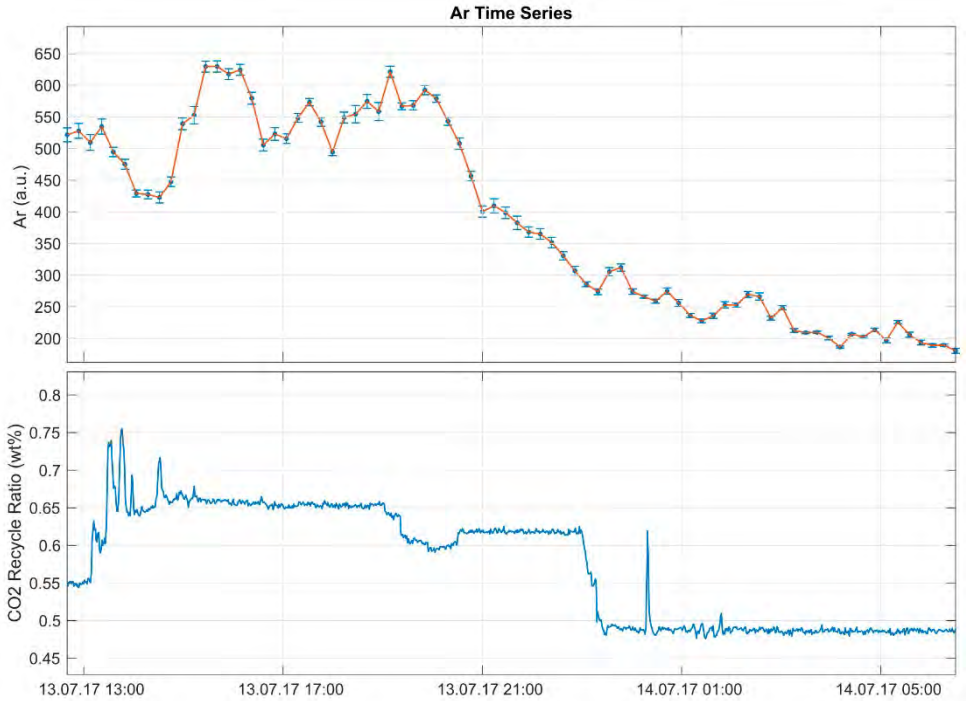

Fig. 4. Measured Ar concentrations (ppm) during the test period 10.07. – 15.07.2017 (upper) displaying co-variance with CO_2 recycle ratio (wt %) at the TCM plant (lower).

analytical error at sampling intervals of 10 - 15 minutes was acceptable, but the standard gas (air) used for calibration was found to be sub-optimal. Ar concentrations appear to be sensitive to changes in the recycle ratio and the capture process (Figs. 4, 5). Preliminary results from single samples confirm that He content is lower in the refinery gas compared to in the natural gas source, and concentrations are expected to vary according to relative contributions from natural gas versus refinery gas (Fig. 6). An observed decline in measured Ar concentrations coincided with reduction of CO_2 recycling in the line, a scheduled process change (Fig. 4).

Fig. 5. Gas flows (kg/h); flue gas, CO_2 product and recycled CO_2.

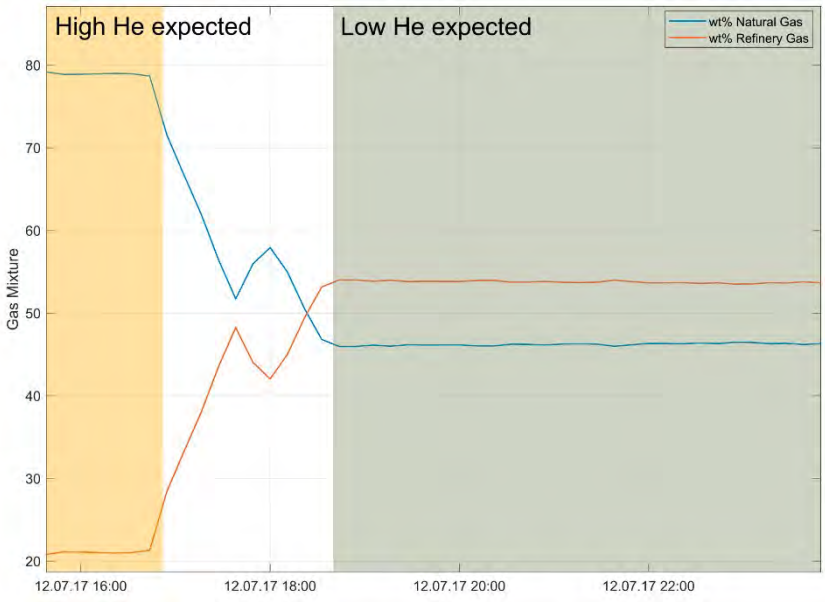

Fig. 6. Change in flue gas composition (wt % refinery gas vs. natural, detail from Fig. 5). Single samples indicate lower He concentrations in RFCC flue gas, such that concentration changes are expected for different mixing ratios.

5. Discussion

The test was successful in that the miniRuedi instrument ran continuously and variation in Ar concentrations were observed and documented. Up to 50 % change in relative concentrations of Ar was observed in the course of 5 days. This shows that there is noble gas variability, and that continuous monitoring is useful to ensure representative sampling in evaluation of inherent fingerprints and traceability. Preliminary single sample results show that concentrations are detectable with our technique before absorption (capture). During gas combustion and in the RFCC process, contamination with air occurs.

Assuming that tests during the capture processing (e.g. recycling) in a regularly working plant are not occurring, variations due to the capture process are expected to be minor. Thus noble gas variation related to source rather than process changes should be measured/detectable at the inlet. This is evaluated in ongoing studies.

The approach of in-line monitoring with a miniRuedi instrument is straightforward. However, optimization is necessary in order to reduce analytical uncertainty. Sample intervals of ~ 10 minutes were found suitable with respect to signal reading time and peak heights, and relative to sample resolution (gradual compositional changes). A customized calibration gas more similar to the CO_2-product should be used in future tests for improved accuracy. Absolute variability in Ar concentrations was registered, and may be used to guide sampling for further chemical analysis and noble gas isotopic signature, ensuring a representative data set of single samples.

TCM is a test facility, and thus the CO_2 product is not stored. There are, however, plans to establish a full value CCS chain in Norway, including storage of CO_2 captured post-combustion [12]. Storage of CO_2 from multiple sources (e.g. fossil fuels, cement, waste incineration) and different capture operations are challenging. Semi-continuous noble gas analysis may allow for pre-injection gas fingerprinting. With regards to detectability at potential leakage sites and separation of different anthropogenic type sources in reservoirs, however, some additional tracer gas may have to be added. At single-source sites (e.g. Snøhvit, Utsira), inherent fingerprints may suffice for source identification. For evaluation of source variability and the effect of the capture process on noble gas signatures, both the flue gas supply (inlet) and CO_2 product (outlet) should be monitored simultaneously. Multiple capillary inlets to the miniRuedi instrument allows for semi-continous monitoring of several sample points. Total variation estimates are useful to guide sampling for isotopic analysis.

Ar concentrations displayed significant variation. During the Ar decrease shown in Fig. 4 the recycling rate was adjusted. Even though this is a change that may not occur in a running large-scale capture site, the dramatic decrease emphasizes that there is a response in the noble gas assembly related to capture process changes. During the test period measurements indicate that noble gases were heavily depleted after capture. He concentrations are significantly lower than atmospheric concentrations (~ 0.00524 hPa). Alternative sampling techniques, e.g. [13], may be tested in further research for gases currently below detection limit (i.e. He, Ne, Kr). Monitoring in-line variation and correlating with isotopic fractions from previous samples will reduce the need for costly and time-consuming lab analysis.

6. Conclusions

The utilization of noble gases as added and/or natural tracers in the context of CO_2 storage monitoring is rather new. As CCS is being upscaled and put into practice, the need for combined and improved monitoring techniques is becoming evident. This feasibility study found that the miniRuedi [2] allows for frequent and accurate measurements of Ar abundance in captured CO_2 from a *post-combustion* like facility (TCM). Preliminary single sample analyses indicate detectability also for continuous measurements of variation in He in the flue gas supply (source) before absorption and depletion during *post-combustion* capture. At *pre-combustion* sites, however, contamination with air is expected to be significantly lower, and considering He concentrations (enriched during radiogenic production) measured in North Sea gas fields [6], monitoring temporal variations for He in the CO_2 product at *pre-combustion* capture sites is feasible. Documentation of variability in live gas streams and guided follow-up sampling for isotopic analysis in the lab will provide an important basis for consideration of noble gas fingerprints in monitoring schemes and leakage detection. This is a new approach that will provide knowledge of the uniqueness of noble gas fingerprints in the product stream from hydrocarbon production, CO_2 capture operations and in the injection line for CO_2 storage.

Acknowledgements

The ICO2P-project is funded by CLIMIT-Demo under grant #616220. The work was also partially funded by the SUCCES FME research center at the Department of Gesociences under grant 193825/S60 from the Research Council of Norway. The authors gratefully acknowledge the staff at TCM DA, Gassnova, Equinor, Shell and Total for their contribution and work at the TCM DA facility. The authors also gratefully acknowledge Gassnova, Equinor, Shell and Total as the owners of TCM DA for their financial support and contribution. We would also like to thank Eawag/ETH for making a miniRuedi instrument available. The project period is scheduled for 2016-2018. A continuation of this project is granted by RCN (#280551), and ICO2P-2 will continue until 2021, including a Ph.D. project. www.mn.uio.no/geo/english/research/projects/ico2p/

References

[1] CLIMIT-Demo feasibility study "ICO2P" under grant 193825/S60: www.mn.uio.no/geo/english/research/projects/ico2p/
[2] Brennwald, M. S., Schmidt, M., Oser, J., and Kipfer, R. (2016). A portable and autonomous mass spectrometric system for on-site environmental gas analysis. *Env.Science & Technology*, 50(24), 13455–13463.
[3] Gilfillan et al. (2008) The noble gas geochemistry of natural CO_2 gas reservoirs from the Colorado Plateau and Rocky Mountain provinces, USA. *Geochimica et Cosmologica Acta*, *72*(4), 1174-1198.
[4] Gilfillan et al. (2017) Using noble gas fingerprints at the Kerr Farm to assess CO_2 leakage allegations linked to the Weyburn-Midale CO_2 monitoring and storage project. *Int. Jour. of Greenhouse Gas Control*, 63, 215-225.
[5] Lollar, B. S., & Ballentine, C. J. (2009). Insights into deep carbon derived from noble gases. *Nature Geosci. 2*(8), 543.
[6] Ballentine, C. J., O'Nions, R. K., & Coleman, M. L. (1996). A Magnus opus: Helium, neon, and argon isotopes in a North Sea oilfield. *Geochimica et Cosmochimica Acta*, *60*(5), 831-849.
[7] Györe et al. (2015). Tracing injected CO_2 in the Cranfield enhanced oil recovery field (MS, USA) using He, Ne and Ar isotopes. *Int. Jour. of Greenhouse Gas Control*, *42*, 554-561.
[8] Flude, S., Johnson, G., Gilfillan, S. M., & Haszeldine, R. S. (2016). Inherent tracers for CCS in sedimentary formations: composition and applications. *Env. Science & Technology*, *50*(15), 7939-7955.
[9] de Koeijer, G., Enge, Y., Sanden, K., Graff, O. F., Falk-Pedersen, O., Amundsen, T., & Overå, S. (2011). CO2 Technology Centre Mongstad–Design, functionality and emissions of the amine plant. *Energy Procedia*, *4*, 1207-1213.
[10] Thimsen et al. (2014). Results from MEA testing at the CO_2 Post-Combstion CO_2 capture testing. Part I: Post-Combstion CO_2 capture testing methodology. *Energy Procedia*, *63*, 5938-5958.
[11] Flø, N. E., Faramarzi, L., de Cazenove, T., Hvidsten, O. A., Morken, A. K., Hamborg, E. S., ... & Fostås, B. F. (2017). Results from MEA degradation and reclaiming processes at the CO2 Technology Centre Mongstad. *Energy Procedia*, *114*, 1307-1324.
[12] Gassnova (2018) Feasibility study for full scale CCS in Norway: www.gassnova.no/en/Documents/Feasibilitystudy...
[13] Manning, C. C., Stanley, R. H., & Lott III, D. E. (2016). Continuous measurements of dissolved Ne, Ar, Kr, and Xe ratios with a field-Deployable gas equilibration mass spectrometer. *Analytical chemistry*, *88*(6), 3040-3048.

CATCHING OUR FUTURE

Dynamic Process Model Validation and Control of the Amine Plant at CO_2 Technology Centre Mongstad

(2017)

energies

MDPI

Article

Dynamic Process Model Validation and Control of the Amine Plant at CO_2 Technology Centre Mongstad

Rubén M. Montañés [1,*], Nina E. Flø [2] and Lars O. Nord [1]

[1] Department of Energy and Process Engineering, NTNU—Norwegian University of Science and Technology, NO-7491 Trondheim, Norway; lars.nord@ntnu.no

[2] CO_2 Technology Center Mongstad, NO-5954 Mongstad, Norway; nflo@tcmda.no

* Correspondence: ruben.m.montanes@ntnu.no; Tel.: +47-73-5073722

Received: 24 August 2017; Accepted: 26 September 2017; Published: 1 October 2017

Abstract: This paper presents a set of steady-state and transient data for dynamic process model validation of the chemical absorption process with monoethanolamine (MEA) for post-combustion CO_2 capture of exhaust gas from a natural gas-fired power plant. The data selection includes a wide range of steady-state operating conditions and transient tests. A dynamic process model developed in the open physical modeling language Modelica is validated. The model is utilized to evaluate the open-loop transient performance at different loads of the plant, showing that pilot plant main process variables respond more slowly at lower operating loads of the plant, to step changes in main process inputs and disturbances. The performance of four decentralized control structures is evaluated, for fast load change transient events. Manipulation of reboiler duty to control CO_2 capture ratio at the absorber's inlet and rich solvent flow rate to control the stripper bottom solvent temperature showed the best performance.

Keywords: pilot plant; transient data; dynamic simulation; flexibility; post-combustion; decentralized control; process dynamics; chemical absorption; CO_2 capture

1. Introduction

Carbon capture and storage (CCS) is a group of technologies that can significantly contribute to the reduction of anthropogenic CO_2 emissions from thermal power generation and other carbon-intensive industries [1]. There are two commercial-scale coal-fired power plants with post-combustion CO_2 capture (PCC) using amines being operated today, at Boundary Dam in Canada [2] and at Petra Nova project at the Parish Power Station in the US [3]. These projects prove the technical feasibility of the technology at commercial scale. Among the different options and technologies for CO_2 capture in thermal power generation, post-combustion CO_2 capture with chemical absorption is considered the more mature technology that can contribute to significantly reducing the carbon intensity ($kgCO_2/kWh_{el}$) of fossil-fueled thermal power plants. In future energy systems with a high penetration of renewable energy sources, the variability in demand and generation will introduce a change in the operating patterns of thermal power generation plants, which will have to change operating conditions [4–6]; there will also be a higher frequency of significant transient events including load changes, and start-up and shut-down events [7,8]. In this regard, Boot-Handford et al.'s carbon capture and storage update 2014 concludes that the financial case for CCS requires that it operates in a flexible manner and that load-following ability is extremely important to the long-term economics [9].

Among the different features of flexible operation of power plants with CCS, an important aspect is the transient behavior of the system when varying operating conditions. This means that efficient operation and emissions and the related operational costs during transient operation will gain importance. However, the operational experience from commercial-scale power plants with post

combustion CO_2 capture is scarce and the published transient pilot plant data from test campaigns is limited. Therefore, there is a need for the development of dynamic process models. Dynamic process models can contribute to developing the learning curve for flexible operation of PCC plants. These tools can assist in evaluating the feasibility of flexible operation strategies as well as design process configurations and operational strategies that can lead to the reduction of operational costs and increased revenue during power plant operation. The study of the transient performance with dynamic process models can contribute to identifying process bottlenecks and ease the process scale-up.

Dynamic process models allow the study of the open-loop transient performance of the plant [10], the evaluation of different process configurations and designs [11], the development and implementation of optimal control strategies [12–20], as well as the study of the plant behavior under different operational flexibility scenarios [21,22]. In addition, the power plant and the PCC unit can be treated as an integrated system and dynamic process models can be utilized to analyze the response of the capture unit to changes that occur upstream in the power plant [12,15,19,23–25]. Furthermore, the operational flexibility of the PCC plant can be improved with plant design or using control strategies [26–29]. The core purpose of dynamic process models is to capture the time-dependent behavior of the process under transient conditions. However, the validation of dynamic process models with experiments and pilot plant data is necessary in order to assess the reliability of simulation results.

Kvamsdal et al. [30] developed a dynamic process model of a CO_2 absorber column and used steady-state data from a pilot plant to validate liquid temperature profiles, capture ratio % and rich loading. That work highlighted the necessity of building up a dynamic process model of the integrated system (including stripper, lean/rich heat exchanger, mixing tank and main process equipment), to understand the complexities of dynamic operation of the plant. Gaspar and Cormos [31] developed a dynamic process model of the absorber/desorber process and validated with steady-state plant data. Several publications are available, in which the models were validated only with steady-state pilot plant data [11,32–35]. Biliyok et al. [36] presented a dynamic model validation study where transient data was driven by decrease in solvent flow rate to the absorber, fluctuating concentration of CO_2 at absorber inlet and a varying absorber's feed flue gas stream temperature to the absorber. A dynamic process model developed in Modelica language was validated with transient data from the Esbjerg pilot plant by Åkesson et al. [37]. That data consisted of the transient performance after one step-change in flue gas mass flow rate. An extensive review work by Bui et al. [38] concluded that research efforts are required on producing transient pilot plant data.

More recent works have included validation of dynamic process models with transient plant data from pilot plants. A K-Spice model by Flø et al. was validated with pilot plant data from the Brindisi pilot plant [39]. Flø et al. [40] validated a dynamic process model of CO_2 absorption process, developed in Matlab, with steady-state and transient pilot plant data from the Gløshaugen (Norwegian University of Science and Technology (NTNU)/SINTEF) pilot plant. Van de Haar et al. [41] conducted dynamic process model validation of a dynamic process model in Modelica with transient data from a pilot plant located at the site of the coal-fired Maasvlakte power plant in the Netherlands. Gaspar et al. [42] conducted model validation with transient data from two step changes in flue gas volumetric flow rate from the Esbjerg pilot plant. Other works include the validation of equilibrium-based models such as that of Dutta et al. [43]; or the work by Chinen et al. [44] which conducted dynamic process model validation of a process model in Aspen Plus® with transient plant data from the National Carbon Capture Center (NCCC) in the US. Manaf et al. [45] developed a data-driven black box mathematical model, based on transient pilot plant data, by means of system identification. In addition, dynamic process models have been developed to study the transient behavior of the chemical absorption CO_2 capture process using piperazine (PZ) as chemical solvent [19,20]. It should be noted that the majority of work has been conducted for typical flue gas compositions from coal-based power plants with CO_2 concentration around 12 vol % [38].

From the literature review it can be concluded that dynamic process model validation is a challenging process due to:

- The scarce availability of transient or dynamic pilot plant data.
- Most available data is found from small-scale pilot plants. That has implications for the reliability of simulation results when applying dynamic process models to scaled-up applications.
- The works involving transient data generally include the response of the plant to disturbances in a few process variables.
- Most of the validation work was done for flue gas with a typical CO_2 content from coal-based power plants.

Flexible operation of PCC plants has been studied with pilot plant test facilities in test campaigns. Faber et al. [46] conducted open-loop step change responses at the Esbjerg pilot plant; this type of analysis helps in understanding the transient performance of the process. They concluded that the overall system acts as a buffer to perturbations at the plant inlet and that the coupled operation of the absorber/desorber unit led to fluctuations in the system when all parameters—flue gas and solvent mass flow rates and reboiler duty—are changed simultaneously. Bui et al. [47] presented a flexible operation campaign conducted at the Commonwealth Scientific and Industrial Research Organization (CSIRO)'s PCC pilot plant in Australian Gas Light Company (AGL) Loy Yang, a brown-coal-fired power station in Australia. The generated transient data included step changes in flue gas flow rate, solvent flow rate and steam pressure. The purpose of the study was to generate a set of data for validation of dynamic process models, and to gain insight into process behavior under varying operating conditions. A different approach was taken by Tait et al. [48] who conducted experiments that simulated flexible operation scenarios on a pilot plant to treat synthetic flue gas with a CO_2 concentration of 4.3 vol%, typical of a natural gas combined cycle (NGCC) plant. Tests for transient operation have been conducted at the amine plant at CO_2 Technology Center Mongstad (TCM DA). De Koeijer et al. presented two cases: a first case with controlled stop-restart of the plant, driven by a controlled stop of flue gas and steam sent to the PCC plant; and a second case with sudden stop of the blower upstream of the absorber [49]. Nevertheless, a limited amount of transient testing can be conducted during test campaigns. A thoroughly validated dynamic process model can help to study the transient performance, controllability, and flexible operation of the plant and process dynamics via dynamic process simulation.

In this work, a suitable set of steady-state and transient plant data, collected from a MEA campaign at CO_2 Technology Center Mongstad, is selected for dynamic process model validation purposes. The plant was operated with flue gas from a natural gas fueled combined heat and power plant. The selected data is utilized to validate a dynamic process model of the amine-based CO_2 absorption-desorption process at TCM DA. Then, the validated model is employed to carry out two case studies on the process dynamics of the TCM DA amine plant. In the first case study, the open-loop transient response of the pilot plant at different operating loads of the plant is analyzed. In the second case study, the performance of four decentralized control structures of TCM DA amine pilot plant is evaluated for fast disturbances in flue gas volumetric flow rate.

2. Materials and Methods

2.1. Plant Description

CO_2 Technology Center Mongstad test site has a pilot-scale amine-based chemical absorption process plant. The amine plant can be configured to treat flue gas from a catalytic cracker from the Mongstad refinery, with CO_2 content of around 13–14 vol%, typically found in flue gas from coal-fired power plants, and also to treat exhaust gas coming from a combined cycle gas turbine combined heat and power plant (CHP), with CO_2 content of around 3.5 vol%. A fraction of the product CO_2 mass flow rate can be re-circulated back upstream of the direct contact cooler (DCC) to increase the CO_2 content, so CO_2 concentrations of between 3.5 and 13–14 vol% could be fed to the plant to simulate the effects of exhaust gas recirculation [50]. Table 1 presents data of the main process equipment of TCM DA amine plant when configured to treat CHP flue gas, which has a total flue gas capacity of

60,000 Sm^3/h and can capture around 80 ton CO_2/day. Figure 1 shows a simplified process flow sheet of the amine plant at TCM DA when configured for CHP gas. A slipstream of exhaust gas is extracted from the CHP plant placed next to the TCM DA facility, and it consists of about 3% of the total exhaust gas. An induced draft blower is utilized to blow the flue gas flow. It has variable speed drives that allow the flue gas volumetric flow rate fed to the absorber column to be manipulated. Upstream the absorber column, a direct contact cooler cools down and saturates the flue gas with water, by means of a counter-current flow stream of water.

Table 1. Size and materials of main process equipment at the amine plant at TCM DA with CHP stripper configuration.

Absorber	
Column cross sectional area (m^2)	3.55 × 2
Column height (m)	62
Packing height (12 + 6 + 6) (m)	24
Water wash section height (3 + 3) (m)	6
Absorber packing type	Koch Glitsch Flexipac 2X
Absorber washer packing type	Koch Glitsch Flexipac 2Y HC
CHP Stripper	
Column cross sectional area (m^2)	1.33
Diameter (m)	1.3
Packing height (m)	8
Water wash section height (m)	1.6
Absorber packing type	Koch Glitsch Flexipac 2X
Absorber washer packing type	Koch Glitsch Flexipac 2Y HC
Heat Exchanger L/Rich	
Duty (kW)	10358
Heat transfer area (m^2)	308
Material	SS 316L
Reboiler	
Duty (kW)	3365
Heat transfer area (m^2)	142
Material	SS 316L
Lean Amine Cooler	
Duty (kW)	5182
Heat transfer area (m^2)	78.8
Material	TITANIUM

A chemical absorption process occurs in the absorber column, where the chemical solvent, flowing from top to bottom, meets the flue gas flowing in counter-current. The absorber column consists of a rectangular polypropylene-lined concrete column with a height of 62 m and a cross-section of 2 × 3.55 m. The absorber-packed sections consisting of Flexipac 2X (Koch-Glitsch Italia, Vimercate, Italy) structured stainless-steel packing are distributed from bottom to top in three sections of 12 m, 6 m and 6 m. Two water-wash systems are installed in the top of the absorption column, consisting of two sections of Flexipac 2Y HC (Koch-Glitsch Italia, Vimercate, Italy) structured stainless-steel packing. The water-wash sections limit emissions and are used to keep the water balance of the plant. The upper water-wash sections can be operated as acid wash [51]. In addition, the plant can be configured to use different packing heights in the absorber column resulting in 12, 18 or 24 m. This can be implemented at TCM plant by introducing all the lean solvent flow at 12 m of absorber packing, 18 m of absorber packing (12 + 6) m or 24 m of absorber packing (12 + 6 + 6) m.

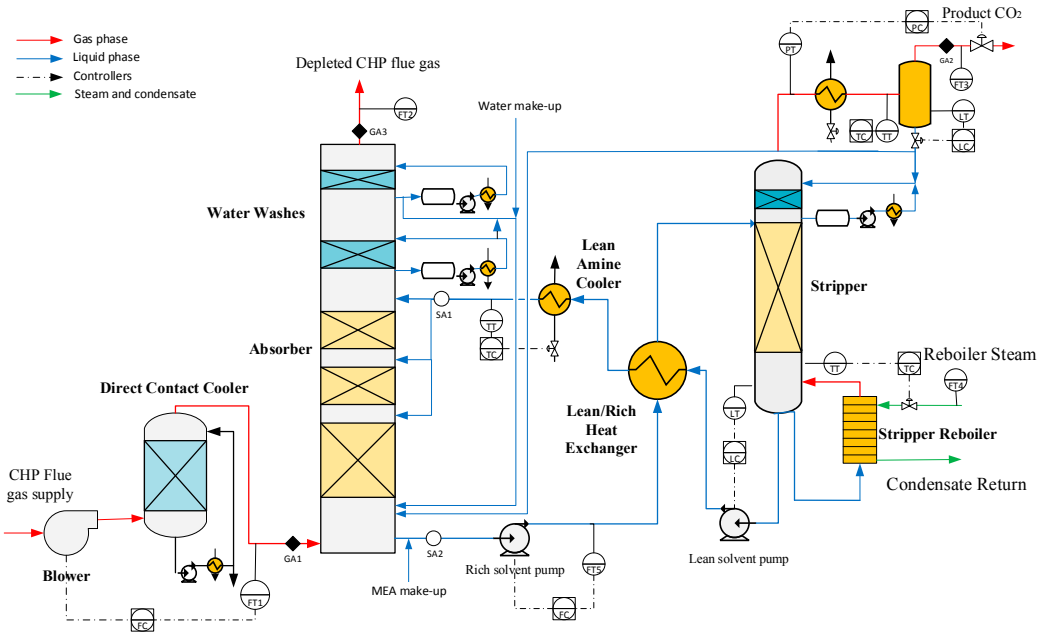

Figure 1. Simplified process flow sheet of the amine plant at CO_2 Technology Center Mongstad, when configured to treat flue gas from a natural gas-fired power plant. The figure shows the location of some gas analyzers (GA), solvent analyzers (SA), flow transmitters (FT), pressure transmitters (PT), temperature transmitters (TT) and level transmitters (LT). The main process controllers of the regulatory control layer are shown, including flow controllers (FC), temperature controllers (TC), pressure controllers (PC) and level controllers (LC).

A 10.4 MW plate and frame heat exchanger is present at the plant where the cold rich amine solution coming from the absorber sump cools down the hot lean amine solution coming from the stripper. In addition, a 5.2 MW lean amine cooler is utilized to set the temperature of the lean solvent conducted to the top of the absorber packing sections, by using a stream of cooling water. The rich solvent is pumped to the top of the stripper column, where it meets the stripping vapors generated in the reboiler. The CHP stripper with overhead condenser system consists of an 8 m column of Koch Glitsch Flexipac 2X structured stainless-steel packing of 1.3-m-diameter, and a water-wash system with Koch Glitsch Flexipac 2Y HC structured stainless-steel packing of 1.6 m of height. The stripper reboiler consists of a 3.4 MW thermosiphon steam-driven system that supplies the heat required for the desorption process. The steam supplied to the reboiler comes from the refinery situated next to the TCM DA facility. Details on the steam supply system can be found in Faramarzi et al. [51].

2.2. Pilot Plant Configuration and Instrumentation

The TCM DA amine plant can be utilized to test various chemical solvents. In this work, the tests were conducted with 30 wt. % aqueous monoethanolamine (MEA). During the tests conducted in the test campaign, the responses and performance of the pilot plant were logged and extracted every 30 s. Gas composition was logged with gas analyzers at the inlet of the absorber, outlet of the absorber, and the product CO_2. A gas chromatograph (GC) installed at TCM DA plant can measure concentrations of CO_2, N_2, H_2O and O_2 at the three locations in a nearly simultaneous manner, which is a desired feature for transient tests; refer to GA1, GA2 and GA3 in Figure 1. Details on gas analyzers and instrumentation at TCM DA plant can be found in [51].

Gas phase flow rates were measured at the plant during the tests. The flue gas volumetric flow rate fed to the absorber is measured with an ultra-sonic flow meter (FT1). As discussed by Faramarzi et al. in [51], the depleted flue gas flow meter (FT2) had a higher degree of variability than FT1, and some transients were observed on the FT2 measurement that were not explained by changes

in process parameters at the plant. Therefore the depleted flue gas flow rate was calculated in the test campaign by considering that all O_2 and N_2 fed to the absorber goes out of the plant with the depleted flue gas. The cooled product CO_2 discharge flow (FT3) was measured with a vortex flow meter. Other flow rates measured at the plant include the steam fed to the reboiler, the lean amine flow rate at the absorber inlet and the rich amine flow rate at the absorber outlet. For flue gas flow meters, the standard conditions are 15 °C and 101.3 kPa [51].

Pressures and pressure drops at different components of the plant were logged. In addition, main process temperatures were logged. For process model validation, it is common to assess the model prediction of the absorber and stripper temperature profiles. Within the absorber and stripper columns of TCM DA's amine plant there are four temperature sensors distributed in the radial plane per meter of packing in the axial direction. Thus, there are 96 temperature sensors within packed segments of absorber column and 28 temperature sensors within the packed segment in the stripper column. These measurements allow the creation of clear temperature profiles of the absorber and stripper columns in the axial direction (at each column height, the resulting temperature value is the average of the four measurements distributed in the radial plane).

Online solvent analysis measurements (SA) were taken at the inlet (SA1) and outlet of the absorber (SA2); refer to Figure 1. The measurements include pH, density and conductivity. In addition, solvent samples were regularly taken manually and analyzed onsite. These analyses allow MEA concentration and CO_2 loadings to be calculated at the sampling points on a periodic basis. The actual reboiler duty was estimated as suggested in Thimsen et al. [52]. Equation (1) shows the calculation of the actual reboiler duty, where F_{steam} is the logged measurement data of steam mass flow rate (refer to FT4 in Figure 1), T_c is the condensate temperature, T_g is the superheated steam inlet temperature, p_g is the steam pressure at inlet, and p_c is the condensate pressure. Enthalpy was calculated with the use of accurate steam tables, with the condensate at the reboiler outlet assumed to be saturated liquid at T_c or p_c. The specific reboiler duty (SRD) in kJ/kgCO_2 is calculated as in Equation (2), where F_{prod} is the CO_2 rich product mass flow rate; refer to FT3 in Figure 1.

$$\dot{Q}_{reb} = F_{steam}\left(h_g\left(T_g, p_g\right) - h_c(T_c, p_c)\right) \quad (1)$$

$$SRD = \frac{\dot{Q}_{reb}}{F_{Prod}} \quad (2)$$

During the tests presented in this work, the averaged total inventory of aqueous MEA was around 38.2 m^3. Averaged values of liquid hold-ups and its distribution at different components of the plant during the steady-state tests included in this work are presented in Table 2. Detailed data on solvent inventory distribution throughout the plant is of importance in order to obtain suitable dynamic process simulation results. The regulatory control layer of the plant was active during the tests conducted in the MEA campaign. The main control loops of the regulatory control layer are presented in Figure 1. Note that the actual regulatory control layer of the amine plant at TCM DA is more complex and includes more control loops for auxiliary equipment, stable and safe operation of the plant, and start-up and shut-down sequences. The control loops included here are those the authors found relevant for the purposes of dynamic process modeling and simulation of this plant during online operation, and considering the time scales of interest for process operation.

Table 2. Averaged values of total solvent inventory and its distribution within the main components of the TCM plant.

PCC Plant Main Components	Solvent Inventory (m^3)
Absorber sump	8.1
Absorber packing	8.4
CHP stripper packing	1.0
CHP stripper sump	2.3
CHP reboiler	0.4
Cold rich solvent pipe	2.2
Cold lean solvent pipes	5.2
Hot rich solvent pipe	1.1
Hot lean solvent pipes (including reboiler pipes)	8.2
Lean/rich hx—lean side	0.5
Lean/rich hx—rich side	0.5
Lean cooler	0.3
TOTAL	38.2

2.3. Dynamic Process Model

Dynamic process modeling was carried out by means of the physical modeling language Modelica [53]. Modelica allows development of systems of differential and algebraic equations that represent the physical phenomena occurring in the different components of the system. The process models of the equipment typically found in a chemical absorption plant were obtained from a Modelica library called Gas Liquid Contactors (Modelon AB, Lund, Sweden) [54], and the commercial tool Dymola (Dassault Systèmes, Vélizy-Villacoublay, France) [55] was utilized to develop the models and carry out the simulations. The component models include absorber and stripper columns, sumps, lean and rich heat exchanger, stripper reboiler, overhead condenser, condensers, pipe models, pumps, valves, measurements and controllers. The dynamic process model of the amine plant at TCM DA presented in Figure 1 was developed by parameterizing, modifying and connecting the different models. For this purpose, the main process equipment, size, geometry and materials were considered; refer to Table 1. A key aspect for obtaining suitable dynamic simulation results is the consideration of the distribution of solvent inventory at the different equipment of the plant. Therefore, solvent inventory distribution was implemented in the dynamic process model; refer to Table 2. Finally, the equivalent regulatory control layer of the plant was applied in the dynamic process model; discussed later in Section 5.2. The models contained in the library have been presented elsewhere [56,57]; therefore only an overview of the models is presented in the following. Numerical integration of the resulting system of differential and algebraic equations was carried out in Dymola with the differential algebraic system solver (DASSL) implemented in Dymola [55]. The main assumptions applied are [56]:

- All chemical reactions occur in the liquid phase and are assumed to be in equilibrium.
- The flue gas into the absorber contains only CO_2, O_2, H_2O and N_2.
- MEA is non-volatile and not present in the gas phase.
- The total amount of liquid in the column is defined as the packing hold-up and the sump liquid hold-up.
- The reboiler is modeled as an equilibrium flash stage.
- The liquid in the column sumps and other large volumes are assumed to be ideally mixed.
- Mass and heat transfer between liquid and gas phase is restricted to packed section.
- Negligible temperature difference between the liquid bulk and interface to gas phase.
- No storage of mass and energy in the gas phase.
- All liquid from the packing bottom in the stripper is fed to the reboiler with a constant liquid level.
- Constant target packing hold-up.

The models of the absorber and stripper columns are developed based on the two-film theory; therefore, at the gas and liquid interface thermodynamic equilibrium is assumed. Interface mass transfer phenomena is modeled in packed sections with a rate-based approach with enhancement factor E [30], which takes into account the enhanced mass transfer due to chemical reactions; refer to Equations (3) and (4), where $c_{i,if}$ and $c_{i,b}$ are molar concentrations at liquid bulk and interface, A_{if} is the contact area, k_i are the mass transfer coefficients by Onda [58], T is the bulk phase temperature, and p_i are the partial pressures of the species in the gas phase. The pseudo-first order enhancement factor E is calculated as in Equation (5), where k_{CO_2} is the overall reaction constant for CO_2 and C_{MEA} the molar free MEA-concentration taken from [59], the diffusivity D_{CO_2} of CO_2 in aqueous MEA is calculated by the Stokes-Einstein relation and the diffusivity of CO_2 in water from [60]. C_{ef} is a pre-multiplying coefficient for calibration of enhancement factor. The packing characteristics of Koch Glitsch Flexipac 2X were considered for parameterizing the packing segments of the dynamic process model for absorber and stripper columns, with a surface area of 225 m^2/m^3 and a void fraction of 0.97.

$$\dot{n}_{i,l} = A_{if} k_{i,l} E\left(c_{i,b} - c_{i,if}\right) \qquad i = CO_2 \tag{3}$$

$$\dot{n}_{i,v} = \frac{A_{if} K_{i,v}\left(p_{i,b} - p_{i,if}\right)}{RT} \qquad i = CO_2,\ H_2O \tag{4}$$

$$E = C_{ef} \frac{\sqrt{C_{MEA} k_{CO_2} D_{CO_2}}}{k_{i,l}} \qquad i = CO_2 \tag{5}$$

Phase equilibrium at the gas-liquid interface is calculated as in Equations (6) and (7), where the solubility of CO_2 in water is considered by Henry's law, with He_i from [61]; activity coefficients γ_i are implemented from [61]; chemical equilibrium is assumed at the interface and liquid bulk, and the chemical equilibrium constants K_i implemented in the process model are obtained from Böttinger [61]. The Van't Hoff equation is utilized in order to infer the heats of reaction ΔH_r from the equilibrium constant; refer to Equation (8). The Chilton-Colburn analogy was employed to correlate sensible heat transfer between phases with the gas phase mass transfer coefficient. Latent heat connected to the transferred mass flow from one phase to the other is considered in the specific enthalpies of the individual species. The heat of evaporation and heat of solution are a function of temperature but are considered constant with solvent CO_2 loading. The gas phase model assumes ideal gas law, and the pressure of the column p is determined by the gas phase pressure drop.

$$y_i p = \gamma_i x_i\ He_i\ i = CO_2 \tag{6}$$

$$y_i p = \gamma_i x_i\ p_{i,sat}(T)\ i = H_2O \tag{7}$$

$$\frac{dlnK}{dT} = \frac{\Delta H_r}{RT^2} \tag{8}$$

The lean-rich heat exchanger is modeled as a static heat exchanger model with the ε-NTU (effectiveness—number of thermal units), and pure transport delay models are used to account for dead times included by the solvent hold-up within piping' volumes.

At the top of the absorber column a washer model is implemented, consisting of a volume model with phase separation that saturates the gas with water at the targeted temperature. A make-up stream of water is injected in the absorber sump to keep the H_2O mass balance of the system. MEA is assumed non-volatile in the model and therefore it is only present in the liquid phase. However, in the actual plant make-up MEA is required for operation and it is injected upstream the rich amine pump; refer to Figure 1.

3. Steady-State Validation of Dynamic Process Model

3.1. Steady-State Operating Cases

A test campaign was conducted at the amine plant at TCM DA using MEA, operated from 6 July until 17 October 2015. Table 3 shows the steady-state cases generated during the test campaign that were used in this work for dynamic process model validation purposes. The plant was operated with 30 wt. % MEA for all cases. The objective was to select a set of steady-state cases from the MEA campaign that could represent a wide range of steady-state operating conditions, including data from full capacity of volumetric flow rate fed to the absorber column. The steady-state cases were generated by varying the set points of the main pilot plant inputs, namely solvent circulation flow rate F_{solv} (refer to FT5 in Figure 1), reboiler duty ($\dot{Q}_{reb}$), and flue gas volumetric flow rate (F_{gas}). The steady-state cases represent a variation in operating conditions of the plant, especially on the flue gas volumetric flow rate load of the absorber, CO_2 capture rate, L/G ratio in the absorber and absorber packing height. Cases 1 to 5 are operated at absorber full flue gas capacity of around 60,000 Sm^3/h. A similar mass-based L/G ratio, of around 0.89, is kept in the absorber column during the steady-state operating cases with full capacity, with the exception of Case 4, where it is changed to 0.8, by varying the rich solvent mass flow rate. The main process variability in these cases is the change in reboiler duty, with CO_2 capture rate ranging from 85 to 68%. CO_2 capture rate was calculated with the method 1 described by Thimsen et al. [52]; refer to Equation (9), where F_{prod} refers to the product CO_2 flow rate (FT3 in Figure 1), and X_{CO_2} is the mass fraction of CO_2 in the absorber inlet (measured at GA1 in Figure 1). Note that here CO_2 capture rate has been named *Des* as it defines the desorption ratio utilized in Section 5.2. In addition, Cases 2 to 5 were operated with 18 m absorber packing, i.e., the uppermost absorber-packing segment is kept dry. Cases 6 to 10 are operated with 24 m absorber packing and the absorber column at 80% volumetric flue gas flow rate capacity. The mass-based L/G ratios on the absorber range from 1.34 to 0.75 for Cases 6 to 10, by varying solvent circulation mass flow rate. The capture rate is kept constant at around 85% by varying the reboiler duty.

Table 3. A selection of steady-state data cases obtained from the test campaign conducted at TCM plant during autumn 2015. The plant was operated with 30 wt. % aqueous MEA.

Case	1	2	3	4	5	6	7	8	9	10
Gas flow rate (Sm^3/h)	59,461	59,468	59,442	59,499	59,544	46,973	46,973	46,973	46,973	46,973
Rich solvent flow rate (kg/s)	17.33	17.31	17.22	15.50	17.24	20.56	17.50	16.11	12.74	11.46
L/G ratio (kg/kg)	0.89	0.89	0.89	0.80	0.89	1.34	1.14	1.05	0.83	0.75
Reboiler duty (kW)	3417	3159	2664	2397	3056	2745	2669	2667	2659	2682
Absorber inlet gas CO_2 (vol%)	3.64	3.61	3.59	3.58	3.59	3.60	3.62	3.62	3.62	3.62
Absorber inlet gas O_2 (vol%)	15.52	15.54	15.55	15.46	15.35	15.30	15.48	15.49	15.51	15.52
Absorber inlet gas H_2O (vol%)	3.98	3.92	3.93	4.01	4.22	3.80	3.36	3.46	3.52	3.43
Absorber inlet gas N_2 (vol%)	79.09	79.02	78.85	78.57	78.20	78.18	78.88	78.94	79.06	78.96
Loading rich (mol/mol)	0.490	0.485	0.498	0.500	0.495	0.475	0.488	0.486	0.493	0.491
Loading lean (mol/mol)	0.280	0.294	0.333	0.341	0.314	0.342	0.329	0.310	0.260	0.229
Stripper bottom temperature (°C)	120.9	121.1	119.1	118.9	120.1	116.6	118.3	119.1	121.4	121.8
CO_2 product flow (kg/s)	0.95	0.89	0.75	0.68	0.84	0.74	0.74	0.75	0.77	0.76
CO_2 capture rate (%)	85	80	68	-	75	85	85	85	85	85
Absorber packing height (m)	24	18	18	18	18	24	24	24	24	24

The first series of tests during the MEA campaign were dedicated to verification of mass balances of the plant [50]. CO_2 mass balance gives results close to 100%, and Gjernes et al. [50] conclude that CO_2 mass balance based on gas phase can be maintained at a level better than 100 ± 5%. In this work, the suggested method in [50] was used during data selection in order to ensure that the steady-state data cases presented in Table 3 have acceptable CO_2 mass balance.

In order to develop the overall dynamic process model of the plant, the steady-state data for Case 1, refer to Table 3, was used as a reference to calibrate the dynamic process model, and the main outputs from the model simulations were compared with the plant data. This data set was chosen since

it represents the baseline operating conditions of the amine plant at TCM DA when using aqueous MEA as chemical solvent, as presented in Faramarzi et al. [51]. The models of the different subsystems of the plant consisting of (i) absorber column; (ii) lean/rich heat exchanger; and (iii) stripper column with overhead condenser and reboiler were calibrated separately, and then linked to form the overall dynamic process model. The model was calibrated by tuning a pre-multiplying coefficient C_{ef} for the enhancement factor E. It was set to 0.28 in absorber packed segments and 0.01 in stripper packed segments. The validation section included in this work extends on work conducted previously [62].

$$Des = \frac{F_{prod}}{F_{gas} \cdot X_{CO_2}} \tag{9}$$

3.2. Validation Results of Dynamic Process Model with Steady-State Plant Data

The results from the simulated dynamic process model for the steady-state operating cases, described in Section 3.1, are displayed in Table 4. The results shown are for main process variables during pilot plant operation, namely CO_2 lean (L_l) and rich (L_r) loadings, product CO_2 flow rate (F_{prod}), specific reboiler duty (SRD) and stripper bottom temperature T_{str}. Possible deviations in dynamic process model prediction arise from errors related to measurement uncertainty and to modeling uncertainty, the latter being related to the fact that a physical model is always a simplification of reality. This means that it is natural to observe some deviation in the prediction of the dynamic process model simulation. Therefore, it is of importance to quantify these errors so that they are kept within reasonable bounds. The absolute percentage errors (AP) and the mean absolute percentage errors (MAP) are calculated as in Equations (10) and (11), where x_m is the value of the process variable predicted by the process model simulation, x_p is the value of the process variable measured at the pilot plant at the given steady-state operation case, and n is the number of steady-state cases studied.

$$AP = 100 \cdot \left| \frac{(x_m - x_p)}{x_p} \right| \tag{10}$$

$$MAP = 100 \cdot \sum_{i}^{n} \frac{\left| \frac{(x_{m,i} - x_{p,i})}{x_{p,i}} \right|}{n} \tag{11}$$

The results for lean CO_2 loading are presented in Figure 2 with a parity plot, where $\pm 5\%$ and $\pm 10\%$ error lines are also shown. It is clear that the dynamic process model under-predicts lean loading for most of the cases, with a $MAP < 6.6\%$. In addition, Figure 2 shows the parity plot for CO_2 product flow rate; in this case, the CO_2 product flow rate is also under-predicted by the dynamic process model, with a $MAP < 5.3\%$. Figure 3 shows the parity plot for stripper bottom temperature, with the $\pm 2\%$ error lines plotted; stripper bottom temperature T_{str} presented a $MAP < 1\%$. From the parity plots, one can observe that, despite the errors found in the absolute values predicted by the dynamic process model with respect to the reference plant data, the dynamic process model can predict the variability in the main process variables for a wide range of steady-state operating conditions.

Table 4. Results from dynamic process simulation of the amine plant at TCM for the 10 steady-state operation cases. The pilot plant data for solvent CO_2 lean loading (L_l), solvent CO_2 rich loading (L_r), CO_2 product flow rate (F_{prod}), specific reboiler duty (SRD) and stripper bottom temperature (T_{str}) are shown. In addition, the model prediction during steady-state simulation for the same process variables is shown. Calculated absolute percentage errors (AP) and mean absolute percentage errors (MAP) between pilot plant measurements and simulated model predictions for the 10 steady-state operating cases are presented.

Case		1	2	3	4	5	6	7	8	9	10
Rich loading L_r (mol/mol)	Pilot plant	0.489	0.485	0.498	0.500	0.495	0.475	0.488	0.486	0.493	0.491
	Model	0.514	0.513	0.514	0.514	0.513	0.512	0.513	0.514	0.514	0.514
	AP	5.01	5.58	3.19	2.91	3.55	7.81	5.17	5.62	4.43	4.70
	MAP										4.80
Lean loading L_l (mol/mol)	Pilot plant	0.282	0.294	0.333	0.341	0.314	0.342	0.329	0.310	0.260	0.229
	Model	0.257	0.273	0.309	0.306	0.279	0.343	0.312	0.292	0.241	0.224
	AP	8.93	7.24	7.16	10.06	11.34	0.35	4.98	5.94	7.10	2.35
	MAP										6.55
CO_2 Product flow F_{prod} (kg/sec)	Pilot plant	0.95	0.89	0.75	0.68	0.84	0.74	0.74	0.75	0.77	0.76
	Model	0.90	0.84	0.72	0.65	0.82	0.70	0.71	0.72	0.70	0.67
	AP	4.97	4.72	5.18	4.38	1.96	4.65	3.50	3.44	8.46	11.42
	MAP										5.27
Specific reboiler duty SRD (kJ/kg)	Pilot plant	3602	3562	3533	3509	3651	3727	3613	3561	3463	3538
	Model	3791	3739	3726	3670	3724	3909	3744	3688	3783	3994
	AP	5.23	4.95	5.46	4.58	2.00	4.88	3.63	3.56	9.24	12.89
	MAP										5.64
Stripper bottom temperature T_{str} (°C)	Pilot plant	120.9	121.1	119.1	118.9	120.1	116.6	118.3	119.1	121.4	121.8
	Model	121.0	119.8	117.2	117.2	119.4	114.7	117.0	118.3	121.0	121.8
	AP	0.08	1.06	1.63	1.42	0.61	1.62	1.10	0.71	0.31	0.04
	MAP										0.86

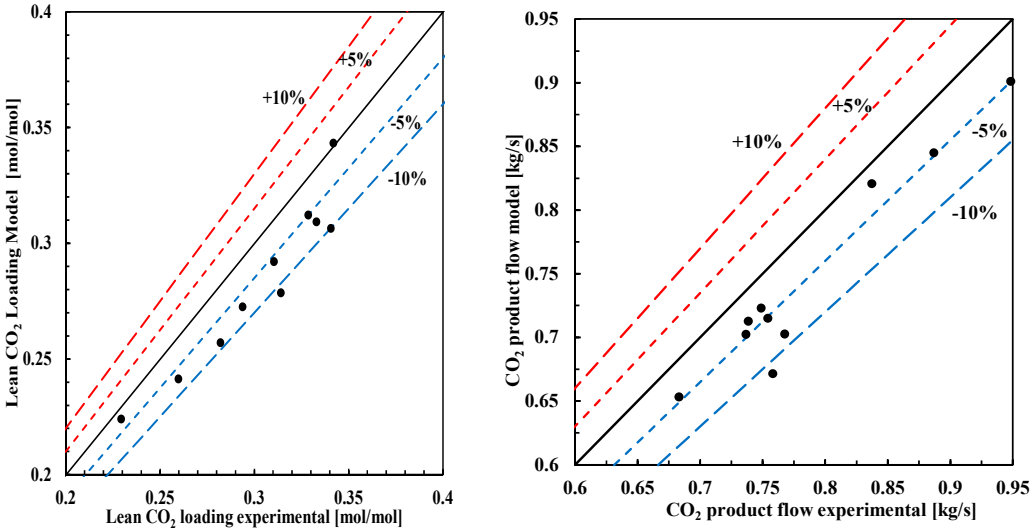

Figure 2. Parity plots of lean CO_2 loading (**left**) and CO_2 product flow rate (**right**). Lines for +10%, +5%, −5% and −10% percentage error are shown. The mean percentage error is <6.6% for CO_2 lean loading and <5.3% for product CO_2 flow rate (F_{prod}).

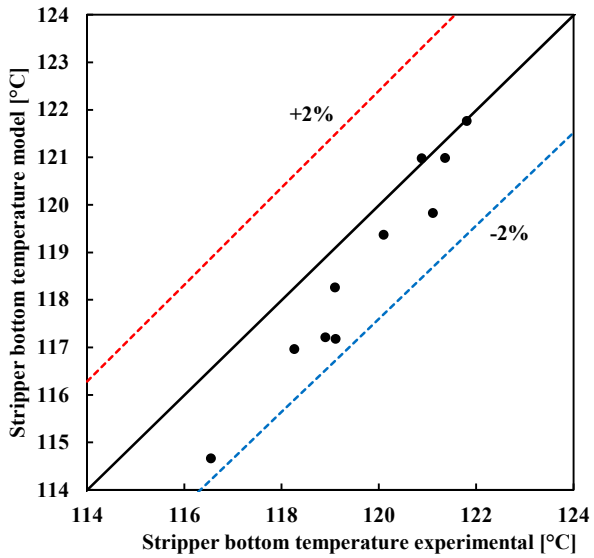

Figure 3. Parity plot for stripper bottom temperature for the 10 steady-state operation cases. Lines for +2% and −2% percentage errors are shown. The mean percentage error is 0.86 for stripper bottom temperature.

Temperature within absorber and stripper column is an important process variable since it affects phase equilibrium at liquid and gas-liquid interface. Some important model parameters and thermophysical properties depend on temperature, including heat capacity, water heat of condensation, heats of reaction, equilibrium constants and CO_2 solubility. Therefore, it is desirable that the dynamic process model can predict with good accuracy absorber and stripper columns' temperature profiles. Figure 4 shows the comparison between the pilot plant temperature profiles of the absorber and desorber columns with the predictions from the simulation of the dynamic process models. Two steady-state operating cases are presented: Case 1 (Table 3) with absorber flue gas volumetric capacity of 100%, mass-based L/G ratio of 0.89 and capture target of 85%; and Case 6 (refer to Table 3) with 80% flue gas volumetric capacity, mass-based L/G ratio of 1.34 and capture target of 85%.

Both cases were operated with 24 m of wet absorber packing, and represent two operating cases with different flue gas capacities and L/G ratios.

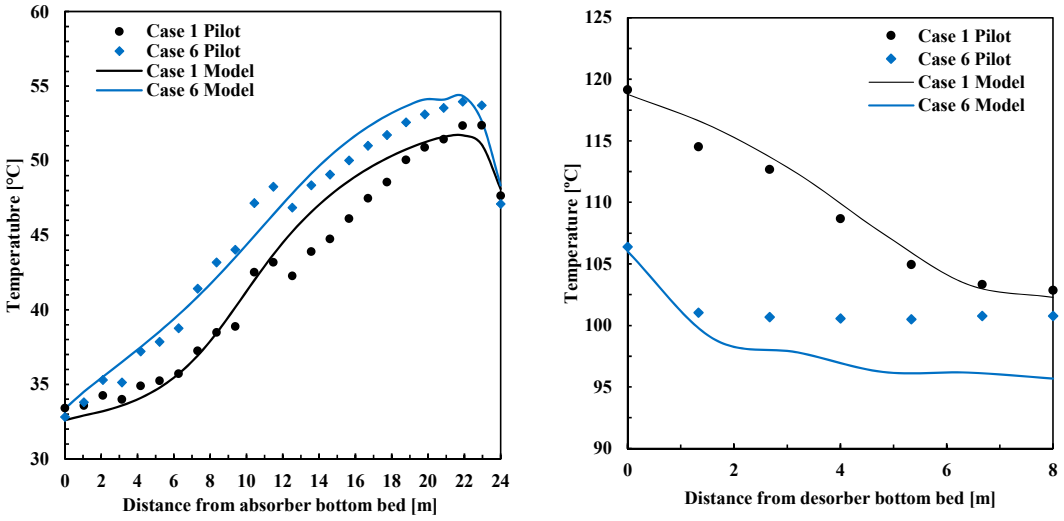

Figure 4. Temperature profiles for absorber column (**left**) and stripper column (**right**) for steady-state cases 1 and 6. In both steady-state operation cases, 24 m of absorber packing were utilized.

Validation of absorber and stripper temperature profiles is normally considered a challenging task for several reasons. At TCM DA the temperature profiles are the resulting averaged values of the 4 measurements distributed radially in a given axial position within the column; refer to Section 3. A given pilot plant temperature value presented in Figure 4 is the resulting average over time during one hour of steady-state operating conditions, of the averaged 4 temperature measurements radially distributed within the absorber or stripper column, at the given axial position of the column. The individual temperature measurements are considered reliable and the resulting temperature profiles are reasonable. However, some sensors are located closer to the center of the packing while others closer to the wall. This results in a maximum variation (<6 °C) which is observed between the measurements in the same radial plane, which depends on operating conditions and is different at different radial planes. Based on the results presented in Figure 4, the dynamic process model can properly predict absorber and stripper column temperature profiles with sufficient accuracy considering the purpose of application. Absorber temperature profiles predicted by the model show a good agreement with the experimental pilot plant data, and the model is capable of properly predicting the trends in temperature along the column. The absorber temperature profiles have a mean absolute percentage error (<2.5%) for Case 1 and (<2.1%) for Case 6, which is within the observed maximum variability of the temperature measurements in a given radial plane. In addition, desorber temperature profiles have a mean average error (<0.6%) for Case 1 and (<3.6%) for Case 6. It is the desorber temperature profile for Case 6 that presents the less accurate prediction. In addition, it can be concluded that the process model is capable of properly predicting the variation of temperature profiles for various steady-state operating conditions.

4. Validation of Dynamic Process Model with Transient Plant Data

For dynamic process model validation purposes transient tests are conducted by means of open-loop step changes in the main process inputs to the plant. The transient behavior occurs between the initial steady-state operating conditions until the new steady-state operating conditions are reached. In this work, the experiments consist of set-point changes in rich solvent flow rate, flue gas volumetric flow rate fed to the absorber and reboiler duty. The output trajectories of main process variables are observed and compared with the model output trajectories. In order to obtain good sets of data

for validation, it is desired to apply the step changes in plant inputs in a non-simultaneous manner. However, this is not normally easy to implement in practice. In order to compare the pilot plant experimental output trajectories with the output trajectories predicted by the dynamic process models, input trajectories were utilized in the dynamic simulations. This means that the measured time series of the inputs applied to the pilot plant during the tests were applied as disturbances or inputs to the dynamic process model; refer to Figures 5a, 6a and 7a. During the three tests, the regulatory control layer of the plant was active. In Figures 5 and 6, the time $t = 0$ corresponds to the point from which the set point of flue gas volumetric flow rate was changed. In Figure 7 the time $t = 0$ is the point from when the set point of rich solvent flow rate was changed.

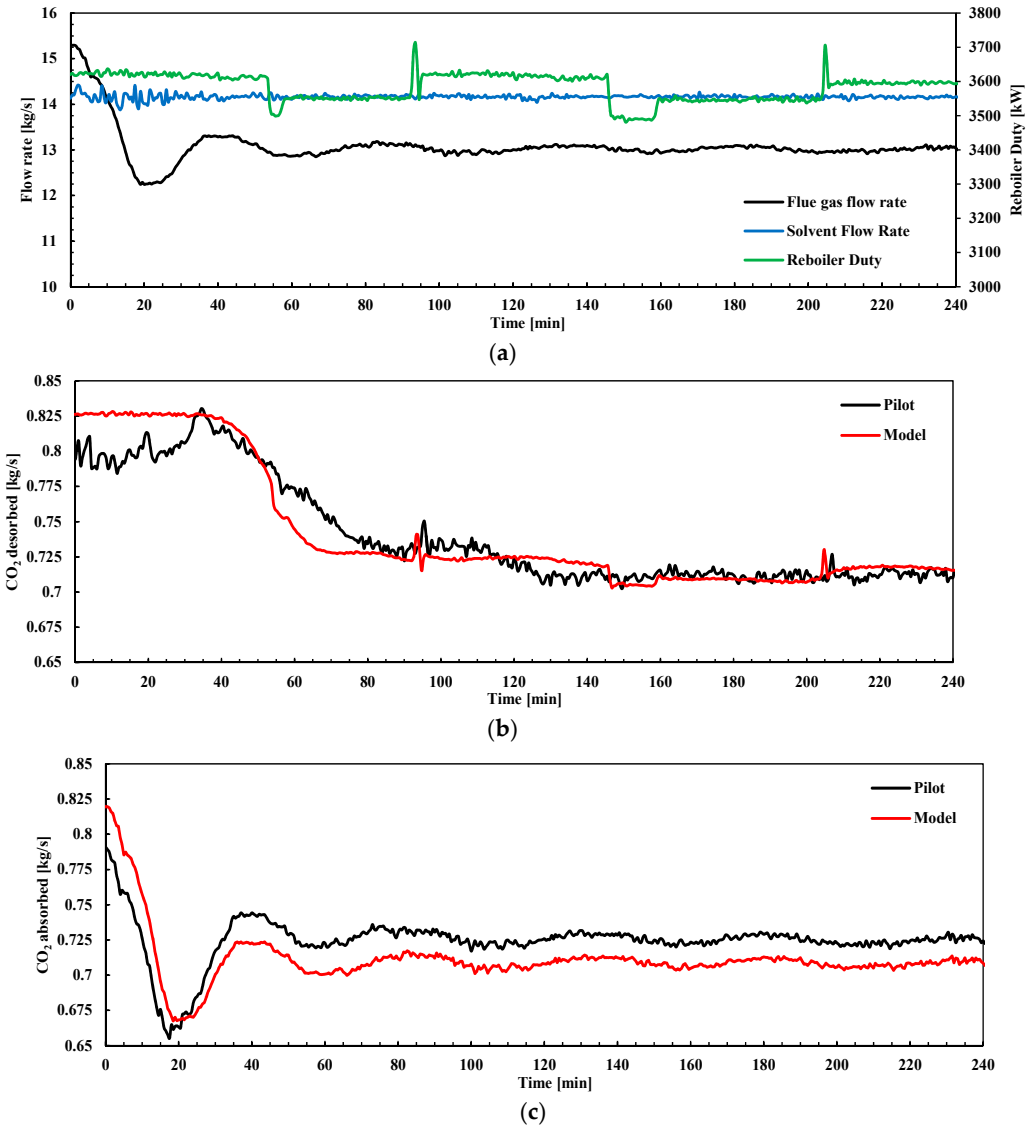

Figure 5. (**a**) Main inputs to the plant for test with flue gas flow rate set-point reduction (kg/s). Rich solvent flow rate from absorber (kg/s) and reboiler duty (kW); (**b**) Pilot plant transient response and model output trajectory for CO_2 product flow rate F_{prod} or CO_2 desorbed (refer to FT3 in Figure 1); (**c**) Pilot plant transient response and model output trajectory for CO_2 absorbed in absorber column, refer to Equation (11). The time $t = 0$ corresponds to the point from which the set point of flue gas volumetric flow rate was changed.

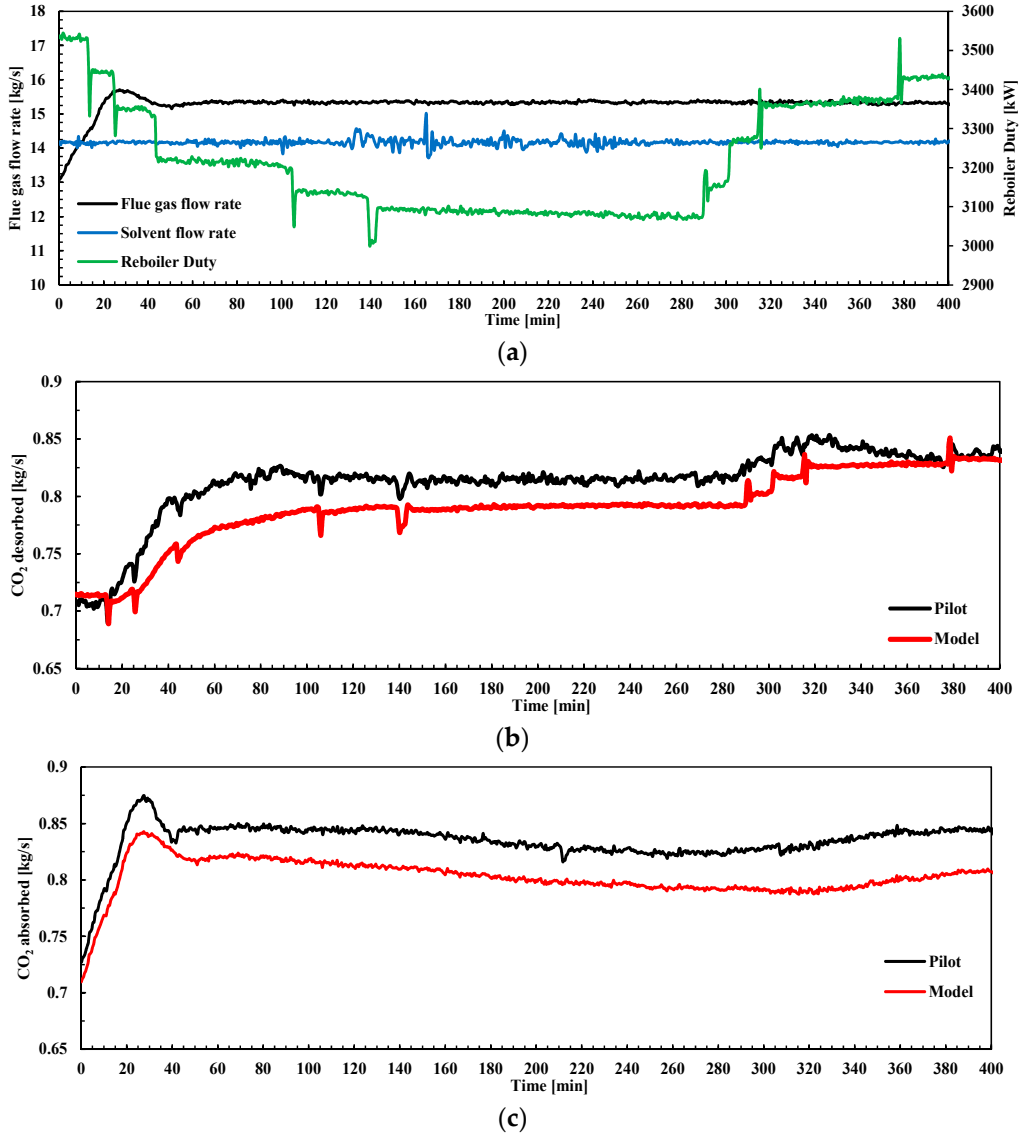

Figure 6. (**a**) Main inputs to the plant for test with flue gas flow rate set-point increase (kg/s). Rich solvent flow rate from absorber (kg/s) and reboiler duty (kW); (**b**) Pilot plant transient response and model output trajectory for CO_2 product flow rate F_{prod} or CO_2 desorbed (refer to FT3 in Figure 1); (**c**) Pilot plant transient response and model output trajectory for CO_2 absorbed in absorber column, refer to Equation (11). The time t = 0 corresponds to the point from which the set point of flue gas volumetric flow rate was changed.

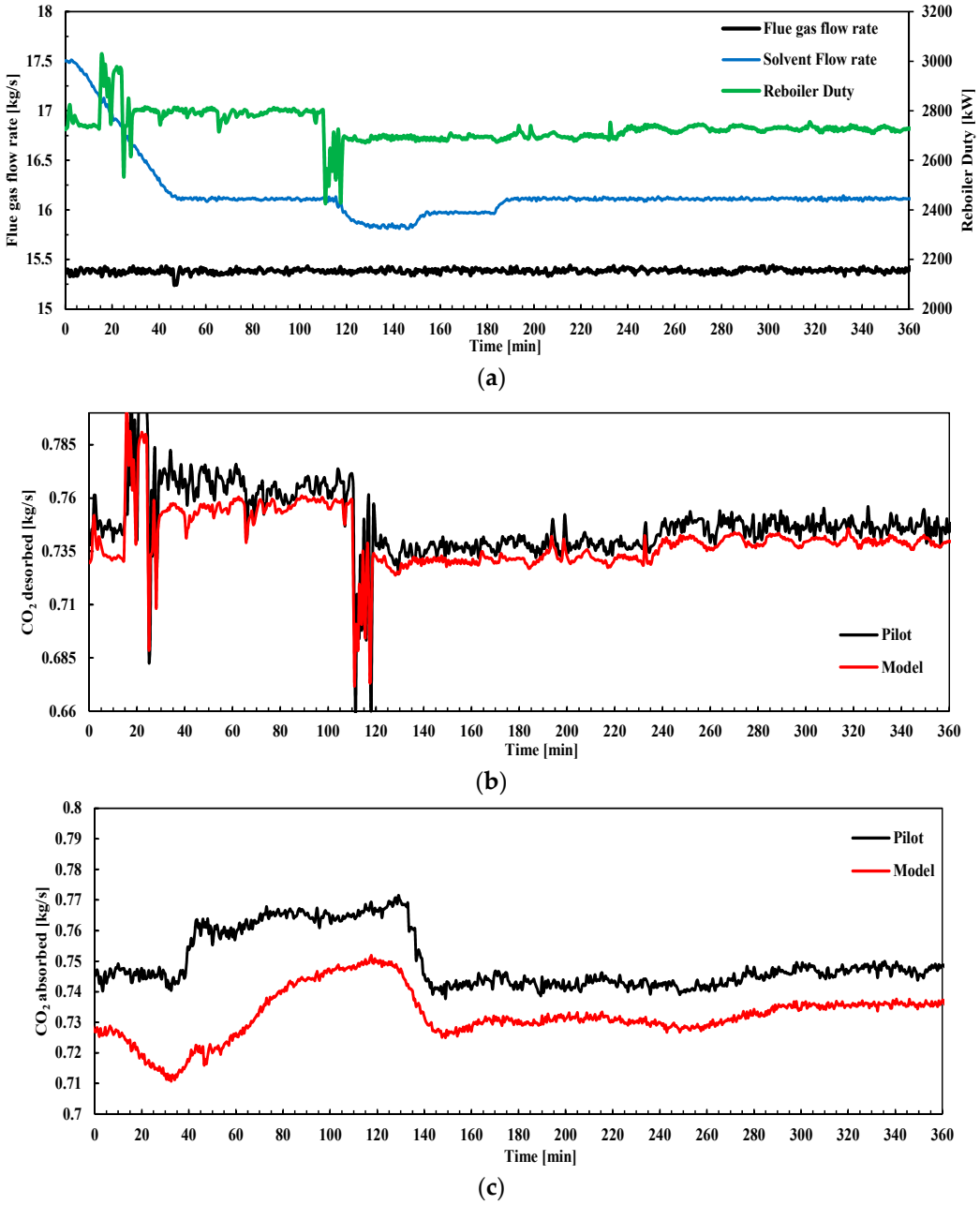

Figure 7. (**a**) Main inputs to the plant. Flue gas volumetric flow rate set-point change increase (kg/s). Rich solvent flow rate from absorber (kg/s) and steam flow to reboiler (kg/s); (**b**) Pilot plant transient response and model output trajectory for CO_2 product flow rate F_{prod} or CO_2 desorbed (refer to FT3 in Figure 1); (**c**) Pilot plant response in CO_2 absorbed mass flow rate (kg/s). The time $t = 0$ corresponds to the point from which the set point of rich solvent flow rate was changed.

4.1. Flue Gas Flow Rate Ramp-Down

The main disturbance applied in this transient test consisted of a reduction in flue gas volumetric flow rate at the inlet of the absorber. It was implemented at TCM DA pilot plant by changing the set point of the blower cascade controller from 47,000 Sm^3 to 40,000 Sm^3; refer to FT1 in Figure 1. This corresponds with flue gas volumetric flow capacities in the absorber column of 80% and 67% respectively. Figure 5a shows the three main inputs of the plant for this test. During the test, reboiler duty was changed in steps around the value of 3550 kW; this might be due to the effects of the

regulatory control layer on steam mass flow rate. The solvent mass flow rate had small amplitude oscillations around the set point.

$$CO_{2,abs} = F_{gas} \cdot X_{CO_2} - F_{depleted} \cdot X_{CO_{2,out}} \quad (12)$$

Figure 5b,c show the output trajectories of CO_2 product flow rate (or CO_2 desorbed) and CO_2 absorbed to the disturbance applied in this test. CO_2 absorbed is calculated as the difference between CO_2 mass flow rate at the absorber inlet and the CO_2 mass flow rate leaving the absorber with the depleted flue gas at the top of the absorber; refer to Equation (12). In Figure 5b, a dead time of around 40 min was observed, i.e., no significant changes are found in the CO_2 desorbed until around 40 min after the disturbance was applied to the pilot plant. In addition, the plant did not reach steady-state operating conditions until around 4 h later. As shown in Figure 5c, there is not significant dead time in the response of CO_2 absorbed. The difference observed between the output trajectories is characteristic of the coupled transient performance of the absorber and stripper columns. Figure 5b,c shows that the process model is capable of predicting the main process dynamics for CO_2 product mass flow rate (CO_2 desorbed), including an adequate prediction of dead times and stabilization time. In addition, the CO_2 absorbed transient performance trends are predicted in a satisfactory manner.

4.2. Flue Gas Flow Rate Ramp-Up and Step Changes in Reboiler Duty

These tests consist of combined input changes to the plant in terms of flue gas volumetric flow rate and reboiler duty. A set-point increase of the flue gas volumetric flow rate fed to the absorber from 40,000 to 47,000 Sm^3/h was applied. This corresponds with 67% and 80% of the absorber column capacity, respectively. In addition, step-changes in reboiler duty were applied during the transient test. Figure 6a shows the three main inputs of the plant during the test. Figure 6b,c show the CO_2 product flow and CO_2 absorbed for the model and the pilot plant data. In this test a dead time of around 20 min in the response of CO_2 desorbed was observed. This confirms the buffering effect by the chemical process in terms of the response of CO_2 desorbed when the flue gas volumetric flow rate is changed. There is evidence to support this observation in previous pilot plant studies [46–48]. The delay in the response is partly attributed to solvent circulation time and the redistribution of liquid. Despite the steady-state offset shown on CO_2 absorbed in Figure 6b, a good prediction of the main transient response is seen. It is possible that the reduction in reboiler duty at around 10 min flattens out the response in CO_2 product flow rate.

4.3. Solvent Flow Rate Ramp-Down

In this test, the plant is operated in steady-state until the rich solvent mass flow rate set point is ramped down from around 17.5 kg/s to around 16.1 kg/s; refer to FT5 in Figure 1. The reboiler duty and flue gas volumetric flow rate were intended to be kept constant. Figure 7a shows the three main inputs of the plant during this transient test. In addition, the pilot plant performance in terms of product CO_2 mass flow F_{prod} (or CO_2 desorbed) and absorbed CO_2 flow rate are presented, together with the dynamic process model simulations for this test. Again, a satisfactory agreement is found between the plant trajectories and the output trajectories predicted by the dynamic process model.

From the three transient tests presented above, it can be concluded that the dynamic process model predicts the transient trends of the main output trajectories of the process for different inputs to the plant. In addition, the dead times and stabilization times of the process are properly predicted by the dynamic process models, despite the steady-state deviations observed and already quantified in Section 3.2. This means that the dynamic process model is suitable for simulation studies at the plant scale, including dynamic process simulations to analyze the plant transient performance, and for control tuning and advanced control layer design, including control structure studies.

5. Case Study: Open-Loop Performance and Decentralized Control Structures

5.1. Open-Loop Step Responses at Different Plant Flue Gas Capacities

A power plant operated in a power market with a high penetration of renewables will most likely be operated in load-following mode [7,63]. This means that the power plant with PCC will be operated during a significant amount of its lifetime at part loads. In the case of a natural gas combined cycle power plant with post-combustion CO_2 capture it means that, at part-load operation, the gas turbine (GT) load will be reduced, generating a reduced mass flow rate of flue gas that would be conducted to the PCC unit. The purpose of this case study is to investigate the transient performance of the PCC pilot plant via dynamic process simulation by implementing open-loop step changes to the dynamic process model, and to compare the response of the plant at different part-load operating points, defined by different mass flow rates of flue gas to be treated. The analysis will assess the transient response of the plant to multiple and non-simultaneous step changes in three key inputs to the plant, namely (i) flue gas flow rate F_{gas} (ii) solvent flow rate F_{solv}; and (iii) reboiler duty $\dot{Q}_{reb}$, at different flue gas mass flow rate capacities of the plant. In order to define the part-load operating points, a decentralized control structure was utilized, in which reboiler duty was the manipulated variable to control stripper bottom temperature T_{str} to 120.9 °C, and the solvent flow rate was the manipulated variable to control CO_2 capture ratio *Cap* to 0.85, as defined in Equation (13). When operating the plant at different flue gas mass flow rates, corresponding to 100%, 80% and 60% of nominal mass flow rate, this results in the three steady-state operating points presented in Tables 5 and 6. The control structure is defined as control structure A in Table 7.

$$Cap = \frac{F_{gas} \cdot X_{CO_2} - F_{depleted} \cdot X_{CO_{2,out}}}{F_{gas} \cdot X_{CO_2}} \quad (13)$$

Table 5. Simulated pilot plant inputs' set points for the three operating points to be studied, corresponding to 100%, 80% and 60% of flue gas mass flow rate capacity of the pilot plant. With *Cap* = 0.85 and T_{str} = 120.9 °C for all cases.

Pilot Load (%)	F_{gas} (kg/h)	F_{solv} (kg/s)	$\dot{Q}_{reb}$ (MW)
100	19.3	17.6	3.5
80	15.3	13.2	2.7
60	11.6	9.5	2.1

Table 6. Simulated pilot plant values for the process variables, lean CO_2 loading L_l, rich CO_2 loading L_r, CO_2 capture ratio *Cap* and CO_2 product flow rate, at three different operating points of the plant, corresponding to 100%, 80% and 60% of flue gas mass flow rate capacity of the pilot plant. With *Cap* = 0.85 and T_{str} = 120.9 °C for all cases.

Pilot Load (%)	L_l (mol/mol)	L_r (mol/mol)	*Cap*	F_{prod} (kg/s)
100	0.280	0.501	0.85	0.91
80	0.246	0.514	0.85	0.72
60	0.228	0.514	0.85	0.55

Table 7. Control structures for the supervisory control layer of the TCM amine plant. Key manipulated variables (MVs) are solvent flow rate F_{solv} and reboiler duty Q_{reb}. Controlled variables are CO_2 capture ratio *Cap* to 85%, defined in Equation (12), and stripper bottom temperature T_{str} to 120.9 °C. Control structure D controls *Cap* via a feed forward FF controller.

	Pairing 1		Pairing 2	
Control Structure	**Manipulated Variable**	**Controlled Variable**	**Manipulated Variable**	**Controlled Variable**
A	F_{solv}	*Cap*	Q_{reb}	T_{str}
B	Q_{reb}	*Cap*	F_{solv}	T_{str}
C	F_{solv}	*L/G*	Q_{reb}	T_{str}
D	F_{solv}	*Cap, with FF*	Q_{reb}	T_{str}

The open-loop response was studied for the process variables (i) CO_2 absorbed $CO_{2,abs}$, in Equation (11); (ii) CO_2 desorbed $CO_{2,abs}$ (or F_{prod}); (iii) lean CO_2 loading L_l at the inlet of the absorber; and (iv) rich CO_2 loading L_r at the outlet of the absorber. To characterize the transient response, dead time θ, settling time t_s, total stabilization time t_t, and relative change (*RC*) were calculated:

- Dead time θ*:* it is the time that takes before a process variable starts to change from the initial steady-state conditions as a response to the disturbance or input.
- Settling time: The 10% settling time t_s is the time taken from when the process variable begins to respond to the input change (dead time) until it remains within an error band described by 10% of the change in the process variable Δy and the final steady-state value of the process variable y_∞, i.e.: $-0.1\ \Delta y + y_\infty < y_\infty < 0.1\ \Delta y + y_\infty$.
- Total stabilization time: the sum of the dead time θ and the settling time t_s is the resulting total stabilization time t_t.
- Relative change *RC:* Change in the observed process variable from initial steady-state conditions y_0 to the final steady-state conditions; refer to Equation (14).

$$RC(\%) = 100 \cdot \frac{y_\infty - y_0}{y_0} \tag{14}$$

The detailed results of the process simulations are presented in Tables A1–A3 in Appendix A. Figure 8 shows the total stabilization times for the selected process variables at the three operating points, for step changes in solvent flow rate and reboiler duty. The responses for step changes in flue gas flow rate are not presented, since it is shown in Table A1 that the relative change *RC* in the output process variables is very small or negligible (*RC* ranges from −0.81% to 0.21%). This can be explained by the highly diluted nature of the CO_2 in the flue gas (ca. 3.5 vol%). The results show the non-linear behavior of the plant, with different transient responses to step change set-point increase and decrease in key plant inputs, and at different loads of the plant.

Figure 8a shows the total stabilization time for lean CO_2 loading L_l at the inlet of the absorber, which ranges from 25 to 45 min in all cases. The results show that the required time for total stabilization increases when the plant is operated at lower loads. As shown in Appendix A (Tables A1 and A2), a general trend was that the dead time θ in the response of L_l to step changes in reboiler duty and rich solvent mass flow rate increases at part-load points. This could be explained by the fact that at lower loads the solvent mass flow rate is smaller (refer to F_{solv} in Table 6), resulting in longer residence times of the solvent through each equipment hold-up, piping, and recycle loop, this is, larger circulation time. This can also explain why dead times are generally larger when decreasing solvent flow rate than when increasing it; refer to Table A2 in Appendix A.

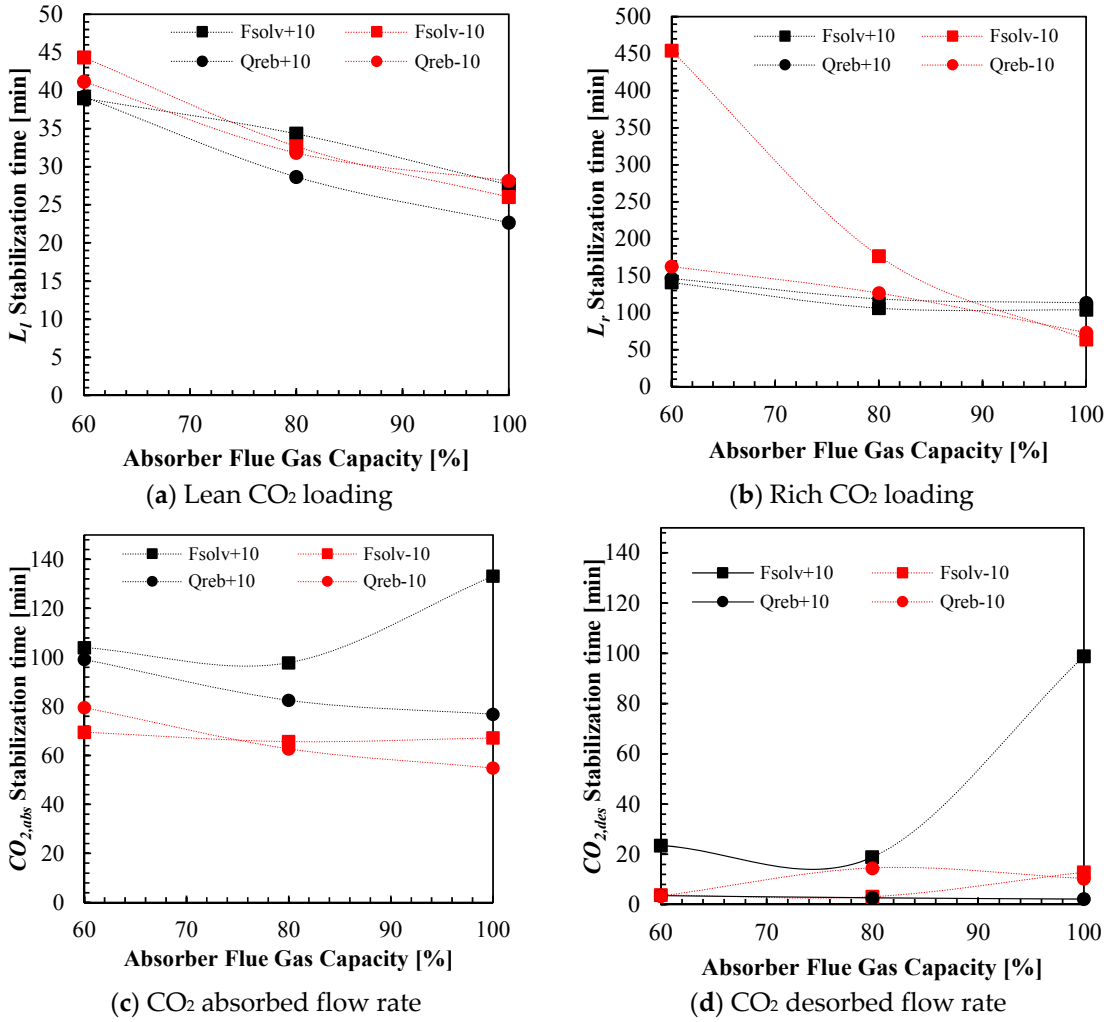

Figure 8. Simulation results. Total stabilization times t_s for open-loop ± 10% step changes in solvent flow rate and reboiler duty for the process variables (**a**) Lean CO_2 loading L_l; (**b**) rich CO_2 loading L_r; (**c**) CO_2 absorbed $CO_{2,abs}$ and (**d**) CO_2 desorbed $CO_{2,abs}$. Stabilization times are calculated for the response when the plant is operated at three different operating points in terms of flue gas mass flow rate, 100%, 80% and 60% of nominal capacity; refer to Tables 5 and 6.

Figure 8b shows the total stabilization times for rich CO_2 loading L_r at the outlet of the absorber sump. In this case, the stabilization times range from 60 to 450 min. It should be mentioned that the relative change *RC* in rich CO_2 loading is also small or negligible for the disturbances studied (see Appendix A), due to the fact that the solvent is operated close to its maximum loading capacity of 0.51 mol/mol CO_2 loading. The total stabilization times of the responses of rich CO_2 loading L_r to disturbances in solvent flow rate and reboiler duty are larger at lower plant loads. At 60% flue gas capacity, a very slow response is found in L_r when the solvent flow rate is decreased by a −10% step change; however, the relative change *RC* of L_r in this process variable is negligible for this plant disturbance; refer to Table A2 in Appendix A.

The total stabilization times for CO_2 absorbed $CO_{2,abs}$ response to disturbances in rich solvent mass flow rate F_{solv} and reboiler duty $\dot{Q}_{reb}$ are shown in Figure 8c. Total stabilization times range from 55 to 135 min. When the rich solvent mass flow rate is increased by 10%, this results in an increase in CO_2 absorbed with a relative change *RC* of 0.35% to 4.18% (refer to Table A2), due to the increased L/G ratio in the absorber column. However, since the reboiler duty is kept constant, the lean loading will increase (see *RC* values of L_l in Table A2). Due to the residence time in the hot solvent piping,

lean/rich heat exchanger and lean amine cooler of the recycle loop, it takes time for the solvent to be distributed towards the inlet of the absorber. A dead time in CO_2 lean loading L_l at the inlet of the absorber of 11 to 22 min is observed (see Table A2). This results in it taking a long time for the $CO_{2,abs}$ to stabilize. When the rich solvent mass flow rate is decreased by 10%, it is observed that the CO_2 absorbed $CO_{2,abs}$ decreases (relative change RC between −3.14% and −5.59% in Table A2). This is a result of the combination of the reduction in L/G ratio and the decrease in lean loading L_l. $CO_{2,abs}$ requiring time for stabilization (stabilization time of 65 to 69 min). When reboiler duty $\dot{Q}_{reb}$ is increased by 10%, the lean loading L_l is decreased significantly (RC ranging from 6.75 to 8.59%), which results in increase of $CO_{2,abs}$ (relative change RC of 4.0% to 6.07%). The change in lean loading L_l is observed at the absorber inlet with a dead time of 13 to 23 min (due to circulation time of the solvent in the recycle loop), and the total stabilization time for $CO_{2,abs}$ for increase in reboiler duty ranges from 76 to 99 min. When reboiler duty $\dot{Q}_{reb}$ is decreased by 10%, the solvent lean loading increases (RC of 6.63% to 8.46%), resulting in less CO_2 being absorbed. Relatively slower response in $CO_{2,abs}$ to disturbances in solvent flow rate and reboiler duty were found when the PCC was operated at lower loads (55 to 99 min). An exception is found for the case when the solvent flow rate is increased at 100% mass flow rate operating conditions of the plant.

Figure 8d shows the stabilization times for CO_2 desorbed $CO_{2,abs}$. For disturbances in rich solvent flow rate and reboiler duty, the desorbed CO_2 stabilizes slightly faster at lower loads (ranging from 2 to 100 min). In general, it was found that the desorption rate stabilized faster than the absorption rate $CO_{2,abs}$ for the disturbances in solvent flow rate and reboiler duty applied to the process. When solvent flow rate is decreased, this results in smaller L/G ratio in the absorber column and less CO_2 being desorbed in the stripper column. Since the rich CO_2 loading does not change significantly (RC in L_r from 0 to 0.08%), the CO_2 desorbed $CO_{2,des}$ stabilizes faster than the CO_2 absorbed (circulation time through the recycle loop is not affecting the stabilization of $CO_{2,abs}$). When the reboiler duty $\dot{Q}_{reb}$ is increased by 10%, the relative change in CO_2 desorbed is large (4 to 6.07% in Table A3), and with fast total stabilization time (2 to 3 min in Table A3). A change in reboiler duty results in a fast response in the produced stripping vapors, which also results in a fast response in CO_2 product flow rate (CO_2 desorbed). The longest stabilization time for CO_2 desorbed is found when the solvent flow rate is increased at 100% operating conditions. It is notable that there is a big difference in total stabilization times for solvent flow rate increase at different loads of the plant.

5.2. Decentralized Control Structures

In this section, four control structures for the TCM DA amine plant were tested via dynamic process model simulations. The scenario considers realistic load changes on the power plant, by changing flue gas flow rate feed to the absorber column. From a control analysis perspective, flue gas flow rate change can be considered as a disturbance applied to the PCC process. A load change event would result in a significant change in flue gas flow rate, at a ramp rate given by GT operation and controls. Fast ramp rates are the goal of power plant operators, since a fast power plant can respond to the variability in costs in a day-ahead power market [7,64]. For a NGCC power plant, a fast ramp rate is considered to be around 10%/min GT load [4,65]. Two tests were considered and simulated:

- Test 1: Ramping down flue gas flow rate from 100 to 70% in 3 min. The transient event starts at t_0 = 0 min, and sufficient simulation time is allowed for the plant to reach the new steady-state.
- Test 2: Flue gas flow rate is ramped up from 70 to 100% in 3 min. The transient event starts at t_0 = 0 min, and sufficient simulation time is allowed for the plant to reach the new steady-state.

The supervisory or advanced control layer of the TCM DA amine plant has three main degrees of freedom, consisting of set point of flue gas volumetric flow rate F_{gas}, set point of rich pump solvent flow rate F_{solv}, and steam flow rate to feed the reboiler duty $\dot{Q}_{reb}$; refer to FT1, FT5 and FT4, respectively in Figure 1. Under normal and stable operation of the pilot plant at TCM DA, such degrees of freedom

are changed manually by the operators to bring the plant to different operating conditions. If flue gas flow rate is considered to be a disturbance, there are two degrees of freedom left for operation. Note that here we do not consider the degrees of freedom available to the operators in the stabilizing or regulatory control layer, or for other auxiliary operations of the plant, or start-up procedures. Several studies in the literature suggest that keeping the capture ratio *Cap* and a temperature in the stripper column constant can lead to efficient operation of the process for varying loads of the PCC absorber-desorber process [13]. In this analysis, four control structures were tested, as presented in Table 7. All the feedback control loops are PI controllers, and were tuned with the simple internal model control (SIMC) tuning rules [66].

- **Control structure A** uses F_{solv} to control capture ratio at the top of the absorber *Cap* defined by Equation (13) to the set point of 0.85, and reboiler duty $\dot{Q}_{reb}$ to control the solvent temperature at the stripper bottom T_{str} to the set point of 120.9 °C. This control structure has been previously proposed in the literature in different studies including [14,16], where it shows a fast response and the capability to reject disturbances.
- **Control structure B** uses F_{solv} to control the solvent temperature at the stripper bottom T_{str} to the set point of 120.9 °C, and reboiler duty $\dot{Q}_{reb}$ to control capture ratio at the top of the absorber *Cap* to the set point of 0.85. Note that changes in reboiler duty result in a big change in solvent lean CO_2 loading (large relative change *RC*; see Appendix A). A similar version was suggested by Panahi and Skogestad [14], where it was found that this control structure showed similar dynamic behavior, in response to disturbances in flue gas flow rate, compared with a model predictive control scheme (MPC).
- **Control structure C** utilizes solvent flow rate F_{solv} to control the mass-based L/G ratio in the absorber column at the same value as that in the close-to-design-point operating conditions. This control structure has been studied previously in [12,15]. This control loop is implemented via ratio control. In addition, reboiler duty is manipulated to control T_{str} to 120.9 °C. The control structure leads to different final steady-state operating conditions when ramping down the plant load than the other three alternatives.
- **Control structure D** is a modification of control structure A. In this control structure, the solvent flow rate set point is changed via a feed forward (FF) action to control the capture ratio *Cap* at 0.85; in addition, the stripper bottom temperature is controlled by manipulating the reboiler duty. The feed forward controller is implemented by a set-point ramp change in the solvent flow rate with the same total duration as the flue gas flow rate ramp change, to the final value that gives a *Cap* of 0.85 under final steady-state conditions.

Figure 9 shows the simulated time input trajectories during the test with flue gas flow rate reduction. The manipulated variables F_{solv} and $\dot{Q}_{reb}$ are shown for the different control structures evaluated. Figure 10 shows the output trajectories of CO_2 capture ratio *Cap*, desorption ratio *Des*, CO_2 absorbed and CO_2 desorbed for the transient tests of flue gas flow rate reduction. Figure 11 shows the trajectories of lean loading L_l and stripper bottom solvent temperature T_{str} for flue gas flow rate reduction. In addition, Figure 12 shows the simulated time input trajectories during the test with flue gas flow rate increase. Figure 13 shows the output trajectories of CO_2 capture ratio *Cap*, desorption ratio *Des*, CO_2 absorbed and CO_2 desorbed for the transient tests of flue gas flow rate increase, and Figure 14 shows the trajectories of lean loading L_l and stripper bottom solvent temperature T_{str} for flue gas flow rate increase. In order to compare the different control structure performances during transient load change, the total stabilization times of the selected process variables are shown in Table 8. These will indicate how fast the plant achieves stabilization of the different floating (not controlled) process variables when moving from one operating condition to the next one. In addition, three transient performance indicators have been considered and presented in Table 9. Note that, for this analysis auxiliary consumptions of the plant are not considered.

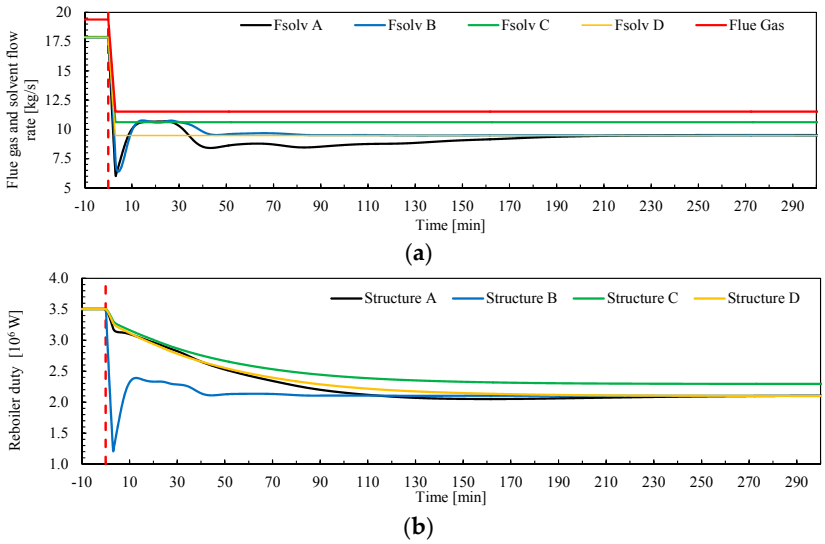

Figure 9. Inputs to the pilot plant during simulations for load change ramp-down (Test 1) from 100 to 70% with a ramp rate of 10%/min reduction in flue gas flow rate, for control structures A, B, C and D. (**a**) Flue gas flow rate (kg/s), as a disturbance, and solvent flow rates (kg/s) of the rich pump as manipulated variables (MVs); (**b**) Reboiler duty (W) as MV. The red vertical dotted line shows when the transient event starts at t_0.

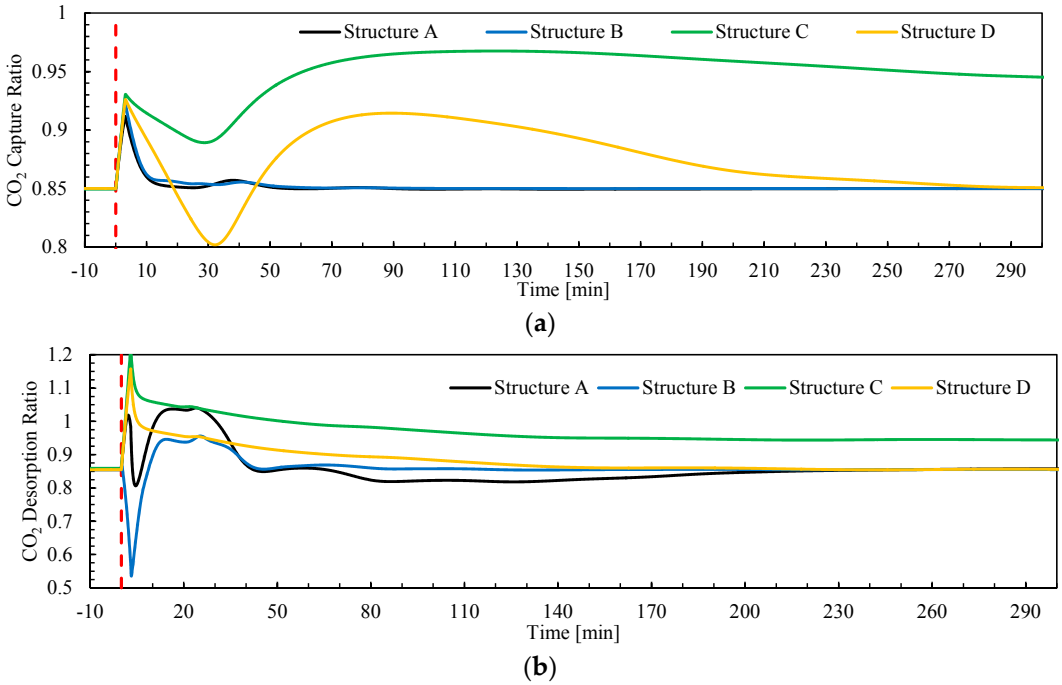

Figure 10. *Cont.*

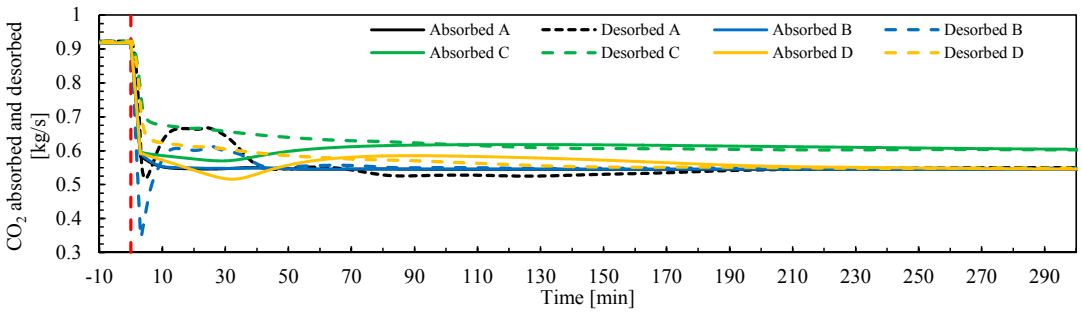

(**c**)

Figure 10. Outputs from pilot plant model during simulations for load change ramp-down (Test 1) from 100 to 70% with a ramp rate of 10%/min reduction in flue gas flow rate, for control structures A, B, C and D. (**a**) CO_2 capture ratio *Cap*, as controlled variable (CV); (**b**) CO_2 desorption ratio *Des*; (**c**) CO_2 absorption and desorption rates (kg/s). The red vertical dotted line shows when the transient event starts at t_0.

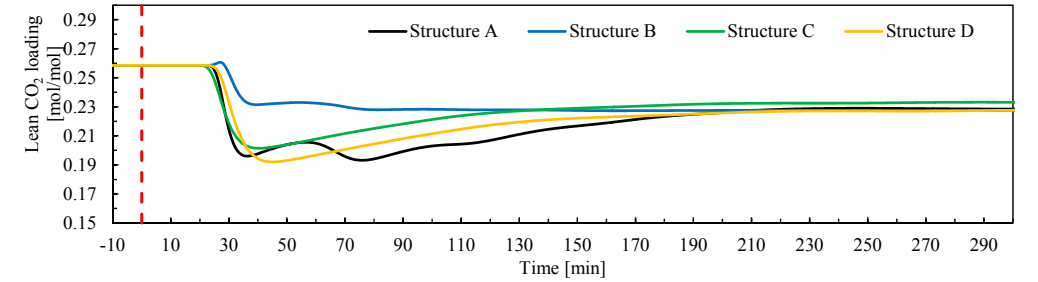

(**a**)

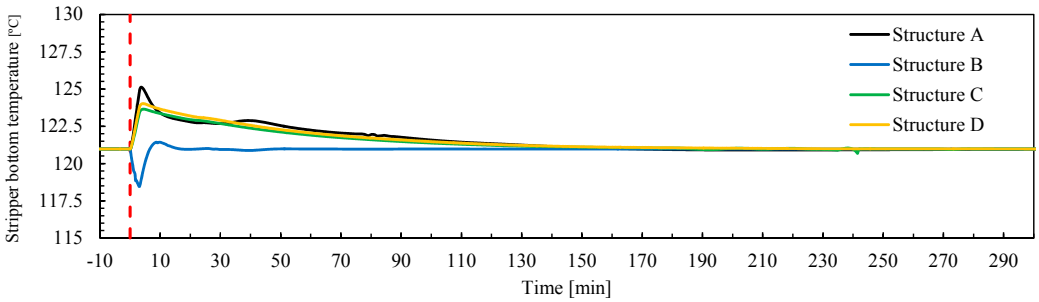

(**b**)

Figure 11. Outputs from pilot plant model during simulations for load change ramp-down (Test 1) from 100 to 70% with a ramp rate of 10%/min reduction in flue gas flow rate, for control structures A, B, C and D. (**a**) Lean CO_2 loading at the inlet of the absorber; (**b**) Stripper bottom temperature as controlled variable (°C). The red vertical dotted line shows when the transient event starts at t_0.

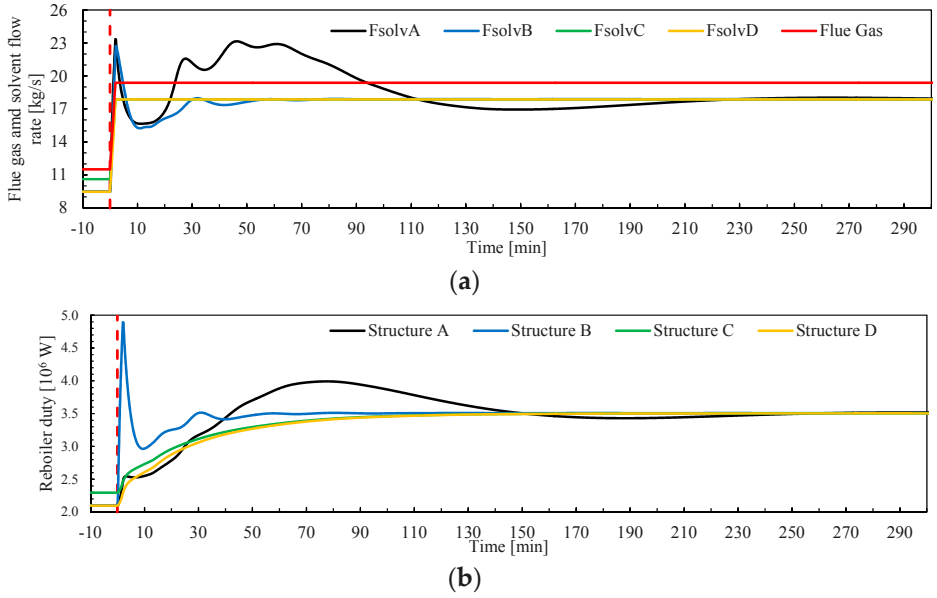

Figure 12. Inputs to the pilot plant during simulations for load change ramp-up (Test 2) from 70 to 100% with a ramp rate of 10%/min increase in flue gas flow rate, for control structures A, B, C and D. (**a**) Flue gas flow rate (kg/s), as a disturbance, and solvent flow rates (kg/s) of the rich pump as manipulated variables (MVs); (**b**) Reboiler duty (W) as MV. The red vertical dotted line shows when the transient event starts at t_0.

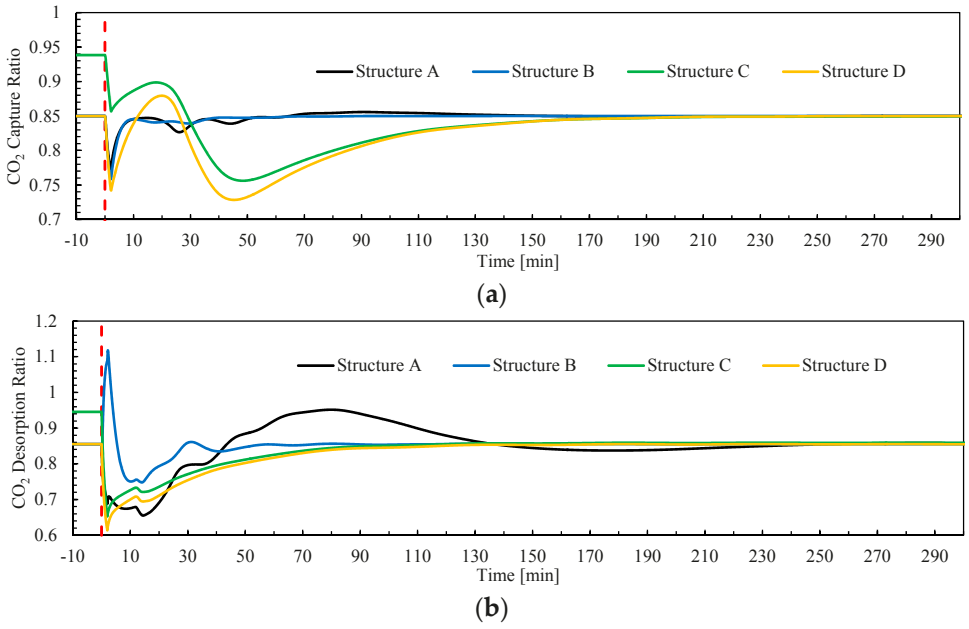

Figure 13. *Cont.*

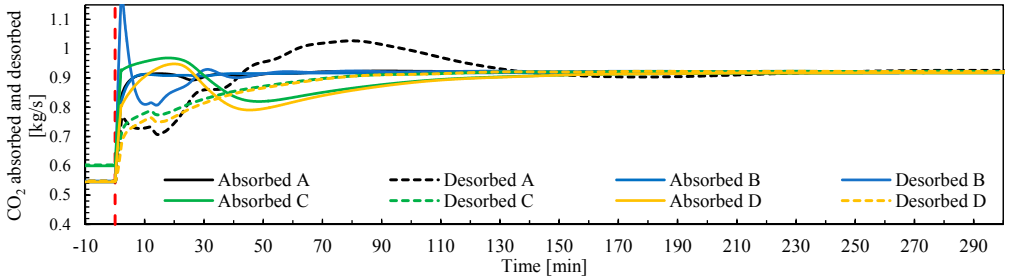

(**c**)

Figure 13. Outputs from pilot plant model during simulations for load change ramp-up (Test 2) from 70 to 100% with a ramp rate of 10%/min increase in flue gas flow rate, for control structures A, B, C and D. (**a**) CO_2 capture ratio *Cap*, as controlled variable (CV); (**b**) CO_2 desorption ratio *Des*; (**c**) CO_2 absorption and desorption rates (kg/s). The red vertical dotted line shows when the transient event starts at t_0.

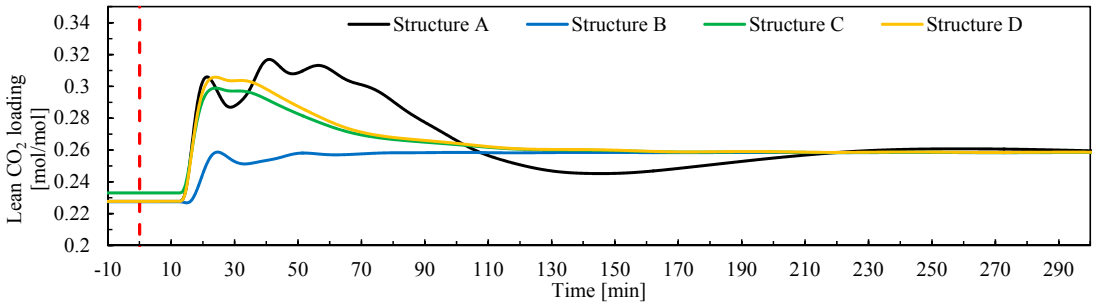

(**a**)

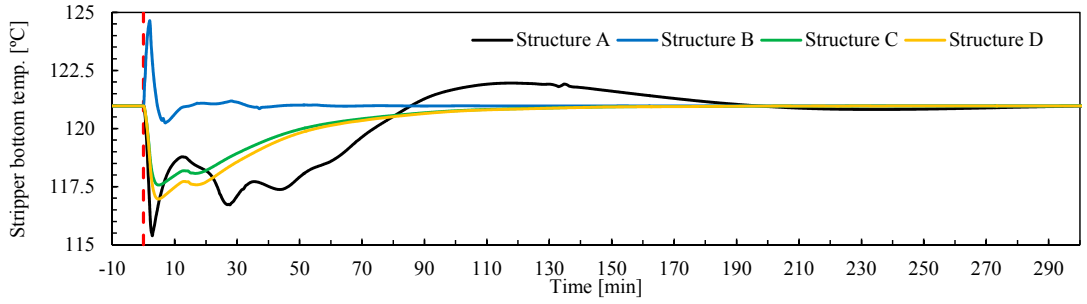

(**b**)

Figure 14. Outputs from pilot plant model during simulations for load change ramp-up (Test 2) from 70 to 100% with a ramp rate of 10%/min increase in flue gas flow rate, for control structures A, B, C and D. (**a**) Lean CO_2 loading at the inlet of the absorber; (**b**) Stripper bottom temperature as controlled variable (°C). The red vertical dotted line shows when the transient event starts at t_0.

Table 8. Total stabilization times of the floating process variables for the different control structures, when ramping down the plant $t_{t,down}$ from 100% flue gas mass flow rate to 70%; and when ramping up the plant $t_{t,up}$ from 70% flue gas mass flow rate to 100%.

Control Structure	Process Variable	$t_{t,down}$ (min)	$t_{t,up}$ (min)
A	CO_2 Absorbed	3.3	71.0
	CO_2 Desorbed	36.3	112.7
	L_l	187.7	201.0
B	CO_2 Absorbed	4.0	5.2
	CO_2 Desorbed	35.3	27.5
	L_l	68.2	46.7
C	CO_2 Absorbed	3.6	97.7
	CO_2 Desorbed	56.5	63.7
	L_l	172.2	115.5
D	CO_2 Absorbed	6.2	96.8
	CO_2 Desorbed	50.3	59.2
	L_l	185.0	113.8

Table 9. Simulation results for accumulated reboiler energy consumption Q_{reb} (MJ), accumulated CO_2 emitted $CO_{2,em}$ and accumulated CO_2 captured $CO_{2,cap}$ during the transient event (8 h) for the different control structures A,B, C and D (refer to Table 7), when ramping up and down the plant (between 100% and 70% of flue gas mass flow rate). Static plant refers to an ideal static plant that changes from the initial operating conditions to the final operating conditions instantaneously at time $t = 0$. An integration time of $t_f = 480$ min was utilized to calculate the values for the ideal static plant.

Transient Event	Indicator	Static Plant	A	B	C	D
Ramp down	Q_{reb} (MJ)	60,441	63,353	60,926	69,045	64,046
	$CO_{2,em}$ (tons)	2.66	2.64	2.65	0.96	2.39
	$CO_{2,cap}$ (tons)	15.70	15.76	15.75	17.44	16.01
Ramp up	Q_{reb} (MJ)	100,924	100,898	100,655	98,973	98,667
	$CO_{2,em}$ (tons)	4.49	4.51	4.53	4.77	4.94
	$CO_{2,cap}$ (tons)	26.41	26.39	26.37	26.13	25.96

- **Accumulated reboiler energy input Q_{reb} (MJ)**: see Equation (15). This is calculated by integration of the $\dot{Q}_{reb}$ trajectory under the transient event, from the initial time $t_0 = 0$ min to the final time $t_f = 480$ min (8 h). The final time was defined to ensure that the plant was already under steady-state conditions at the final operating point. This value Q_{reb} represents the main energy consumption of the process during the transient event of load change. In addition, the consumption of an ideal static plant is included for comparison (see Table 9). The ideal static plant is assumed to change from initial to the final steady-state operating conditions instantaneously at time t_0, and would operate until t_f. The static plant value represents the minimum value when ramping down and a maximum value when ramping up.

$$Q_{reb} = \int_{t_0}^{t_f} \dot{Q}_{reb}(t)dt \tag{15}$$

- **Accumulated CO_2 emitted $CO_{2,em}$ (tons)**: see Equation (16). This is calculated by integration of the $\dot{m}_{CO_2}$ trajectory under the transient event, from the initial time $t_0 = 0$ min to the final time $t_f = 480$ min; this represents the CO_2 emitted at the absorber stack. The final time was defined to ensure that the plant was already under steady-state conditions at the final operating point. This measure represents the CO_2 emitted during the transient event of load change.

For comparison, the CO_2 emitted by an ideal static plant is calculated (considered as the maximum value when ramping down and a minimum value when ramping up), shown in Table 9.

$$CO_{2,em} = \int_{t_0}^{t_f} \dot{m}_{CO_2}(t)dt = \int_{t_0}^{t_f} \dot{m}_{depleted}(t) \cdot X_{CO_2}(t)dt \quad (16)$$

- **Accumulated CO_2 captured $CO_{2,cap}$ (tons)**: see Equation (17). This is calculated by integration of the CO_2 absorbed $CO_{2,abs}$ trajectory (Equation (12)) under the transient event, from the initial time t_0 = 0 min to the final time t_f = 480 min. The final time was defined to ensure that the plant was already under steady-state conditions at the final operating point. This measure represents the CO_2 captured during the transient event of load change. For comparison, the CO_2 captured by an ideal static plant is calculated (considered as the minimum value when ramping down and a maximum value when ramping up), shown in Table 9.

$$CO_{2,cap} = \int_{t_0}^{t_f} \left(F_{gas}(t) \cdot X_{CO_2}(t) - F_{depleted}(t) \cdot X_{CO_{2,out}}(t) \right) dt \quad (17)$$

Figure 10 shows that the CO_2 capture ratio *Cap* had similar trajectories for control structures A and B during Test 1 (flue gas ramp-down), and that *Cap* reached stabilization conditions faster (20–50 min) than control structures C and D (around 270 min). *Cap* had also larger excursions from the set point than when control structures A and B are utilized. The same trends are found for Test 2 with flue gas flow rate ramp-up (Figure 13). When ramping up, control structures C and D stabilize faster (around 160 min) than when ramping down. This showed that the utilization of close-loop feedback control (structures A and B) allows shorter stabilization times to be reached for the controlled variable CO_2 capture ratio *Cap*. The desorption ratio *Des* trajectories in Figure 10 show that the plant requires the shortest stabilization time for this process variable when employing control structure B (around 60 min), followed by control structure A and C (around 200 min). This can be explained by the fact that for a change in reboiler duty the response of CO_2 desorbed has a fast total stabilization time and a large static relative change *RC* (where *RC* ranges from 4 to 6.29% and total stabilization time range from 2.2 to 3.5 min for a +10% step in reboiler duty); refer to Table A3. When it comes to the stabilization time required for *Des* for Test 1, structures C and D presented a poorer performance as the trajectories for *Cap* and *Des* deviate from the set point significantly. For control structure A, *Des* showed slow performance for Test 2 (around 210 min total stabilization time) with significant oscillations around set point; refer to Figure 13.

When ramping down the plant, CO_2 absorbed and CO_2 desorbed require similar stabilization times for control structures A and B (around 3 min for $CO_{2,abs}$ and 36 min for $CO_{2,abs}$), while the control structures C and D require longer stabilization times for CO_2 desorbed (around 50 to 57 min); refer to Table 8. The trajectory of CO_2 lean loading again shows shorter stabilization time for control structure B. This can be explained by the large static relative change *RC* of the response of CO_2 lean loading to changes in reboiler duty (where *RC* ranges from −6.29% to −4.97% and total stabilization time range from 22.7 to 39.2 min for a +10% step in reboiler duty); refer to Table A3. This contributes to the tight control of CO_2 capture ratio *Cap* achieved by control structure B, since the CO_2 lean loading L_l is a key process variable that connects the operation of the stripper and the absorber columns via the recycle loop. In addition, control structure B shows the shortest stabilization times and smaller excursions of the stripper bottom temperature T_{str} (around 15 to 30 min), in Figures 11 and 14.

When the plant load is ramped up from 70 to 100% (Test 2), the control structure B in general showed a faster dynamic performance with significantly shorter stabilization times required for the floating process variables considered (5.2 min for $CO_{2,abs}$, 27.5 min for $CO_{2,abs}$ and 46.7 min for L_l), see Table 9; followed by C, D and A. Note that control structure B presented a faster dynamic performance towards stabilization while ramping up (L_l stabilizes in 46.7 min) than when ramping down the process (L_l stabilizes in 68.2 min). Control structures A, C and D required shorter stabilization

times for CO_2 absorption and CO_2 desorption when ramping down the process load, while CO_2 lean loading stabilized faster when ramping up the plant load; refer to the stabilization time values in Table 9. When the plant is operated under control structure C, the optimum solvent flow rate F_{solv} and lean loading L_l are not reached at the 70% absorber capacity steady-state operating conditions; refer to time >250 min in Figures 9a and 11a, and time <0 min in Figures 12a and 14a. This leads to a higher *Cap* than specified (refer time $t > 290$ min in Figure 10a and time $t < 0$ min in Figure 13a), and therefore higher reboiler duty (time $t > 290$ min in Figure 9b and time $t < 0$ min in Figure 12b), even though the stripper bottom temperature T_{str} criterion is satisfied.

During the ramp-down transient event of the plant (i.e., period of 8 h from the time change was implemented), the least energy-intensive performance measured by Q_{reb} in Table 9 was observed for control structure B. In addition, this structure shows the largest CO_2 emissions during the transient event, albeit still lower than the ideal static plant. The fast stabilization time of the plant process variables achieved by control structure B provides a transient performance that is the closest to the ideal static plant. Control structures C and D showed the largest CO_2 captured during the transient event. However, when ramping down the plant load, this means that the plant is emitting less CO_2 during the transient event with control structures A, B, C and D than that established by the operational objective and represented by the ideal static plant case. Consequently, when ramping down the plant load, CO_2 emissions will always be lower than those of the equivalent ideal static plant. In addition, the plant is capturing more CO_2 than the ideal static plant. Figure 10a shows how there are periods of time in which the capture ratio *Cap* is above the target of 0.85, leading to more CO_2 being captured than the ideal static plant during the transient event. Control structures A and B showed the largest CO_2 emitted when compared with the ideal static case. Despite control structure A presenting a similar amount of CO_2 emitted during the transient event, it requires a larger amount of energy input during this period than control structure B. Therefore, control structure B shows the best performance in terms of energy consumption and CO_2 emissions during the transient load change event of ramping down the PCC plant load. When ramping up the plant load the most energy-intensive control structure is control structure B. However CO_2 emissions are the lowest, being closer to the minimum established by the static plant. This means that, when ramping up the plant load, CO_2 emissions will always be higher than those of the equivalent ideal static plant. While control structure D is the least energy-intensive process during the transient event of load change increase, it is the control structure with the largest CO_2 emissions during this transient event.

6. Conclusions

The pilot plant data obtained in this work from an MEA campaign at TCM DA amine plant includes ten steady-state operating data sets. The data sets consist of a wide range of steady-state operating conditions of the chemical absorption process in terms of L/G ratio in the absorber column, different absorber packing heights, CO_2 capture ratios, reboiler duty and flue gas flow rate fed to the absorber. The data is considered reliable and valid and can be used for process model validation purposes. In addition, the three transient data sets presented in this work represent transient operation of the pilot plant driven by set-point changes in flue gas flow rate, solvent circulation flow rate and reboiler duty. The transient data sets are considered reliable and suitable for dynamic process model validation purposes, provided that input trajectories can be applied to the dynamic process model.

The validation of the dynamic process model with the steady-state and transient data shows that the process model has a good capability of predicting the steady-state and transient behavior of the plant for a wide range of operating conditions. The validation included in this work proves the capacities of dynamic process modeling applied to large-scale experimental data. The model is considered suitable for studies including transient performance analysis and control structure evaluation studies at the plant scale. In addition, it provides confidence towards using the dynamic process model for analysis of larger-scale PCC plants.

The case study carried out in this work via dynamic process simulations with the validated model shows that, generally, the plant responds more slowly at lower operating loads (the load being defined by the flow rate fed to the absorber). A general trend is observed, in which it takes a longer time to stabilize the main process variables of the pilot plant under open-loop step changes in the main inputs of the process, namely solvent flow rate, flue gas flow rate and reboiler duty. From the process simulations, it is found that, in general, the desorption rate stabilizes faster than the absorption rate for set-point step changes in solvent flow rate and reboiler duty. In addition, $\pm 10\%$ step changes in flue gas flow rate around a given operating point do not cause a large relative change in the main process variables of the process (RC ranges from -0.81% to 0.21%).

The evaluation of the decentralized control structures shows that by adding closed-loop controllers on the two main degrees of freedom of the plant—solvent flow rate and reboiler duty—to control two other process variables, including CO_2 capture ratio and stripper bottom solvent temperature, the plant can be stabilized faster and more efficiently under varying loads. The control structure that showed the best performance was control structure B, in which the reboiler duty is manipulated to control CO_2 capture ratio at the inlet of the absorber and the rich solvent flow rate to control the stripper bottom solvent temperature. It was observed that control structure B provides the fastest stabilization times for the main process variables under scenarios when the plant load is ramped down and up, with ramp rates typically found in NGCC power plants with fast-cycling capabilities. When reducing the PCC process load, this control structure is the least energy-intensive of those evaluated in this work. When increasing the plant load, this control structure is the one with the lowest accumulated CO_2 emissions imposed by the process inertia during load-change transient operation.

Acknowledgments: The authors acknowledge the Department of Energy and Process Engineering at NTNU-Norwegian University of Science and Technology and TCM DA owners Gassnova, Shell, Statoil and Sasol, for funding this project. The funds for covering the costs to publish in open access were provided by the Norwegian University of Science and Technology—NTNU.

Author Contributions: Rubén M. Montañés contributed to the selection of experimental data; processed the experimental data; developed the models; carried out the calibration, validation and simulation of the dynamic process models; defined and carried out the case studies; analyzed the results; and wrote the manuscript. Nina E. Flø contributed to the experimental data selection; contributed to the critical analysis of the results; and reviewed the manuscript. Lars O. Nord contributed to the critical analysis of the results; reviewed the manuscript; and supervised the work.

Conflicts of Interest: The authors declare no conflict of interest.

Abbreviations and Symbols

A_{if}	Contact area
AP	Absolute percentage error
Cap	CO_2 capture ratio
CHP	Combined heat and power
CCS	Carbon capture and storage
CO_2	Carbon dioxide
$CO_{2,em}$	CO_2 emitted (kg/s)
c_i	Molar concentration
C_{ef}	Pre-multiplying coefficient
DCC	Direct contact cooler
Des	Desorption ratio
D_{CO2}	Diffusivity of CO_2 in aqueous monoethanolamine
E	Enhancement factor
F	Mass flow rate (kg/s)

FB	Feedback
FC	Flow controller
FF	Feed-forward
FT	Flow transmitter
GA	Gas analyzer
GC	Gas chromatograph
GT	Gas turbine
He_i	Henry's constant
H_2O	Water
HX	Heat exchanger
k_i	Mass transfer coefficient
K_i	Equilibrium constant
LC	Level controller
L_l	Lean CO_2 loading
L_r	Rich CO_2 loading
L/G	Mass-based liquid to gas ratio (kg/kg)
LT	Level transmitter
MAP	Mean absolute percentage error
MEA	Monoethanolamine
MPC	Model predictive control
N_2	Nitrogen
NCCC	National carbon capture center
NGCC	Natural gas combined cycle
O_2	Oxygen
p	Pressure (Pa)
PC	Pressure controller
PCC	Post-combustion CO_2 capture
PT	Pressure transmitter
PZ	Piperazine
$\dot{Q}_{reb}$	Reboiler duty (W)
Q_{reb}	Reboiler energy input (J)
RC	Relative change
SA	Solvent analyzer
SIMC	Simplified internal model control
SRD	Specific reboiler duty (kJ/kgCO_2)
T	Temperature (K)
TC	Temperature controller
TCM DA	CO_2 Technology Cener Mongstad
t_s	Settling time
t_t	Total stabilization time
TT	Temperature transmitter
X	Mass fraction
x_p	Value measured at pilot plant
x_m	Value simulated model
y_∞	Steady-state final value
θ	Dead time
γ_i	Activity coefficient
ΔH_r	Heat of reaction
Δy	Change in process variable
ε-NTU	Effectiveness number of thermal units

Appendix A

Tables A1–A3 show the simulation results in terms of the dead time θ, 10% settling time t_s, total stabilization time t_t and relative change RC %, for the open-loop response to step-changes in the main inputs to the plant. The step changes are applied to the plant when it is operated at three different steady-state operating conditions defined by three different mass flow rate capacities of the absorber column. The inputs are:

- Flue gas mass flow rate ±10% step-change.
- Solvent mass flow rate ±10% step-change.
- Reboiler duty ±10% step-change.

The output process variables studied are:

- CO_2 lean loading L_l (mol/mol).
- CO_2 rich loading L_r (mol/mol).
- CO_2 absorbed $CO_{2,abs}$ (kg/s).
- CO_2 desorbed $CO_{2,abs}$ (kg/s).

Table A1. Open-loop response to ±10% step-changes in flue gas mass flow rate for three different operating points of the pilot plant. Responses in CO_2 lean loading L_l, CO_2 rich loading L_r, CO_2 absorbed, and CO_2 desorbed.

	Input	F_{gas} +10%				F_{gas} −10%			
Plant Load	**Process Variable**	***θ* (min)**	***t_s* (min)**	***t_t* (min)**	***RC* (%)**	***θ* (min)**	***t_s* (min)**	***t_t* (min)**	***RC* (%)**
100%	L_l	40.5	296.5	337.0	0.01	33.5	133.2	166.7	−0.35
	L_r	0.0	41.7	41.7	0.09	19.0	116.3	135.3	−0.76
	$CO_{2,abs}$	0.0	95.2	95.2	0.05	0.0	168.7	168.7	−0.81
	$CO_{2,abs}$	22.2	244.3	266.5	0.04	22.7	128.7	151.3	−0.80
80%	L_l	50.3	260.8	311.2	−0.03	42.7	442.0	484.7	0.04
	L_r	0.0	53.3	53.3	0.21	67.2	117.5	184.7	−0.15
	$CO_{2,abs}$	0.0	61.8	61.8	−0.03	0.0	334.5	334.5	−0.06
	$CO_{2,abs}$	25.5	393.7	419.2	−0.03	23.8	364.7	388.5	−0.06
60%	L_l	51.9	424.9	476.8	−0.03	53.7	318.5	372.2	0.08
	L_r	0.0	96.1	96.1	0.00	0.0	192.8	192.8	−0.05
	$CO_{2,abs}$	0.0	113.7	113.7	−0.05	0.0	141.2	141.2	0.09
	$CO_{2,abs}$	27.7	363.4	391.1	−0.05	25.6	369.9	395.5	0.09

Table A2. Open-loop response to ±10% step-changes in solvent mass flow rate for three different operating points of the pilot plant. Responses in CO_2 lean loading L_l, CO_2 rich loading L_r, CO_2 absorbed, and CO_2 desorbed.

	Input	F_{solv} +10%				F_{solv} −10%			
Plant Load	**Process Variable**	***θ* (min)**	***t_s* (min)**	***t_t* (min)**	***RC* (%)**	***θ* (min)**	***t_s* (min)**	***t_t* (min)**	***RC* (%)**
100%	L_l	11.8	15.8	27.7	8.59	14.5	11.5	26	−7.50
	L_r	14.2	89.7	103.8	−0.10	0	63.83	63.83	0.08
	$CO_{2,abs}$	0.0	133.2	133.2	0.35	0	67.16	67.16	−3.14
	$CO_{2,abs}$	0.0	98.8	98.8	0.35	0	12.83	12.83	−3.15
80%	L_l	15.8	18.5	34.3	7.85	19.5	13.16	32.66	−6.87
	L_r	0.0	106.3	106.3	−0.04	0	176.66	176.66	0.02
	$CO_{2,abs}$	0.0	97.8	97.8	2.09	0	65.66	65.66	−4.38
	$CO_{2,abs}$	0.0	18.8	18.8	2.09	0	3.16	3.16	−4.39
60%	L_l	22.0	17.0	39.0	6.75	27	17.33	44.33	−6.28
	L_r	0.0	141.0	141.0	−0.02	0	454	454	0.00
	$CO_{2,abs}$	0.0	104.0	104.0	4.18	0	69.5	69.5	−5.59
	$CO_{2,abs}$	0.0	23.5	23.5	4.18	0	3.8	3.8	−5.59

Table A3. Open-loop response to ±10% step-changes in reboiler duty for three different operating points of the pilot plant. Responses in CO_2 lean loading L_l, CO_2 rich loading L_r, CO_2 absorbed, and CO_2 desorbed.

	Input	$\dot{Q}_{reb}$ +10%				$\dot{Q}_{reb}$ −10%			
Plant Load	**Process Variable**	***θ (min)***	***t_s (min)***	***t_t (min)***	***RC* (%)**	***θ (min)***	***t_s (min)***	***t_t (min)***	***RC* (%)**
100%	L_l	13.0	9.7	22.7	−6.29	12.7	15.5	28.2	8.46
	L_r	31.8	81.5	113.3	−0.22	29.5	43.3	72.8	0.00
	$CO_{2,abs}$	6.0	70.8	76.8	6.07	5.0	49.8	54.8	−8.48
	$CO_{2,abs}$	0.0	2.2	2.2	6.07	0.0	10.3	10.3	−8.48
80%	L_l	17.0	11.7	28.7	−5.60	17.0	14.8	31.8	7.78
	L_r	40.7	78.0	118.7	−0.03	38.3	88.0	126.3	0.02
	$CO_{2,abs}$	7.8	74.7	82.5	5.19	5.7	57.0	62.7	−7.16
	$CO_{2,abs}$	0.0	2.7	2.7	5.19	0.0	14.5	14.5	−0.05
60%	L_l	23.2	16.0	39.2	−4.97	23.8	17.3	41.2	6.63
	L_r	47.0	99.3	146.3	−0.01	47.8	114.7	162.5	0.00
	$CO_{2,abs}$	9.5	89.6	99.1	4.00	7.5	72.0	79.5	−5.30
	$CO_{2,abs}$	0.0	3.5	3.5	4.00	0.0	3.3	3.3	−5.30

References

1. The International Energy Agency (IEA). *CO_2 Capture and Storage: A Key Carbon Abatement Option*; International Energy Agency: Paris, France, 2008.
2. Singh, A.; Stéphenne, K. Shell Cansolv CO_2 capture technology: Achievement from first commercial plant. *Energy Procedia* **2014**, *63*, 1678–1685. [CrossRef]
3. Laboratory, N.E.T. Petra Nova Parish Holdings. W.A. Parish Post-Combustion CO_2 Capture and Sequestration Project. Available online: https://www.netl.doe.gov/research/coal/project-information/fe0003311-ppp (accessed on 28 September 2017).
4. Hentschel, J.; Babić, U.A.; Spliethoff, H. A parametric approach for the valuation of power plant flexibility options. *Energy Rep.* **2016**, *2*, 40–47. [CrossRef]
5. Mac Dowell, N.; Staffell, I. The role of flexible CCS in the UK's future energy system. *Int. J. Greenh. Gas Control* **2016**, *48*, 327–344. [CrossRef]
6. Gaspar, J.; Jorgensen, J.B.; Fosbol, P.L. Control of a post-combustion CO_2 capture plant during process start-up and load variations. *IFAC-PapersOnLine* **2015**, *48*, 580–585. [CrossRef]
7. Montañés, R.M.; Korpås, M.; Nord, L.O.; Jaehnert, S. Identifying operational requirements for flexible CCS power plant in future energy systems. *Energy Procedia* **2016**, *86*, 22–31. [CrossRef]
8. Johnsson, F.; Odenberger, M.; Göransson, L. Challenges to integrate CCS into low carbon electricity markets. *Energy Procedia* **2014**, *63*, 7485–7493. [CrossRef]
9. Boot-Handford, M.E.; Abanades, J.C.; Anthony, E.J.; Blunt, M.J.; Brandani, S.; Mac Dowell, N.; Fernandez, J.R.; Ferrari, M.-C.; Gross, R.; Hallett, J.P.; et al. Carbon capture and storage update. *Energy Environ. Sci.* **2014**, *7*, 130–189. [CrossRef]
10. Flø, N.E.; Kvamsdal, H.M.; Hillestad, M.; Mejdell, T. Dominating dynamics of the post-combustion CO_2 absorption process. *Comput. Chem. Eng.* **2016**, *86*, 171–183. [CrossRef]
11. Karimi, M.; Hillestad, M.; Svendsen, H.F. Investigation of the dynamic behavior of different stripper configurations for post-combustion CO_2 capture. *Int. J. Greenh. Gas Control* **2012**, *7*, 230–239. [CrossRef]
12. Garðarsdóttir, S.Ó.; Montañés, R.M.; Normann, F.; Nord, L.O.; Johnsson, F. Effects of CO_2-absorption control strategies on the dynamic performance of a supercritical pulverized-coal-fired power plant. *Ind. Eng. Chem. Res.* **2017**, *56*, 4415–4430. [CrossRef]
13. Panahi, M.; Skogestad, S. Economically efficient operation of CO_2 capturing process part i: Self-optimizing procedure for selecting the best controlled variables. *Chem. Eng. Process. Process Intensif.* **2011**, *50*, 247–253. [CrossRef]
14. Panahi, M.; Skogestad, S. Economically efficient operation of CO_2 capturing process. Part II. Design of control layer. *Chem. Eng. Process. Process Intensif.* **2012**, *52*, 112–124. [CrossRef]

15. Montañés, R.M.; GarÐarsdóttir, S.Ó.; Normann, F.; Johnsson, F.; Nord, L.O. Demonstrating load-change transient performance of a commercial-scale natural gas combined cycle power plant with post-combustion CO_2 capture. *Int. J. Greenh. Gas Control* **2017**, *63*, 158–174. [CrossRef]
16. Nittaya, T.; Douglas, P.L.; Croiset, E.; Ricardez-Sandoval, L.A. Dynamic modelling and control of MEA absorption processes for CO_2 capture from power plants. *Fuel* **2014**, *116*, 672–691. [CrossRef]
17. Zhang, Q.; Turton, R.; Bhattacharyya, D. Development of model and model-predictive control of an MEA-based postcombustion CO_2 capture process. *Ind. Eng. Chem. Res.* **2016**, *55*, 1292–1308. [CrossRef]
18. International Energy Agency Greenhouse Gas R&D Programme (IEAGHG). *Evaluation of Process Control Strategies for Normal, Flexible, and Upset Operation Conditions of CO_2 Post Combustion Capture Processes*; July 2016; IEAGHG: Cheltenham, UK, September 2016.
19. Walters, M.S.; Edgar, T.F.; Rochelle, G.T. Regulatory control of amine scrubbing for CO_2 capture from power plants. *Ind. Eng. Chem. Res.* **2016**, *55*, 4646–4657. [CrossRef]
20. Gaspar, J.; Ricardez-Sandoval, L.; Jørgensen, J.B.; Fosbøl, P.L. Controllability and flexibility analysis of CO_2 post-combustion capture using piperazine and MEA. *Int. J. Greenh. Gas Control* **2016**, *51*, 276–289. [CrossRef]
21. Mac Dowell, N.; Shah, N. The multi-period optimisation of an amine-based CO_2 capture process integrated with a super-critical coal-fired power station for flexible operation. *Comput. Chem. Eng.* **2015**, *74*, 169–183. [CrossRef]
22. Flø, N.E.; Kvamsdal, H.M.; Hillestad, M. Dynamic simulation of post-combustion CO_2 capture for flexible operation of the brindisi pilot plant. *Int. J. Greenh. Gas Control* **2016**, *48 Pt 2*, 204–215. [CrossRef]
23. Ceccarelli, N.; van Leeuwen, M.; Wolf, T.; van Leeuwen, P.; van der Vaart, R.; Maas, W.; Ramos, A. Flexibility of low-CO_2 gas power plants: Integration of the CO_2 capture unit with CCGT operation. *Energy Procedia* **2014**, *63*, 1703–1726. [CrossRef]
24. Wellner, K.; Marx-Schubach, T.; Schmitz, G. Dynamic behavior of coal-fired power plants with postcombustion CO_2 capture. *Ind. Eng. Chem. Res.* **2016**, *55*, 12038–12045. [CrossRef]
25. Olaleye, A.K.; Oko, E.; Wang, M.; Kelsall, G. Dynamic modelling and analysis of supercritical coal-fired power plant integrated with post-combustion CO_2 capture. In *Clean Coal Technology and Sustainable Development, Proceedings of the 8th International Symposium on Coal Combustion, Beijing, China, 19-22 July 2015*; Yue, G., Li, S., Eds.; Springer: Beijing, China, 2016; pp. 359–363.
26. Mechleri, E.; Lawal, A.; Ramos, A.; Davison, J.; Dowell, N.M. Process control strategies for flexible operation of post-combustion CO_2 capture plants. *Int. J. Greenh. Gas Control* **2017**, *57*, 14–25. [CrossRef]
27. Mechleri, E.; Fennell, P.S.; Dowell, N.M. Optimisation and evaluation of flexible operation strategies for coal- and gas-CCS power stations with a multi-period design approach. *Int. J. Greenh. Gas Control* **2017**, *59*, 24–39. [CrossRef]
28. Sanchez Fernandez, E.; Sanchez del Rio, M.; Chalmers, H.; Khakharia, P.; Goetheer, E.L.V.; Gibbins, J.; Lucquiaud, M. Operational flexibility options in power plants with integrated post-combustion capture. *Int. J. Greenh. Gas Control* **2016**, *48*, 275–289. [CrossRef]
29. Dutta, R.; Nord, L.O.; Bolland, O. Selection and design of post-combustion CO_2 capture process for 600 MW natural gas fueled thermal power plant based on operability. *Energy* **2017**, *121*, 643–656. [CrossRef]
30. Kvamsdal, H.M.; Jakobsen, J.P.; Hoff, K.A. Dynamic modeling and simulation of a CO_2 absorber column for post-combustion CO_2 capture. *Chem. Eng. Process. Process Intensif.* **2009**, *48*, 135–144. [CrossRef]
31. Gaspar, J.; Cormos, A.-M. Dynamic modeling and absorption capacity assessment of CO_2 capture process. *Int. J. Greenh. Gas Control* **2012**, *8*, 45–55. [CrossRef]
32. Harun, N.; Nittaya, T.; Douglas, P.L.; Croiset, E.; Ricardez-Sandoval, L.A. Dynamic simulation of MEA absorption process for CO_2 capture from power plants. *Int. J. Greenh. Gas Control* **2012**, *10*, 295–309. [CrossRef]
33. Jayarathna, S.A.; Lie, B.; Melaaen, M.C. Amine based CO_2 capture plant: Dynamic modeling and simulations. *Int. J. Greenh. Gas Control* **2013**, *14*, 282–290. [CrossRef]
34. He, Z.; Sahraei, M.H.; Ricardez-Sandoval, L.A. Flexible operation and simultaneous scheduling and control of a CO_2 capture plant using model predictive control. *Int. J. Greenh. Gas Control* **2016**, *48*, 300–311. [CrossRef]
35. Luu, M.T.; Abdul Manaf, N.; Abbas, A. Dynamic modelling and control strategies for flexible operation of amine-based post-combustion CO_2 capture systems. *Int. J. Greenh. Gas Control* **2015**, *39*, 377–389. [CrossRef]
36. Biliyok, C.; Lawal, A.; Wang, M.; Seibert, F. Dynamic modelling, validation and analysis of post-combustion chemical absorption CO_2 capture plant. *Int. J. Greenh. Gas Control* **2012**, *9*, 428–445. [CrossRef]

37. Åkesson, J.; Laird, C.D.; Lavedan, G.; Prölß, K.; Tummescheit, H.; Velut, S.; Zhu, Y. Nonlinear model predictive control of a CO_2 post-combustion absorption unit. *Chem. Eng. Technol.* **2012**, *35*, 445–454. [CrossRef]
38. Bui, M.; Gunawan, I.; Verheyen, V.; Feron, P.; Meuleman, E.; Adeloju, S. Dynamic modelling and optimisation of flexible operation in post-combustion CO_2 capture plants—A review. *Comput. Chem. Eng.* **2014**, *61*, 245–265. [CrossRef]
39. Enaasen, N.; Zangrilli, L.; Mangiaracina, A.; Mejdell, T.; Kvamsdal, H.M.; Hillestad, M. Validation of a dynamic model of the brindisi pilot plant. *Energy Procedia* **2014**, *63*, 1040–1054. [CrossRef]
40. Enaasen Flø, N.; Knuutila, H.; Kvamsdal, H.M.; Hillestad, M. Dynamic model validation of the post-combustion CO_2 absorption process. *Int. J. Greenh. Gas Control* **2015**, *41*, 127–141. [CrossRef]
41. Van De Haar, A.; Trapp, C.; Wellner, K.; De Kler, R.; Schmitz, G.; Colonna, P. Dynamics of postcombustion CO_2 capture plants: Modeling, validation, and case study. *Ind. Eng. Chem. Res.* **2017**, *56*, 1810–1822. [CrossRef] [PubMed]
42. Gaspar, J.; Gladis, A.; Jørgensen, J.B.; Thomsen, K.; von Solms, N.; Fosbøl, P.L. Dynamic operation and simulation of post-combustion CO_2 capture. *Energy Procedia* **2016**, *86*, 205–214. [CrossRef]
43. Dutta, R.; Nord, L.O.; Bolland, O. Prospects of using equilibrium-based column models in dynamic process simulation of post-combustion CO_2 capture for coal-fired power plant. *Fuel* **2017**, *202*, 85–97. [CrossRef]
44. Chinen, A.S.; Morgan, J.C.; Omell, B.P.; Bhattacharyya, D.; Miller, D.C. Dynamic data reconciliation and model validation of a MEA-based CO_2 capture system using pilot plant data. In Proceedings of the 11th IFAC Symposium on Dynamics and Control of Process Systems, Including Biosystems, Trondheim, Norway, 6–8 June 2016.
45. Abdul Manaf, N.; Cousins, A.; Feron, P.; Abbas, A. Dynamic modelling, identification and preliminary control analysis of an amine-based post-combustion CO_2 capture pilot plant. *J. Clean. Prod.* **2016**, *113*, 635–653. [CrossRef]
46. Faber, R.; Köpcke, M.; Biede, O.; Knudsen, J.N.; Andersen, J. Open-loop step responses for the MEA post-combustion capture process: Experimental results from the esbjerg pilot plant. *Energy Procedia* **2011**, *4*, 1427–1434. [CrossRef]
47. Bui, M.; Gunawan, I.; Verheyen, V.; Feron, P.; Meuleman, E. Flexible operation of CSIRO's post-combustion CO_2 capture pilot plant at the AGL Loy Yang power station. *Int. J. Greenh. Gas Control* **2016**, *48*, 188–203. [CrossRef]
48. Tait, P.; Buschle, B.; Ausner, I.; Valluri, P.; Wehrli, M.; Lucquiaud, M. A pilot-scale study of dynamic response scenarios for the flexible operation of post-combustion CO_2 capture. *Int. J. Greenh. Gas Control* **2016**, *48*, 216–233. [CrossRef]
49. De Koeijer, G.M.; Aasen, K.I.; Steinseth Hamborg, E. *Scale-Up and Transient Operation of CO_2 Capture Plants at CO_2 Technology Centre Mongstad*; Society of Petroleum Engineers: Abu Dhabi, UAE, 2014.
50. Gjernes, E.; Pedersen, S.; Cents, T.; Watson, G.; Fostås, B.F.; Shah, M.I.; Lombardo, G.; Desvignes, C.; Flø, N.E.; Morken, A.K.; et al. Results from 30 wt % MEA performance testing at the CO_2 Technology Centre Mongstad. *Energy Procedia* **2017**, *114*, 1146–1157. [CrossRef]
51. Faramarzi, L.; Thimsen, D.; Hume, S.; Maxon, A.; Watson, G.; Pedersen, S.; Gjernes, E.; Fostås, B.F.; Lombardo, G.; Cents, T.; et al. Results from MEA testing at the CO_2 Technology Centre Mongstad: Verification of baseline results in 2015. *Energy Procedia* **2017**, *114*, 1128–1145. [CrossRef]
52. Thimsen, D.; Maxson, A.; Smith, V.; Cents, T.; Falk-Pedersen, O.; Gorset, O.; Hamborg, E.S. Results from MEA testing at the CO_2 Technology Centre Mongstad. Part I: Post-combustion CO_2 capture testing methodology. *Energy Procedia* **2014**, *63*, 5938–5958. [CrossRef]
53. Modelica Association. Available online: https://www.Modelica.Org/ (accessed on 28 September 2017).
54. Modelon. Post-Combustion Capture with Amine Solutions. Available online: http://www.Modelon.Com/industries/energy-process/carbon-capture-and-sequestration/ (accessed on 28 September 2017).
55. Dassault Systems, Dymola. Available online: http://www.3ds.Com/products-services/catia/products/dymola (accessed on 28 September 2017).
56. Prölß, K.; Tummescheit, H.; Velut, S.; Åkesson, J. Dynamic model of a post-combustion absorption unit for use in a non-linear model predictive control scheme. *Energy Procedia* **2011**, *4*, 2620–2627. [CrossRef]
57. Garðarsdóttir, S.Ó.; Normann, F.; Andersson, K.; Prölß, K.; Emilsdóttir, S.; Johnsson, F. Post-combustion CO_2 capture applied to a state-of-the-art coal-fired power plant—The influence of dynamic process conditions. *Int. J. Greenh. Gas Control* **2015**, *33*, 51–62. [CrossRef]

58. Onda, K.; Takeuchi, H.; Okumoto, Y. Mass transfer coefficients between gas and liquid phases in packed columns. *J. Chem. Eng. Jpn.* **1968**, *1*, 56–62. [CrossRef]
59. Versteeg, G.F.; Van Dijck, L.A.J.; Van Swaaij, W.P.M. On the kinetics between CO_2 and alkanolamines both in aqueous and non-aqueous solutions. An overview. *Chem. Eng. Commun.* **1996**, *144*, 113–158. [CrossRef]
60. Holst, J.V.; Versteeg, G.F.; Brilman, D.W.F.; Hogendoorn, J.A. Kinetic study of CO_2 with various amino acid salts in aqueous solution. *Chem. Eng. Sci.* **2009**, *64*, 59–68. [CrossRef]
61. Böttinger, W. *Nmr-Spektroskopische Untersuchung der Reaktivabsorption von Kohlendioxid in Wässrigen Aminlösungen*; VDI-Verlag: Düsseldorf, Germany, 2006.
62. Montañés, R.M.; Flø, N.E.; Dutta, R.; Nord, L.O.; Bolland, O. Dynamic process model development and validation with transient plant data collected from an mea test campaign at the CO_2 technology center mongstad. *Energy Procedia* **2017**, *114*, 1538–1550. [CrossRef]
63. International Energy Agency Greenhouse Gas R&D Programme (IEAGHG). *Operating Flexibility of Power Plants with CCS*; IEAGHG: Cheltenham, UK, June 2012.
64. Christopher, H.J.; James, K. How to Determine a Unit Ramp Rate (MW/min) for Lowest Total Production Cost. Available online: http://www.heatrate.com/docs/Value-of-Ramp-Rate-1987.pdf (accessed on 28 September 2017).
65. Genrup, M.; Thern, M. *Ny Gasturbinteknik 2012–2014: Gas Turbine Developments*; Report 2012; ELFORSK: Stockholm, Sweden, 2013.
66. Skogestad, S.; Grimholt, C. The SIMC method for smooth PID controller tuning. In *Pid Control in the Third Millennium: Lessons Learned and New Approaches*; Vilanova, R., Visioli, A., Eds.; Springer: London, UK, 2012; pp. 147–175.

CATCHING OUR FUTURE

Dynamic process model development and validation with transient plant data collected from an MEA test campaign at the CO_2 Technology Center Mongstad

(2016)

Available online at www.sciencedirect.com

ScienceDirect

Energy Procedia 114 (2017) 1538 – 1550

Energy Procedia

13th International Conference on Greenhouse Gas Control Technologies, GHGT-13, 14-18 November 2016, Lausanne, Switzerland

Dynamic process model development and validation with transient plant data collected from an MEA test campaign at the CO_2 Technology Center Mongstad

Rubén M. Montañés[a]*, Nina E. Fløb, Rohan Dutta[a], Lars O. Nord[a], Olav Bolland[a]

[a]*Department of Energy and Process Engineering, NTNU - Norwegian University of Science and Technology, NO-7491 Trondheim, Norway.*
[b]*CO_2 Technology Center Mongstad (TCM DA), 5954 Mongstad, Norway.*

Abstract

This work focuses on the development and validation of a dynamic process model of the post-combustion CO_2 chemical absorption process with temperature swing absorption (TSA) using aqueous monoethanolamine (MEA) as solvent. A new set of steady-state and transient cases were generated during an MEA test campaign at the amine pilot plant at CO_2 Technology Center Mongstad (TCM DA). Nine steady-state cases comprising a wide range of operating conditions of the plant and two transient tests consisting of flue gas volumetric flow rate step-changes were utilized for the purpose of dynamic process model validation of the overall pilot plant process model. It is concluded that the dynamic process model is capable of estimating the absorber and stripper columns temperature profiles with good accuracy after tuning of model parameters. An over-prediction of the model for lean and rich CO_2 loadings has been reported, being mean percentage errors <1.5% for lean loading and <6.7% for rich loading. In addition, an under prediction of CO_2 product flow rate has been observed (<5%). The process model is capable of predicting the variability of lean and rich loadings for the range of steady-state operating conditions. The main process dynamics of the pilot plant under flue gas volumetric flow rate set-point step changes is captured by the process model.

Peer-review under responsibility of the organizing committee of GHGT-13.

Keywords: Post-combustion; natural gas; transient data; rate-based model; model validation; pilot plant; dynamic modeling; Modelica.

* Corresponding author. Tel.: +47 735093722;
E-mail address: ruben.m.montanes@ntnu.no

Peer-review under responsibility of the organizing committee of GHGT-13.
doi:10.1016/j.egypro.2017.03.1284

1. Introduction

Post-combustion CO_2 capture (PCC) with amines is considered one of the more mature technologies that can contribute to reduce anthropogenic CO_2 emissions to the atmosphere from fossil-fueled thermal power plants. It is considered that thermal power plants with CO_2 capture and storage (CCS) might be operated as load-following units in future energy systems with higher integration of variable renewable energy sources [1]. The Carbon Capture and Storage update 2014 concludes that the financial case for CCS requires that it operates in a flexible manner, and considers load-following ability as extremely important to the long-term economics [2]. Therefore, interest has grown in the field of operational flexibility of thermal power plants with CCS. A key aspect of operational flexibility of power plants with post-combustion CO_2 capture using amines is the transient behavior of the capture process, i.e. the time dependent behavior of the PCC plant when varying operating conditions. Pilot plant testing allows analyzing flexible operation of the process [3-5]. Nevertheless, pilot plant testing requires expensive resources and normally a limited amount of transient testing can be conducted during test campaigns.

The scarcity of published transient performance data from pilot plants together with the limited operational experience from commercial-scale post-combustion capture plants, claims for an interest within the research community for the development of dynamic process simulation models. Dynamic process models are considered as invaluable tools that can help studying different aspects of the transient behavior of PCC plants. The models allow studying various transient events, as well as developing and implementing optimal control strategies. In addition, computational tools and process models can contribute to identify process bottlenecks and develop useful knowledge that will contribute to technology development and ease process scale-up. However, the reliability of results from dynamic simulations might be questioned if the dynamic process models have not been validated against experiments or pilot plant transient data. Thus, validation of dynamic process models is necessary [6-9]. According to Bui et al. [10], further research must focus on producing transient pilot plant data for increasing knowledge on real plant transient performance and for dynamic process model validation in order to ensure reliability of simulation results.

The objectives of this work were:

- Generate a set of steady-state and transient plant data that can be used for dynamic process model validation.
- Develop and validate a dynamic process model of the amine-based TSA plant at CO_2 Technology Center Mongstad for flue gas from a natural gas fueled power plant.

Steady-state and dynamic experiments were conducted by TCM DA during an MEA test campaign at the post-combustion amine pilot plant at TCM DA treating flue gas from a natural gas fueled power plant. The steady-state data sets reflect a wide range of operating conditions while the dynamic experiments consist of set-point changes in exhaust gas volumetric flow rate fed to the absorber. In this work, a dynamic process model of the amine-based plant at TCM DA was built with the open physical modeling language Modelica [11], by means of the commercial tool Dymola [12]. After processing the pilot plant data, validation of the overall process model has been conducted with the steady-state and transient data by comparing the prediction of the overall process model of the PCC plant with the pilot plant data. In this paper, the validation with nine steady-state cases and two transient events is presented.

Nomenclature

TSA	Temperature swing absorption
MEA	Monoethanolamine
TCM DA	CO_2 Technology Center Mongstad
PCC	Post combustion CO_2 capture
CCS	CO_2 Capture and Storage
CHP	Combined heat and power
FMI	Functional Mock-up Interface
FMU	Functional Mock-up Unit

2. TCM DA amine pilot plant configured for CHP flue gas treatment

CO_2 Technology Centre Mongstad has an installed pilot-scale amine-based temperature swing absorption (TSA) process plant next to the Statoil refinery in Mongstad, Norway. TCM DA has recently conducted a test campaign with 30% aqueous monoethanolamine (MEA), operated from 6 July until 17 October 2015. The work is part of the continuous effort of TCM DA on generating better understanding of the performance of the non-proprietary aqueous MEA solvent system. From TCM DA's perspective, one of the objectives of MEA test campaigns is to provide understanding of the transient operations of the amine plant [13]. A detailed description of the flexible and fully instrumented TCM DA plant can be found in Hamborg et al. [14]. In the following it is presented a brief description of the TCM DA PCC pilot plant configured for flue gas cleaning from natural gas fueled power plant.

The exhaust gas, with a CO_2 content of about 3.5 vol%, comes from the natural gas combined heat and power plant (CHP) placed next to the TCM DA facility. The amine pilot plant treats a fraction of about 3% of the total exhaust gas originating from the two GE 9001E gas turbines operating at design load at the CHP plant. The total capacity of the pilot plant for CHP flue gas is 60000 Sm^3/hr and it is capable of capturing around 80 ton CO_2/day. Figure 1 shows a simplified process flowsheet for TCM DA amine plant operated with CHP flue gas. An induced draft blower is present at the plant to overcome pressure drops and blow the flue gas flow. It has variable speed drives that allow manipulating the flue gas volumetric flow rate fed to the absorber. The flue gas flows through a direct contact cooler that cools down and saturates the flue gas by a counter-current water flow.

The absorber column consists of a rectangular polypropylene-lined concrete column with a cross-section of 3.55 x 2 m and a total height of 62 m. It has three absorber packed sections consisting of Koch Glitsch Flexipac 2X structured stainless-steel packing of 12 m, 6 m and 6 m. Two water-wash systems are operated in the upper part of the absorption tower, consisting of two sections of Koch Glitsch Flexipac 2Y HC structured stainless-steel packing. The absorber in TCM DA has the flexibility option to use different packing heights (12, 18 or 24 m). During the tests presented in this paper, 24 m of absorber packing were utilized (12 bottom + 6 middle + 6 top). There are 4 temperature sensors radially distributed in the absorber column per meter of absorber packing in the axial direction. This makes a total of 96 temperature sensors within packed segments.

The CHP stripper with overhead condenser system consists of a 1.3 m diameter column of Koch Glitsch Flexipac 2X structured stainless-steel packing of 8 m, and a rectifying water-wash region with Koch Glitsch Flexipac 2Y HC structured stainless-steel packing of 1.6 m of height. There are 4 temperature sensors radially distributed in the

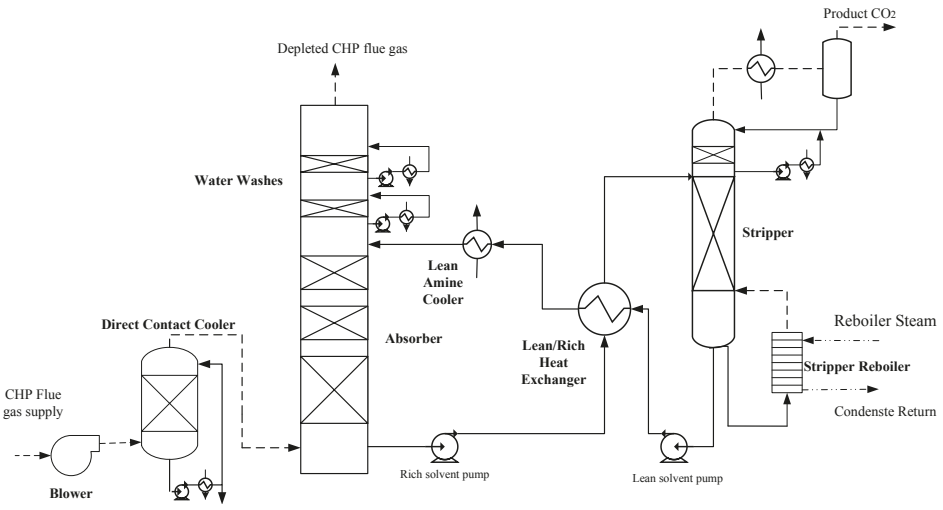

Figure 1. Simplified flowsheet of the TCM amine plant for CHP flue gas.

absorber column per meter of absorber packing in the axial direction. The total number of temperature sensors within packed segments is therefore 28. The stripper reboiler consists of a thermosiphon steam-driven system that provides the required heat for the stripping process. A plate and frame heat exchanger allows heat integration between the absorber and stripper columns, where the hot lean amine solution coming from the stripper heats up the rich amine solution. In addition, a lean amine cooler is utilized to control the lean solution temperature introduced at the top of the absorber packing sections.

3. Steady-state and transient operating cases from the MEA test campaign

With the purpose of dynamic model validation under steady-state operating conditions, a set of nine steady-state plant operation cases from the MEA test campaign were utilized. The tests were conducted with 30 wt% aqueous MEA, and comprise a wide range of operating conditions with various combinations of rich solvent flow rate and reboiler duty. Table 1 shows the steady-state cases generated during the test campaign that are used in this work. Cases 1 to 5 were obtained by varying rich solvent mass flow rate when operating the absorber at 80% volumetric flue gas flow rate capacity with a CO_2 capture target of 85%. The mass based L/G ratios on the absorber range from 1.34 to 0.75 for cases 1 to 5. Cases 6 to 9 were obtained from the steady-state operation of the plant achieved in between the four transient tests (refer to Table 2).

A transient event happens when the plant is brought from one operating point to another. During transient testing key manipulated variables (inputs) of the plant are changed to observe how the process variables evolve over time from one steady-state operating point until a new steady-state operating point is reached. The purposes of these experiments are to increase knowledge of the process under transient conditions and to generate a set of data for assessing the validity of dynamic process models at the plant scale. It is desirable that the transient data represents the main dynamics of the plant. Table 2 includes the test matrix for the set-point change experiments conducted during the autumn 2015 MEA test campaign at TCM DA. The experiments consist of set-point changes in main inputs to the pilot plant, i.e., rich solvent flow rate, flue gas volumetric flow rate into the absorber and steam flow rate to reboiler. In this paper, tests 2 and 3 are presented for the purpose of dynamic process model validation. These two tests represent set point step-changes in flue gas volumetric flow rate fed to the absorber.

The responses and performance of the pilot plant was logged. The data was extracted every 30 seconds in order to reduce the data load. Logged data includes:

- Gas analyzers at the inlet of the absorber, outlet of the absorber, and CO_2 rich to stack.
- Main liquid and gas flow rates.
- Main process temperatures, including absorber and stripper temperatures.
- Pressures and pressure drops at different components of the plant.
- Online solvent analysis measurements include pH, density and conductivity, at the inlet and outlet of the absorber (lean and rich solvent).
- Liquid hold-ups distribution at different components of the plant.
- Main active controller set-points and tuning parameters.

Solvent samples were taken during steady-state conditions at the inlet and outlet of the absorber for posterior analysis in the lab, in order to obtain the CO_2 lean and rich solvent loadings. Actual reboiler duty was estimated based on logged measurement data of steam temperatures, pressures and mass flow rate as indicated in Thimsen et al. [15]. In order to assess the validity of the process model, temperature profiles of the absorber and stripper columns were utilized. Each of the measured temperature points included in the steady-state absorber temperature profiles is the average over time during steady-state conditions, of the averaged 4 temperature measurements of the sensors radially distributed within the absorber column, at the given axial position of the column.

The tests were run with a total inventory of aqueous MEA of about 38.2 m^3. For process simulations, it is of importance to understand how the solvent inventory is distributed within the different components of the plant. Therefore, liquid hold-ups at different parts of the plant were registered for the steady-state operating cases.

Table 1. Steady-state data for the nine operating cases selected from the MEA test campaign. The plant was operated with 30 wt% aqueous MEA and 24 meters of absorber packing. Note that standard conditions are 15 ºC and 1 atm. The tag IDs for the instrumentation utilized are included.

Case	1	2	3	4	5	6	7	8	9
Gas flow rate [Sm^3/hr] (8610-FT-0150)	47000	47000	47000	47000	47000	47000	47000	40000	47000
Rich solvent [kg/s] (8611-FIC-2004)	20.56	17.50	16.11	12.74	11.46	13.04	14.16	14.17	13.06
Reboiler duty [kW] (estimated [15])	2156.2	2093.3	2104.4	2102.8	2137.3	3901.3	3698.7	3549.7	2929.2
Absorber inlet CO_2 [%](8610-ai-2036a)	3.60	3.62	3.62	3.62	3.62	3.47	3.48	3.48	3.46
Absorber inlet O_2 [%](8610-ai-2036b)	15.30	15.48	15.49	15.51	15.52	14.70	14.74	14.84	14.77
Absorber inlet H_2O [%](8610-ai-2036c)	3.80	3.36	3.46	3.52	3.43	4.19	4.11	3.66	4.23
Absorber inlet N_2 [%](8610-ai-2036d)	78.18	78.88	78.94	79.06	78.96	75.51	75.53	75.87	75.40
Loading rich [mol/mol] (lab samples)	0.47	0.49	0.49	0.49	0.49	0.43	0.42	0.37	0.43
Loading lean [mol/mol] (lab samples)	0.34	0.33	0.31	0.26	0.23	0.21	0.19	0.18	0.17
CO_2 Product [kg/s] (C-8615-FT-0010)	0.74	0.74	0.75	0.77	0.76	0.80	0.80	0.70	0.82

Table 2. Test matrix for the set-point change experiments conducted during the Autumn 2015 MEA test campaign at TCM DA. The tag IDs for the instrumentation used is included.

Input	Test 1	Test 2	Test 3	Test 4
Rich amine mass flow rate [kg/hr]	47000	51000	51000	47000
(8611-FIC-2004)	51000			
Flue gas volumetric flow rate [Sm^3/hr]	47000	47000	40000	47000
(8610-FT-0150)		40000	47000	
Steam flow rate [kg/hr]	5300	5300	5300	5300
(8655-FI-2368B)				4615

4. Dynamic process models of the CO_2 chemical absorption process with aqueous MEA

A dynamic process model of the amine-based TSA plant at TCM DA was built with the open physical modeling language Modelica [11], by means of the commercial modeling and simulation tool Dymola [12]. Modelica allows for component-based modeling, and the component models consist of systems of differential and algebraic equations. The overall plant model consists of models for the absorber and stripper columns, sumps, internal heat exchanger, reboiler, condensers, flow resistances, pumps, valves, measurements and controllers. The process models were obtained from a Modelica library from Modelon AB [16] and have been presented elsewhere [17, 18]. In this work, the component models were configured, parameterized and modified in order to obtain a dynamic process model of the TSA plant at TCM DA considering the main process equipment, size, geometry, material and solvent inventory during the experiments. In addition, the regulatory control layer of the plant was implemented in the process model, considering the control structure at the PCC pilot plant.

Absorption and desorption columns are modeled considering the two-film theory approach, thus thermodynamic equilibrium is assumed at the liquid and gas interface. Packed sections consider rate-based approach for modeling interface mass transfer, with mass transfer coefficients for CO_2 and H_2O by Onda et al. [19], and enhanced mass transfer due to chemical reactions is implemented via a pseudo-first order enhancement factor [7]. Chemical equilibrium is considered in all model parts, both at interface and liquid bulk, with chemical equilibrium constants obtained empirically from Bötinger [20].

Heats of reaction are inferred from the equilibrium constant via the van't Hoff equation. Sensible heat transfer between phases is correlated to gas-phase mass transfer coefficient (Cohilton-Colburn analogy), while heat of solution and evaporation is calculated as a function of temperature but is constant with solvent loading. Ideal gas law applies

to the gas phase, which is only composed of CO_2, O_2, H_2O and N_2. The pressure of the system p is determined by gas phase pressure drop from a known operating point and a quadratic correlation with gas velocity.

A simplified washer component is included in the head of the column. It is modelled as a simple volume with phase separation. Its purpose is to cool down the gas flow to a temperature given as an input signal and condense as much vapor as required to reach saturation in the gas phase. Water balance is ensured by a make-up water source in the absorber sump that controls the H_2O mass balance of the plant. Note that in this model MEA is considered non-volatile, which means that it is only present in the liquid phase. This implies that MEA make-up source is not required in the overall dynamic process model. This is not the case for the real plant, where MEA make-up is required for operation.

The numerical solver DASSL was selected in Dymola for solution of the resulting system of differential and algebraic equations. The process model was exported as a co-simulation Functional Mock-up Unit (FMU) via FMI technology (Functional Mockup Interface) [21]. Simulations and validation were carried out in Microsoft Excel® environment via a FMI-add-in for Excel® [22].

5. Dynamic model validation results

5.1. Dynamic model validation using steady-state operational data.

The approach to overall PCC plant model development and validation followed in this work was to initially separate the plant in three main parts: absorber, lean/rich cross heat exchanger and stripper with reboiler. Proper boundary conditions were specified for each part of the process. Steady-state data measured at the pilot plant were used as inputs to the boundary conditions of each section of the process, and the main outputs from the model were compared with the plant data. This involves checking absorption and desorption rates, temperature profiles in the absorber and stripper, and lean and rich CO_2 loadings. The task required tuning of uncertain model parameters (tuners) in order to obtain a better agreement between measured plant performance and behavior predicted by the model. Uncertain parameters include enhancement factors and pre-multiplying factors for adjustment of effective interface area correlations. Then, the overall PCC plant process model was closed by connecting the different sections of the process and implementing the suitable regulatory control layer. The main model outputs were compared with measured plant data in steady-state for the overall plant. In the following, the results from the overall plant process model validation are presented.

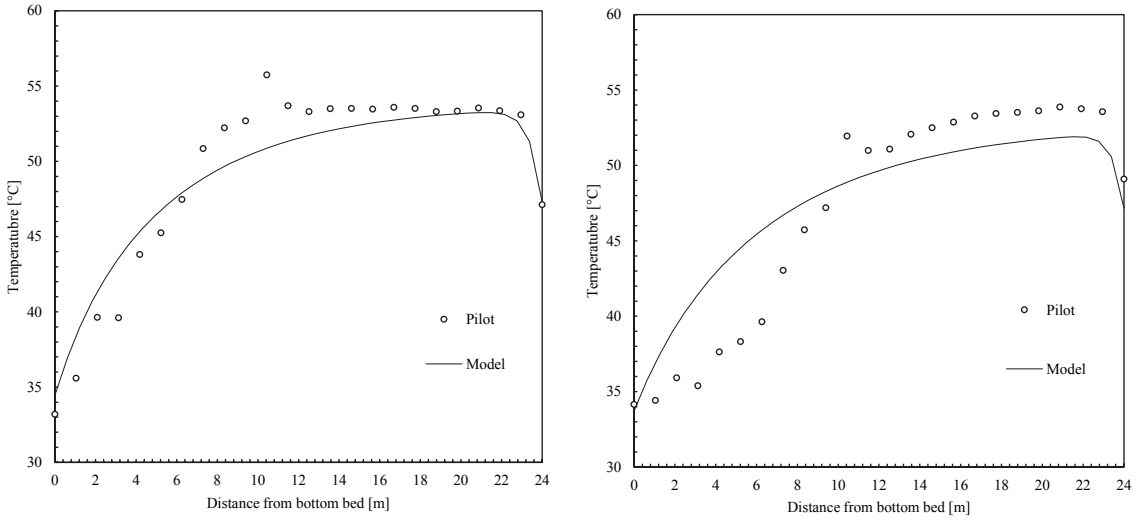

Figure 2. Examples of temperature profiles in absorber and stripper columns during steady-state operating conditions. Left: Case 8. Right: Case 9.

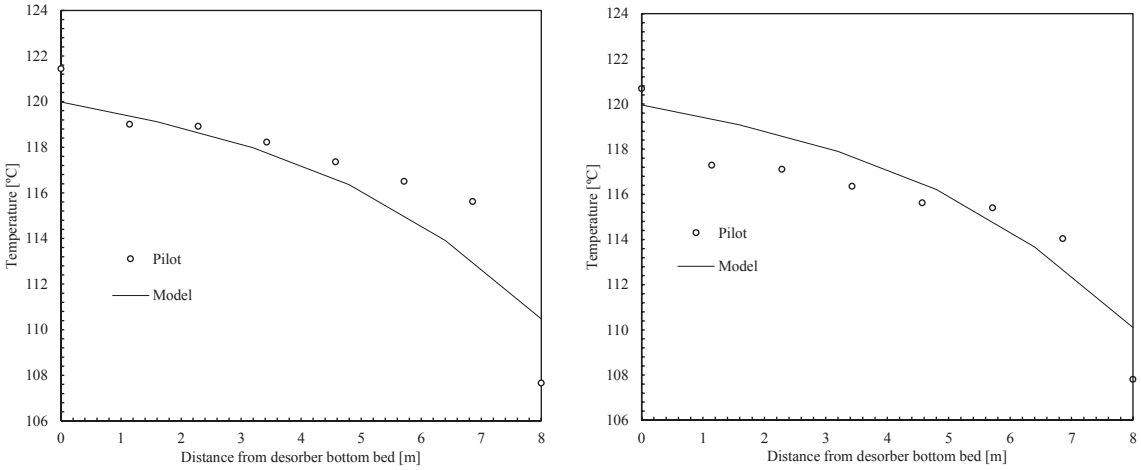

Figure 3. Examples of stripper temperature profiles for two steady-state operating conditions of the PCC pilot plant. Left: Case 8. Right: Case 9 (refer to Table 1).

Examples of temperature profiles within the absorber are shown in Figure 2. Figure 2 (left) shows the absorber temperature profile for the case 8, whereas Figure 2 (right) shows the absorber temperature profile for case 9. Figure 3 (left) shows temperature profiles in the stripper for case 8, whereas Figure 3 (right) shows temperature profiles for stripper in case 9. Note that for cases 8 and 9 the PCC plant is operated with 67 and 80 % flue gas volumetric flow rate capacity in the absorber respectively. Absorber temperature profiles predicted by the model show a good agreement with plant data, especially for case 8. The model is capable to predict properly the trends in temperature along the column. An over prediction is observed in case 9, at the bottom packing below the temperature bulge, while an under prediction is observed from the temperature bulge, within the middle and upper packing. The stripper temperature profile predicted by the process model shows also good agreement with plant data, as illustrated with steady-state cases in Figure 3.

Figure 4 shows the parity plot for lean and rich solvent loadings for the nine steady-state operating cases. It can be observed that the model over predicts the lean and rich loading when compared with the experimental data. The mean percentage error for lean loading is 1.4% and for rich loading 6.7%. There are two steady-state cases where the model shows an under prediction of lean solvent loading. This could be explained by the fact that these two steady-state cases are obtained prior to the injection of anti-foam solution in the plant (cases 6 and 7). Anti-foam is periodically used during MEA test campaigns at TCM to tackle the unideal phenomena in the stripper, and has a direct impact in the performance of the stripper [13]. From the results shown in Figure 4 it can be concluded that the dynamic process model is capable to predict the variability in solvent loading for the steady-state operating cases. The CO_2 product flow is under predicted with an average percentage error of 5% for the simulated cases.

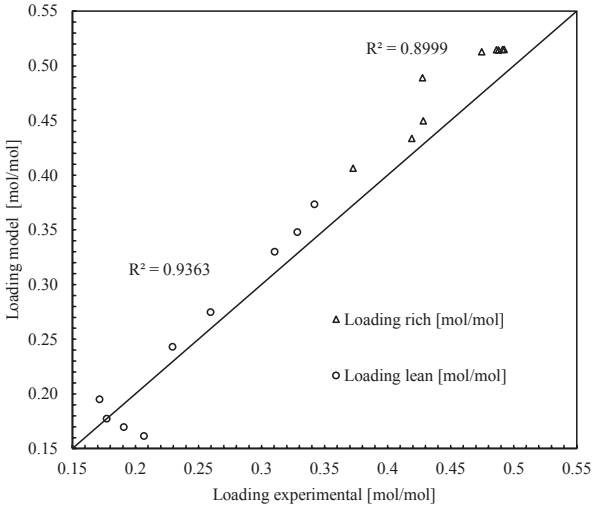

Figure 4. Lean and rich amine CO_2 loading parity plots. Model results from overall pilot plant model for nine steady-state operating cases. The mean percentage error for lean loading is 1.4% and for rich loading is 6.7%.

5.2. Dynamic model validation using transient operational data.

Once the steady-state estimation performance of the dynamic process model is validated for the full plant model, the dynamic process model is validated with transient plant data. Transient performance of this process is characterized by long dead times and large lag times in main process variables, resulting in relatively large total stabilization times. This means that this process is considered slow, when it is compared with a change in load in the steam cycle of a power plant. During the test campaign four transient tests were conducted, here two of them involving flue gas volumetric flow rate ramp-down and ramp-up will be presented.

5.2.1. Flue gas volumetric flow rate reduction

The test consisted of set-point reduction of the exhaust gas volumetric flow rate fed to the absorber, from 80% to 67% of the plant capacity, i.e. 47000 Sm^3/hr to 40000 Sm^3/hr. The purpose was to change the flue gas volumetric flow rate while keeping the rest of the plant process variables constant. Figure 5 shows the three main inputs of the plant for this test. The main controlled drifting variables of the plant during the test were kept constant by the action of the controllers of the regulatory control layer of the plant.

The plant was disturbed by manipulating the speed of the induced draft blower located upstream the direct contact cooler. The blower speed was changed in order to set the flue gas volumetric flow rate at the inlet of the absorber. Step set-point reduction in flue gas volumetric flow rate was applied. As shown in Figure 5, this has resulted in an oscillatory flue gas volumetric flow rate as disturbance to the plant, due to the fact that the blower speed/volumetric flue gas flow rate controller is a PI controller. Steam mass flow rate was maintained constant, while the solvent mass flow rate had small amplitude oscillations around the set-point. In order to compare the transient plant data with the actual plant data, the measured flue gas volumetric flow rate was introduced as an input trajectory to the dynamic process model. This means that the same disturbance applied to the plant during the test campaign, was applied to the dynamic process model for simulation. In addition, averaged value of the time series of the measured rich solvent mass flow rate and the estimated reboiler duty was applied as input to the dynamic process model.

Figure 6 shows the response on CO_2 product flow rate to the plant input. It was observed an input/output dead time of 40 minutes between flue gas volumetric flow rate and CO_2 product mass flow rate. This means that for a change in the flue gas flow rate input to the plant, no changes are observed in the product CO_2 flow until around 40 minutes later. Therefore, the system acts as a buffer to load change driven by flue gas volumetric flow rate change at absorber inlet. In addition, it takes around 4 hours to reach the new steady-state operating point. In addition, a significant lag time was found in stabilization of temperature profiles in the absorber (1 hour) and stripper columns (3-4 hours), not shown. It can be observed in Figures 6 and 7 that the process model is capable of predicting the main process dynamics for CO_2 product mass flow rate and rich and lean solvent CO_2 loadings.

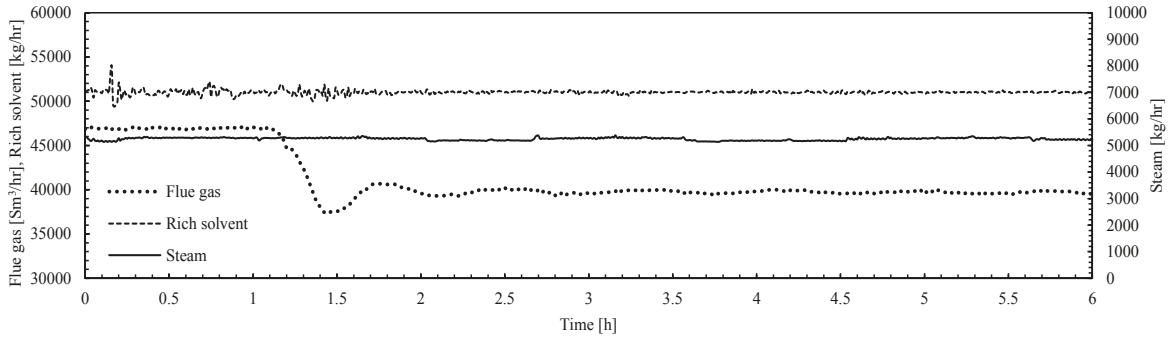

Figure 5. Main inputs to the plant for test with flue gas volumetric flow rate set-point reduction from 47000 [Sm3/hr] to 40000 [Sm3/hr] (8610-FT-0150). Rich solvent flow rate from absorber [kg/hr] (8611-FIC-2004) and steam flow to reboiler [kg/hr] (8655-FI-2368).

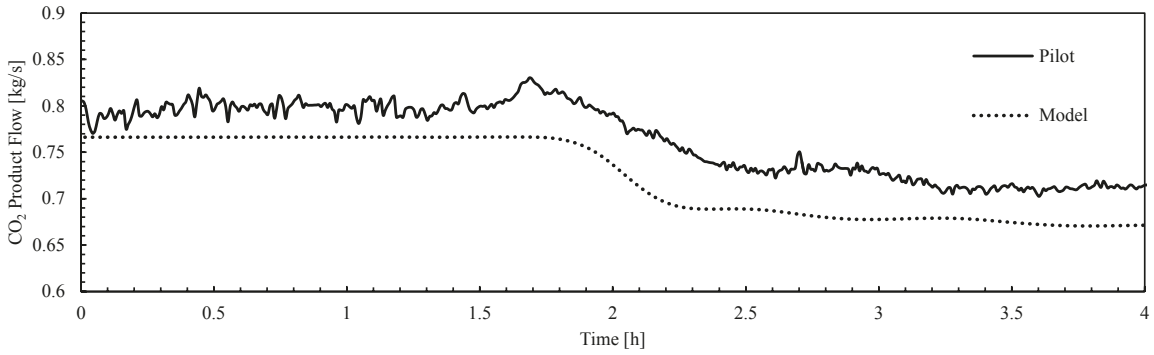

Figure 6. CO_2 Product flow rate [kg/s] (C-8615-FT-0010).

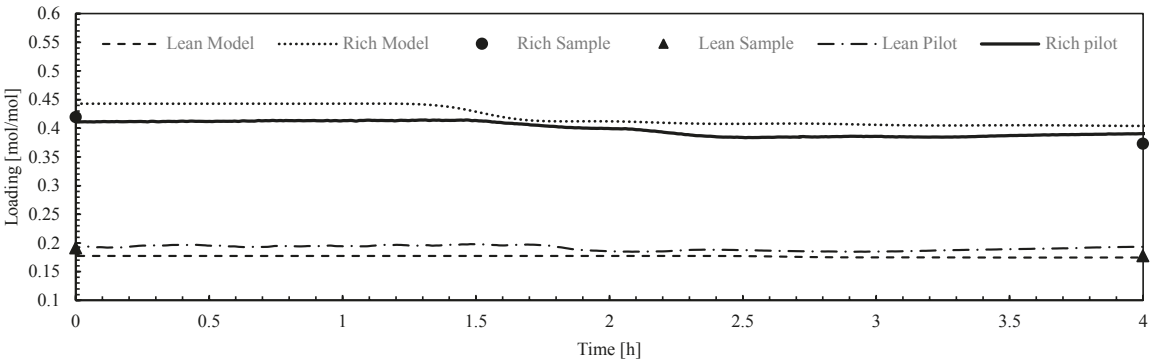

Figure 7. CO_2 lean and rich solvent loadings during test 2 (refer to table 2). Lean and rich pilot curves are based on a correlation for total alkalinity, density and temperature of the solvent, measured online at the plant. Lab samples were taken before and after the test.

5.2.2. Flue gas volumetric flow rate increase.

This test consist of set-point increase of the flue gas volumetric flow rate fed to the absorber, from 67% to 80% of the plant capacity, i.e. 40000 Sm^3/hr to 47000 Sm^3/hr. Figure 8 shows the three main inputs of the plant during the test. As in the previous test, an oscillatory behavior of the flue gas volumetric flow rate around the new set point is observed. The same approach with the measured input to the plant as input trajectory to the dynamic process model was applied. The plant acts as a buffer for flue gas volumetric flow rate changes as shown in Figure 9. Around 20 minutes dead time input/output from flue gas volumetric flow rate to CO_2 product mass flow rate was observed. Figure 9 shows the CO_2 product flow for the model and the pilot plant data and Figure 10 shows the plant and model response for this disturbance in terms of CO_2 lean and rich solvent loadings. A mismatch of 15 min for CO_2 product flow rate predicted by the process model is observed. A similar offset as in the previous test is observed, with a steady-state under prediction of CO_2 product flow rate. Despite of the steady-state offset shown on solvent CO_2 loadings prediction, it is observed a good prediction of the main dynamics, refer to Figure 10. It can be concluded that the process dynamics are well captured by the process model.

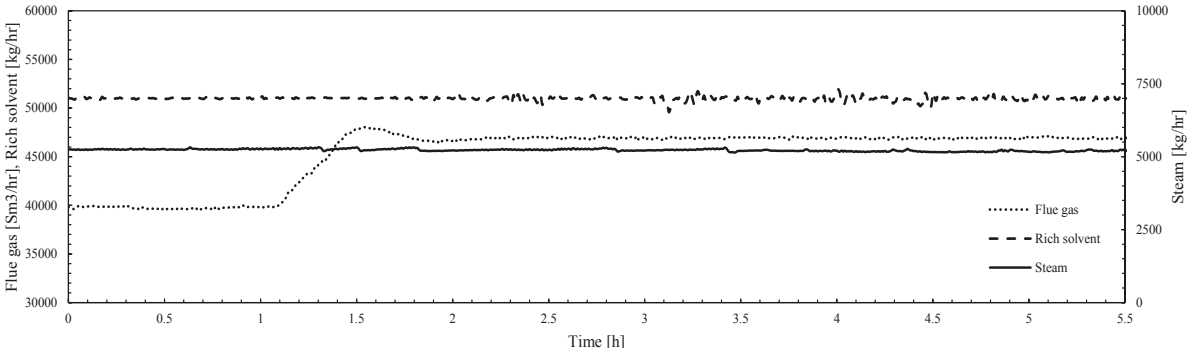

Figure 8. Main inputs to the plant. Flue gas volumetric flow rate set-point change from 47000 [Sm^3/hr] to 40000 [Sm^3/hr] (8610-FT-0150). Rich solvent flow rate from absorber [kg/hr] (8611-FIC-2004) and steam flow to reboiler [kg/hr] (8655-FI-2368).

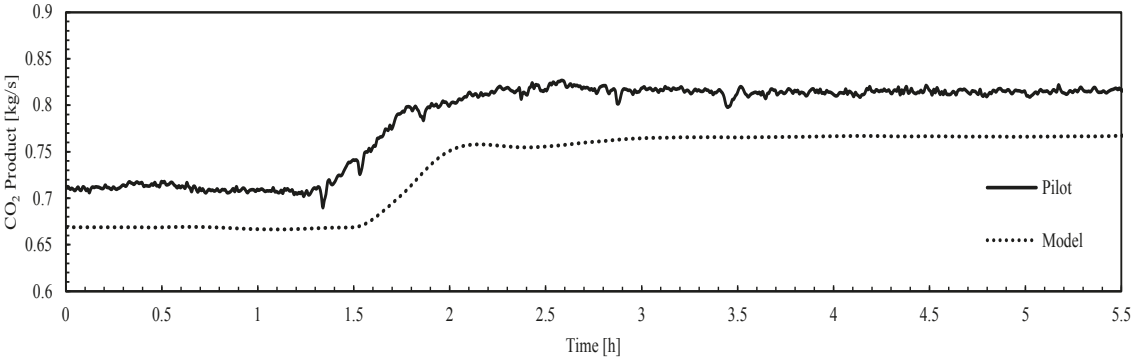

Figure 9. CO_2 product [kg/hr] (C-8615-FT-0010). Results from test 3 on flue gas volumetric flow rate set-point increase (refer to Table 2).

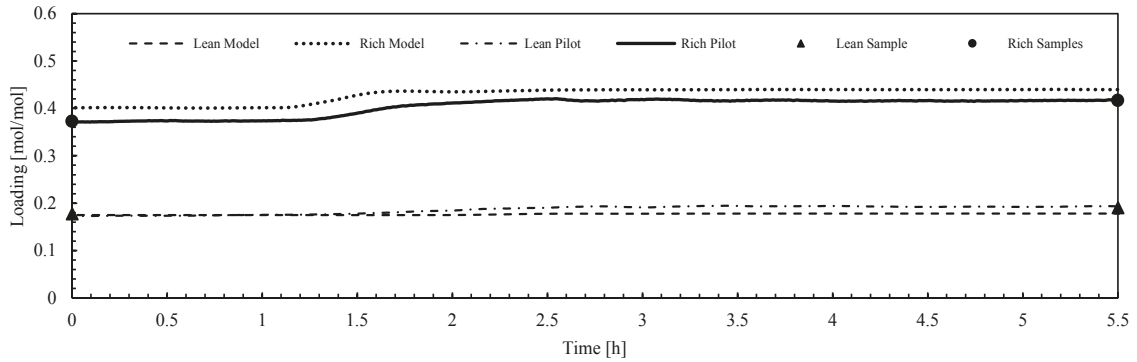

Figure 10. CO_2 lean and rich solvent loadings during test 3 (refer to Table 2). Loading pilot curves are based on a correlation for total alkalinity, density and temperature of the solvent, measured at the plant. Lab samples were taken before and after the test.

6. Discussion

The task of dynamic process model validation of the post-combustion CO_2 absorption with aqueous MEA requires the generation of suitable data sets including both steady-state and transient data. Ideally, the steady-state data should reflect a wide range of operating conditions of the PCC plant. The steady-state data utilized in this work consists of a wide range of operating conditions achieved by changing rich solvent mass flow rate and reboiler heat duty. As shown in Table 1, nine steady-state cases were gathered from the MEA test campaign. The cases include operation of the PCC plant with mass based L/G ratios on the absorber ranging from 1.34 to 0.75, when operating the absorber at 80% capacity and with a capture rate of 85% (cases 1 to 5).

During campaigns at TCM with 30% aqueous MEA, unideal behaviour occurs in the stripper bed and it is handled by addition of anti-foam solution. As shown in literature [13], the addition of anti-foam solution has a significant effect on stripper temperature profile at TCM DA pilot plant for CHP, and especially on specific reboiler duty at low lean amine loadings. Cases 6 and 7 were run before the addition of the anti-foam solution and it has been shown in Figure 4 that the model prediction under estimates lean loading only for these two specific cases. It is advised to check if anti-foam solution was used during the tests, if the data is to be used for process model validation. Anti-foam was introduced in the plant between the transient tests presented in this paper. If required, sufficient time between the tests should be allowed so that steady-state conditions are reached before and after adding anti-foam solution.

The post-combustion TSA process design with solvent recirculation from the stripper to the absorber in a closed-loop makes modeling and validation of the full plant challenging. Modeling errors and inaccuracies in one component of the plant will easily propagate towards other parts of the process. Therefore, a systematic approach is recommended beginning with validation of the separate models of absorber, stripper with reboiler, and heat exchanger sections. In this work, the overall process model is finally developed by joining the different sections and validated with the steady-state and transient pilot data. The intended application of the process model is for transient estimation and plantwide control studies.

Column temperature profiles accurate prediction is of importance since temperature affects phase equilibrium calculation at the gas-liquid interface and liquid phase. In addition, several model parameters and thermophysical properties depend on temperature. These include heat capacity, CO_2 solubility, water heat of condensation, heats of reaction and equilibrium constants. The pilot plant absorber and stripper columns temperature profiles are calculated as an averaged value of the temperature measurements from the sensors distributed in the radial plane at the given axial position of the column. The individual temperature measurements are considered reliable, and the resulting temperature profiles are clear and reasonable. Nevertheless, it should be mentioned that some sensors are closer to the wall while some are closer to the center of the packing, thus a small maximum variation (<6 ºC) is observed between the measurements at a given radial position. The variation is different for different operating conditions of the columns and radial planes. The aggregated effect of above-mentioned aspects makes validation of the absorber temperature profiles challenging. Based on the results presented in Figures 2 and 3, it is considered that the dynamic process model is capable of predicting temperature profiles of both absorber and stripper columns with good accuracy for the purpose considered in this work. Tuning of the pre-multiplying factor of the mass transfer enhancement factor has been required (0.2 in absorber and 0.09 in stripper).

Lean and rich CO_2 loadings are over-predicted by the dynamic process model. Lean and rich loadings are dependent of each other, and modeling errors will easily propagate. In addition, actual reboiler heat duty has been estimated from steam measurements in the plant as suggested by Thimsen et al. [15]. Nevertheless, that value is not truly representative of regeneration energy due to external factors such as changes in ambient conditions and heat loses through non-insulated pipes and equipment [5]. An under-prediction of lean loading is found on cases 6 and 7. It is believed that this is because the plant was operated before addition of anti-foam solution during these cases as well as due to small deviations on MEA concentration from 30 wt% during that period. The mean percentage error for lean loading is 1.4 % and for rich loading 6.7%. It can be concluded that the process model is capable of predicting the variability in lean and rich loading for the range of operating conditions of the PCC plant. The process model under-predicts CO_2 product mass flow rate within <5% for all steady-state cases, being the precision uncertainty of the product CO_2 flow measurement 1% (Vortex FT-0010) [13]. This under prediction is illustrated in the transient cases (Figures 6 and 9).

Dynamic process validation with the two tests involving volumetric flue gas flow rate reduction and increase has been presented in this paper. The experiment shows that the system acts as a buffer to load change driven by flue gas volumetric flow rate change at absorber inlet, and long dead times input/output in terms of CO_2 product flow are observed (around 20-40 minutes). The results from the model show that the model development has been successful to predict the main process dynamics. This includes CO_2 lean and rich loadings and CO_2 product flow response to the disturbances.

7. Conclusions

A dynamic process model of the overall amine-based TSA plant at TCM DA was built for the purpose of model validation with a new set of steady-state and transient plant data. It is concluded that the dynamic process model is capable of estimating the temperature profiles of absorber and stripper columns with good accuracy for the purpose of application. Tuning of the pre-multiplying factor for calibration of the enhancement factor has been required. An over prediction of the model for lean and rich CO_2 loadings has been reported, being mean percentage errors <1.5% and <6.7%. The process model is capable of predicting the variability of lean and rich loadings for a wide range of steady-state operating conditions. In addition, an under prediction of CO_2 product flow rate has been observed (<5%). The main process dynamics of the pilot plant under flue gas volumetric flow changes is captured by the process model.

The validated process model developed in this work will be used to analyze the TCM plant transient performance and expanded to a full-scale plant model to predict transient performance of a natural gas combined cycle power plant integrated with post-combustion CO_2 capture.

Acknowledgements

The authors acknowledge TCM DA and the Department of Energy and Process Engineering at NTNU-Norwegian University of Science and Technology for funding this project. The Faculty of Engineering Science NTNU-Statoil Publication Grant 2016 is also acknowledged. The authors want to acknowledge Espen S. Hamborg from TCM DA for his contribution to establish the ongoing collaboration between TCM DA and the Thermal Energy Research Group at the Department of Energy and Process Engineering at NTNU.

References

[1] R.M. Montañés, M. Korpås, L.O. Nord, S. Jaehnert, Identifying Operational Requirements for Flexible CCS Power Plant in Future Energy Systems, Energy Procedia, 86 (2016) 22-31.
[2] M.E. Boot-Handford, J.C. Abanades, E.J. Anthony, M.J. Blunt, S. Brandani, N. Mac Dowell, J.R. Fernandez, M.-C. Ferrari, R. Gross, J.P. Hallett, R.S. Haszeldine, P. Heptonstall, A. Lyngfelt, Z. Makuch, E. Mangano, R.T.J. Porter, M. Pourkashanian, G.T. Rochelle, N. Shah, J.G. Yao, P.S. Fennell, Carbon capture and storage update, Energy & Environmental Science, 7 (2014) 130-189.
[3] R. Faber, M. Köpcke, O. Biede, J.N. Knudsen, J. Andersen, Open-loop step responses for the MEA post-combustion capture process: Experimental results from the Esbjerg pilot plant, Energy Procedia, 4 (2011) 1427-1434.
[4] P. Tait, B. Buschle, I. Ausner, P. Valluri, M. Wehrli, M. Lucquiaud, A pilot-scale study of dynamic response scenarios for the flexible operation of post-combustion CO_2 capture, International Journal of Greenhouse Gas Control.
[5] M. Bui, I. Gunawan, V. Verheyen, P. Feron, E. Meuleman, Flexible operation of CSIRO's post-combustion CO_2 capture pilot plant at the AGL Loy Yang power station, International Journal of Greenhouse Gas Control.
[6] N. Enaasen Flø, H. Knuutila, H.M. Kvamsdal, M. Hillestad, Dynamic model validation of the post-combustion CO_2 absorption process, International Journal of Greenhouse Gas Control, 41 (2015) 127-141.
[7] H.M. Kvamsdal, J.P. Jakobsen, K.A. Hoff, Dynamic modeling and simulation of a CO_2 absorber column for post-combustion CO_2 capture, Chemical Engineering and Processing: Process Intensification, 48 (2009) 135-144.
[8] C. Biliyok, A. Lawal, M. Wang, F. Seibert, Dynamic modelling, validation and analysis of post-combustion chemical absorption CO_2 capture plant, International Journal of Greenhouse Gas Control, 9 (2012) 428-445.
[9] J. Gaspar, A.-M. Cormos, Dynamic modeling and absorption capacity assessment of CO_2 capture process, International Journal of Greenhouse Gas Control, 8 (2012) 45-55.
[10] M. Bui, I. Gunawan, V. Verheyen, P. Feron, E. Meuleman, S. Adeloju, Dynamic modelling and optimisation of flexible operation in post-combustion CO_2 capture plants—A review, Computers & Chemical Engineering, 61 (2014) 245-265.
[11] Modelica Association, https://www.modelica.org/.
[12] Dassault Systems, Dymola, http://www.3ds.com/products-services/catia/products/dymola.
[13] N. Brigman, M.I. Shah, O. Falk-Pedersen, T. Cents, V. Smith, T. De Cazenove, A.K. Morken, O.A. Hvidsten, M. Chhaganlal, J.K. Feste, G.

Lombardo, O.M. Bade, J. Knudsen, S.C. Subramoney, B.F. Fostås, G. de Koeijer, E.S. Hamborg, Results of Amine Plant Operations from 30 wt% and 40 wt% Aqueous MEA Testing at the CO_2 Technology Centre Mongstad, Energy Procedia, 63 (2014) 6012-6022.
[14] E.S. Hamborg, V. Smith, T. Cents, N. Brigman, O.F. Pedersen, T. De Cazenove, M. Chhaganlal, J.K. Feste, Ø. Ullestad, H. Ulvatn, O. Gorset, I. Askestad, L.K. Gram, B.F. Fostås, M.I. Shah, A. Maxson, D. Thimsen, Results from MEA testing at the CO_2 Technology Centre Mongstad. Part II: Verification of baseline results, Energy Procedia, 63 (2014) 5994-6011.
[15] D. Thimsen, A. Maxson, V. Smith, T. Cents, O. Falk-Pedersen, O. Gorset, E.S. Hamborg, Results from MEA testing at the CO_2 Technology Centre Mongstad. Part I: Post-Combustion CO_2 capture testing methodology, Energy Procedia, 63 (2014) 5938-5958.
[16] Modelon, Post-combustion capture with amine solutions. http://www.modelon.com/industries/energy-process/carbon-capture-and-sequestration/.
[17] K. Prölß, H. Tummescheit, S. Velut, J. Åkesson, Dynamic model of a post-combustion absorption unit for use in a non-linear model predictive control scheme, Energy Procedia, 4 (2011) 2620-2627.
[18] S.Ó. Garðarsdóttir, F. Normann, K. Andersson, K. Prölß, S. Emilsdóttir, F. Johnsson, Post-combustion CO_2 capture applied to a state-of-the-art coal-fired power plant—The influence of dynamic process conditions, International Journal of Greenhouse Gas Control, 33 (2015) 51-62.
[19] K. Onda, H. Takeuchi, Y. Okumoto, Mass transfer coefficients between gas and liquid phases in packed columns, Journal of Chemical Engineering of Japan, 1 (1968) 56-62.
[20] W. Böttinger, NMR-spektroskopische Untersuchung der Reaktivabsorption von Kohlendioxid in wässrigen Aminlösungen, VDI-Verlag, 2006.
[21] Functional Mock-up Interface. https://www.fmi-standard.org/.
[22] Modelon, FMI-Add-In for Excel. http://www.modelon.com/products/fmi-tools/fmi-add-in-for-excel/.

Technology Centre Mongstad (TCM) is the largest and most flexible test centre for verification of CO_2 capture technologies and a world leading competence centre for CCS.

Here is an overview of the main topics where TCM has gathered together its professional contributions:

tcmda.com